POLITECNICO DI MILANO

Scuola di Ingegneria Industriale e dell'Informazione

Corso di Laurea Magistrale in Engineering Physics

Cluster Monte-Carlo for Random-Bond Ising Model

Advisor: Prof. Paolo BISCARI
Co-Advisor: Prof. Stefano Simone TURZI

Author:
Filippo PERANI
Matr. 920441

Anno Accademico 2019-2020

Acknowledgements

Vorrei ringraziare il Professore Paolo Biscari per avermi dato la possibilità di svolgere questo lavoro di tesi, per la sua disponibilità a chiarire ogni mio dubbio e per la pazienza mostrata nel lanciare le simulazioni che gli inviavo...a qualunque orario della giornata! Un sentito ringraziamento anche al Professore Stefano Simone Turzi per il suo supporto nella comprensione del metodo numerico utilizzato nelle simulazioni. Ringrazio anche il Professore Ezio Puppin e il Professore Maurizio Zani, i cui studi sperimentali hanno reso possibile questo progetto.
Grazie ai miei genitori e a mia sorella Ottavia per avermi consigliato, supportato e, soprattuto, sopportato in questi cinque anni universitari.
Non posso mancare di ringraziare i miei cari e fidati amici Carlo, Erjon e Pietro, per quel supporto che solo i veri amici sanno dare.
Infine, vorrei ringraziare il mio Professore di Fisica del Liceo, Luigi Togliani. É grazie alla sua passione per le discipline scientifiche e al suo coinvolgente ed efficace metodo di insegnamento che è nata in me la passione per la fisica.

Grazie.

Sommario

Lo scopo di questa tesi è riprodurre l'effetto della temperatura sulle proprietà del fenomeno fisico noto come Rumore di Barkhausen (BK) attraverso il Random-Bond Ising Model (RBIM). Tale analisi ci permetterà di individuare un legame tra i fenomeni microscopici interni a un ferromagnete e gli effetti macroscopici come il rumore di Barkhausen. Il metodo numerico utilizzato per implementare il modello fisico è il metodo Monte Carlo. Precisamente, la variante proposta da Wolff è stata utilizzata per simulare il comportamento di un reticolo di spin quadrato e bidimensionale. Tale metodo numerico è stato implementato tramite un codice $C++$. Per simulare le proprietà dell'effeto Barkhausen, abbiamo calibrato il parametro di disordine incluso nel modello. La comparsa delle proprietà tipiche del rumore di BK è stata rilevata grazie ad un'analisi sulla statistica dei salti di magnetizzazione. Per completare il nostro studio, abbiamo condotto un'analisi sul rumore di BK negativo. Il coefficiente che abbiamo studiato per confrontare i nostri risultati teorici con quelli sperimentali è l'esponente (τ) della legge di potenza tipica della distribuzione di valanghe del rumore di BK. In particolare, abbiamo stimato la dipendenza di tale coefficiente dalla temperatura. I risultati si sono dimostrati in accordo con il trend del coefficiente τ osservato sperimentalmente al variare della temperatura. Anche i valori numerici di τ da noi trovati sono coerenti con i risultati di molti esperimenti sul rumore di BK. Entro l'intervallo di temperature studiato, anche i risultati sul rumore di BK negativo sono coerenti con le osservazioni sperimentali. Infine, abbiamo anche esplorato la possibile transizione di un RBIM a una fase vetro di spin, costruendo un diagramma di fase per le transizioni para-ferro-vetro grazie a un codice apposito. Tale diagramma ci ha permesso di mantenere il sistema in fase ferromagnetica durante tutta l'analisi sul rumore di BK.

Parole Chiave: Rumore di Barkhausen, Rumore di Barkhausen negativo,

Modello di Ising, Random-Bond Ising Model, Metodo Monte Carlo, Algoritmo Wolff, Meccanica Statistica, Vetro di Spin, Transizioni di Fase, Leggi di Potenza, Magnetismo nell Materia Condensata.

Abstract

The scope of this thesis is reproducing the effect of the temperature on the properties of the Barkhausen (BK) noise through the Random-Bond Ising model (RBIM). This kind of analysis can help us to find a microscopical description to the macroscopic effects of BK noise. The algorithm used in order to implement the physical model is the Montecarlo method. More precisely, the Wolff (cluster) variant was used in order to simulate the behaviour of a 2D square lattice of spins. Such numerical method was implemented on a C_{++} code. In order to mimic the BK noise properties, we calibrated the disorder parameter included in the RBIM. The appearance of the typical properties of BK noise were detected thanks to a magnetization jumps' distribution analysis. To complete the BK noise analysis, the negative BK noise was studied too. The coefficient that we studied in order to compare our results with the experimental data, is the so called power-law coefficient (τ) of the BK avalanches' distribution. In particular, we estimated its dependence from the temperature. The results are in agreement with the trend of the coefficient τ observed experimentally by tuning the temperature. Even the numerical values that we found are within the range of many experimental results. Within the temperature range studied in this thesis, the negative BK noise results are in agreement with experimental observations too. Finally, we also estimated the phase diagram for the para-ferro-glass phase transition, by developing a further code for the identification of the ferro-glass transition. This diagram helped us to keep our system within the ferromagnetic regime for our analysis on BK noise.

Keywords: Barkhausen Noise, Negative Barkhausen Noise, Ising Model, Random-Bond Ising Model, Monte Carlo Method, Wolff algorithm, Statistical Mechanics, Spin Glass, Phase Transitions, Power-Laws, Magnetism in Condensed Matter Physics.

Contents

Introduction

The main scope of this thesis is to study the role of temperature and frozen disorder in the magnetization reversal process, by exploiting a theoretical model implemented on a computer. In particular, the experimental data, to be compared with the results of our computations, refer to a thin Fe film grown on MgO [23]. More in details, the physical process of our interest is called Barkhausen (BK) noise. In 1919, Barkhausen [2] discovered that iron (an example of magnetic material) produces a jerky noise when magnetized by a field smoothly changing in time. This noise was not expected from the macroscopically continuous process of magnetization reversal. It was the first indirect experimental evidence to support the model of ferromagnetism based on magnetic domains, postulated in 1906 by Pierre-Ernest Weiss. Because of the external applied field, magnetic domains change in size or orientation. Thus, minute jumps of the magnetization are produced (so, the variation of the magnetization is not continuous). These jumps are the cause of this noise, since they induce magnetic flux variations in a coil close to the magnetic sample, and consequently voltage variations at the end of the same coil. By amplifying these voltage signals and using a loudspeaker, we can ear crackles: hence the name, Barkhausen noise. Actually, we have to be more precise. By talking about change in size and rotation of domains we are actually moving a step away from Barkhausen's belief that the noise was produced by the sudden reversal of the entire magnetic domain. In fact, in 1938, Elmore observed for the first time the motion of domain boundaries (referred as Bloch walls since described theoretically in 1932 by Bloch) in a cobalt crystal. Then, Williams and Shockley showed that the Barkhausen noise is due to irregular fluctuations in the motion of a domain boundary (fig.1). These irregularities are due to the presence of defects in the spin lattice (e.g. impurities, dislocations). From now on, we will call avalanches the magnetization jumps. In an ideal lattice the wall motion would be a

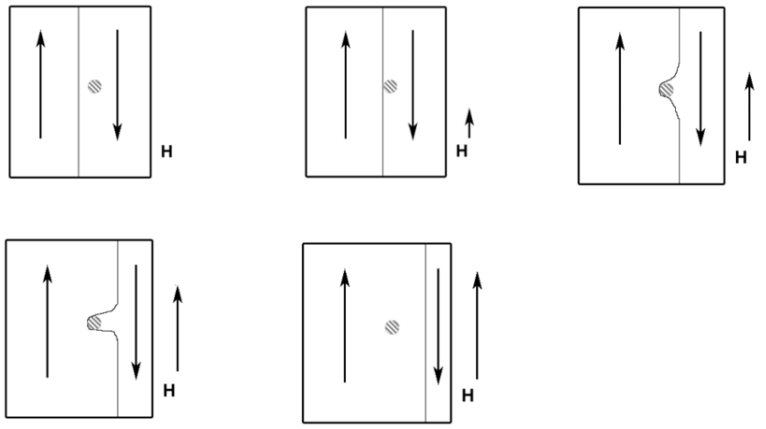

Figure 1: From the left to the right, moving downward: an example of magnetic domain's wall motion. The wall gets caught into the defect and, only when the external magnetic field is big enough, it moves on producing a jump in the magnetization of the material (for the source of the image, look at [1]).

continuous process.
In literature, we can find many experiments that deepened the knowledge about the characteristics of this phenomenon. The surprising result is that BK shows scaling invariance (that is a perfect form of self similarity) and power laws. Actually, these are some of the typical features of a critical phenomenon. In 1991, Cote and Meisel [4, 5] claimed that the Barkhausen effect is an example of self-organized criticality (SOC) [6]. Instead, Sethna, in 1995 [10], said that SOC is not needed. Nowadays, out of the large production of data and ideas of the past years, we still do not have a single framework to interpret the phenomenon.

This project focuses on the study of the avalanches distribution, one of the features of the BK noise showing power law behaviour. And, as previously said, the role of temperature is taken into consideration. This differentiates our work from all the others that we are aware of about the same topic, as these latter always refer to the zero-temperature condition, like [7, 10]. Actually, in [15] the role of temperature in BK noise has been studied but a different algorithm has been used. Here, the cluster algorithm developed by Wolff [22] is used. In particular, it is exploited in order to study a theoretical

model made of interacting spins, the Ising model, in order to understand the Barkhausen avalanches behaviour. This approach, of deriving macroscopic properties from a microscopic model, was suggested by Sethna [8] for the case of the Barkhausen noise with the Random Field Ising Model (RFIM). In fact, the idea rests on the universality feature typical of critical phenomena, according to which the behaviour of a system is independent of many details of the system itself. Indeed, it depends only on the dimension, the range of interaction and the symmetries system. More precisely, we used a variant of the Ising model characterized by a source of disorder (otherwise, it would be impossible to observe BK noise in a perfect spin lattice, as we have already said): the Random Bonds Ising Model (RBIM). Within RBIM, we have also been able to study a different phase transition, from ferromagnetic to spin glass phase.

Chapter 1

Barkhausen noise

In this chapter we will start by deepening our knowledge about the physics behind the BK noise, i.e. the mechanism of ferromagnetism, moving through a brief and general introduction to the magnetism in the matter. Then we will focus on the BK effect itself. All of this will allow us to understand the physical meaning of the mathematical model that we used to simulate a ferromagnet. Indeed, we will come to write the ferromagnet quantum Hamiltonian, which is the one from which the Ising model Hamiltonian comes from. Also the phenomenon of phase transitions will be introduced.

1.1 Magnetism in condensed matter

The magnetic properties of matter are known since nearly three thousand years. In the ancient Greece, people were attracted by the mysterious (at the time) properties of lodestone. The first technological application of magnetic materials was the magnetic compass. Then, in the last two centuries the progress about magnetism has been more rapid. It was discovered that magnetism and electricity are two sides of the same coin, and they make up light which is an electromagnetic wave. This achievement, derived from the special relativity theory. Nowadays, the magnetism in condensed matter (ferromagnetism, spin glasses, ...) is under the lens of many scientific research groups.

1.1.1 Phenomenology

From electromagnetism theory, we know that there are three physical quantities needed to describe magnetism in the matter: **B** (magnetic induction), **H** (magnetic field), and **M** (the magnetization). All three are vector fields. The magnetization is defined as the magnetic moment per unit volume within a material (i.e. in free space it is always zero). In free space, **B** and **H** are just scaled versions of each other

$$\mathbf{B} = \mu_0 \mathbf{H}, \tag{1.1}$$

the former measured in T (Tesla) and the latter measured in $\frac{A}{m}$. μ_0 is the permeability if free space. In a magnetic solid, the relation between **B** and **H** is more complicated

$$\mathbf{B} = \mu_0(\mathbf{H} + \mathbf{M}). \tag{1.2}$$

The magnetization M depends on the external field H. The *magnetic susceptibility* is defined as the coefficient providing the variation of the magnetization when the external field varies

$$\chi = \frac{dM}{dH}. \tag{1.3}$$

In the simplest case, χ is a scalar, but in general it may be a tensor. When the magnetization varies linearly with the external field, the magnetic susceptibility is a constant and (1.3) provides

$$\mathbf{M} = \chi \mathbf{H}. \tag{1.4}$$

A first (experimental) way to characterize magnetic materials is to study them under the action of an external magnetic field. By putting them within the cavity of an electromagnet (i.e. a coil, with a current running within it, generating a tunable magnetic field, see fig.1.1), we would observe different behaviours for different substances. Indeed, some materials are pushed out from the cavity (e.g. H_2O,Cu,...), some others are attracted within it (e.g. Na,Al,O_2 (L),Fe,...). For the greatest part of the materials, the effect due to the magnetic field is weak, except for some substances (O_2 (L),Fe, other Fe compounds,...). This allows us to identify the three main categories of magnetic materials: diamagnetic (weak repulsive force felt within

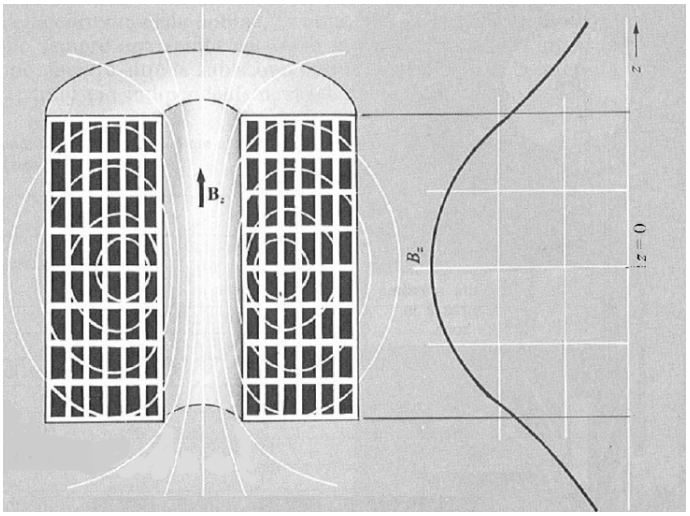

Figure 1.1: Qualitative example of the experimental set-up described above. Also, the typical behaviour of the magnetic field in a finite coil, along its axis, is shown (From [9]). Along such axis, the field is parallel to the axis itself.

the electromagnet), paramagnetic [1](weak attractive force), and ferromagnetic (strong attractive force, and our main interest in this work) materials. Another way to characterize magnetic materials comes from their magnetic

Table 1.1: In this table we can see a few examples of materials for each type of magnetic substance.

Diamagnet	**Paramagnet**	**Ferromagnet**
H_2O	Na	Fe
Cu	Al	Fe_3O_4
Pb	O_2	Co
$N_2(L)$	Ca	Ni

susceptibility (χ). In particular, the diamagnets have $\chi < 0$, the paramagnets and ferromagnets have $\chi > 0$. This can be easily derived by thinking at

[1]Actually, the liquid oxygen is a paramagnet even if characterized by a strong attractive force. Here the main culprit of this "apparently" strange behaviour is the low temperature needed to get liquid oxygen.

the experiment described above and using some notions of electromagnetism. If I_c is the current within the coil, $B_0 = \mu_0 n I_c$ [2] is the magnetic induction within the void electromagnet's cavity, where n is the number of coils per unit length. If we fully fill up the solenoid with a linear magnetic material, $B = \mu_r B_0$ is the field within the material, where $\mu_r = 1 + \chi$ is the magnetic permeability of the material. This variation of the magnetic induction can be seen as the effect of the variation of the total current within the coil. Since

$$B - B_0 = (\mu_r - 1)B_0 = \chi B_0, \tag{1.5}$$

we can rewrite the magnetic induction

$$B = B_0 + \chi B_0 = \mu_0 n(I_c + \chi I_c). \tag{1.6}$$

This works as if a magnetization current $I_m = \chi I_c$ is generated on the surface of the magnetic material. Arrived to this point, by exploiting the Laplace

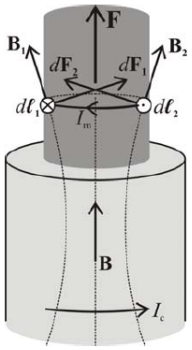

Figure 1.2: Force acting on the magnetic sample. Here the sample is a diamagnet, since the forces push it away from the coil due to the I_m running in the opposite direction respect to the coil current I_c.

formula about the force acting on an infinitesimal length element in which a current runs

$$d\vec{F} = I_m d\vec{l} \times \vec{B} \tag{1.7}$$

and looking at fig.1.2, we can deduce that if the magnetization current runs in the opposite direction of I_c (i.e. $\chi<0$), the resultant force points outward

[2]Here we are using scalar quantities because what we are actually considering is the value of the magnetic induction, B, along the axis of the electromagnet, at $z = 0$ (in the ideal case of an infinite solenoid). This is enough for our scope. Note that $H = nI_c$.

the electromagnet. So, the sample is rejected by the electromagnet. We have previously seen that this is typical of a diamagnet. Instead, if I_m runs in the same direction of I_c (i.e. $\chi > 0$), the resultant will point inward the electromagnet. This is what happens with paramagnets and ferromagnets. So, we have proved that diamagnets have negative susceptibility, against the positive one of paramagnets and ferromagnets.

1.1.2 Quantum-Mechanical description: Pauli Hamiltonian

The three magnetic effects in the matter that we have seen above can be correctly explained only through Quantum Mechanics. Nonetheless, the foundation of the classical theory of magnetism in condensed matter deserves a mention (even if wrong).
In general, at the basis of the theory of magnetism there is the concept of magnetic moment. According to the Ampere equivalence principle, a magnetic dipole is equivalent to a current loop. This is the starting point for the classical theory of magnetism, due to the works of Ampère, Oersted and Arago at the beginning of the 19^{th} century. These scientists believed that magnetism in the matter derived from the presence of magnetization currents (like the one we have talked previously) in the matter itself. By following this ideas, we can link the magnetic moment of an atomic electron to the orbital angular momentum of the electron itself through the gyromagnetic ratio (we simply have to see electrons' orbitals within an atom like if they were current loops). This last relation is demonstrated by the Einstein-de Haas effect and by the inverse Barnett effect[3]. By keeping this way of reasoning, classical theories for diamagnetism and paramagnetism were derived by Langevin (and Larmor). Arrived to this point, there is a problem to take into account. According to a theorem from Statistical Mechanics, known as Bohr-van Leeuwen theorem, since discovered separately by Bohr in 1911 and Hendrika Johanna van Leeuwen in 1919, in a classical system there is no thermal equilibrium magnetization. This means that a quantum mechanics theory for magnetism in condensed matter is needed.

[3]Actually, these two effects also reveal that ferromagnetism (we will talk about it later on) is mainly due to another type of angular momentum: the spin angular momentum, which is an intrinsic property of elementary particles, with a quantum mechanical nature.

So, a quantum Hamiltonian is needed for this kind of problem. First of all, the kinetic energy operator has to face some little variations. From electromagnetism theory, we know that the canonical momentum of a particle moving within an electromagnetic field is

$$\mathbf{p} = m\mathbf{v} + q\mathbf{A}, \tag{1.8}$$

where $\mathbf{A}$ is the magnetic vector potential associated with the magnetic field and such that $\mathbf{B} = \nabla \times \mathbf{A}$. This will be useful in a few moments. Before moving on, let us introduce the operator of the spin angular momentum (see previous note). The behaviour of the electron spin[4] turns out to be connected to an algebra based on the three Pauli spin matrices, which are defined as

$$\hat{\sigma}_x = \begin{pmatrix} 0 & 1 \\ 1 & 0 \end{pmatrix}, \qquad \hat{\sigma}_y = \begin{pmatrix} 0 & -i \\ i & 0 \end{pmatrix}, \qquad \hat{\sigma}_z = \begin{pmatrix} 1 & 0 \\ 0 & -1 \end{pmatrix}. \tag{1.9}$$

For our scope, it will be useful to write them as a vector of matrices

$$\sigma = (\hat{\sigma}_x, \hat{\sigma}_y, \hat{\sigma}_z). \tag{1.10}$$

Between the many properties of these three matrices, we will exploit the following identity

$$(\sigma \cdot \mathbf{a})(\sigma \cdot \mathbf{b}) = (\mathbf{a} \cdot \mathbf{b})\mathbb{1} + i\sigma \cdot (\mathbf{a} \times \mathbf{b}), \tag{1.11}$$

where

$$\mathbf{a} = \begin{pmatrix} a_1 \\ a_2 \\ a_3 \end{pmatrix} \tag{1.12}$$

is a generic vector belonging to $\mathbb{C}^3$, $\mathbb{1}$ is the identity matrix belonging to $M_2(\mathbb{C})$ and

$$\sigma \cdot \mathbf{a} = \begin{pmatrix} a_3 & a_1 - ia_2 \\ a_1 + ia_2 & -a_3 \end{pmatrix} = \hat{\sigma}_x a_1 + \hat{\sigma}_y a_2 + \hat{\sigma}_z a_3, \tag{1.13}$$

in order to obtain our quantum Hamiltonian for a spin-1/2 particle interacting with an external electromagnetic field, described by the magnetic vector

[4]The spin comes out naturally only from combining quantum mechanics and special relativity (i.e. from Dirac equation).

potential $\mathbf{A}$ and the electric potential energy V. First step, we have to introduce the Pauli matrices within our Hamiltonian. According to eq.(1.11), the kinetic energy operator for an electron $\hat{K} = \frac{\hat{\mathbf{p}}^2}{2m}$ can be rewritten [5] as

$$\hat{K} = \frac{(\sigma \cdot \hat{\mathbf{p}})^2}{2m}. \tag{1.14}$$

By remembering eq.(1.8), $\hat{K}$ becomes

$$\hat{K} = \frac{[\sigma \cdot (\hat{\mathbf{p}} + e\mathbf{A})]^2}{2m}. \tag{1.15}$$

Once again, identity 1.11 comes to our help

$$[\sigma \cdot (\hat{\mathbf{p}} + e\mathbf{A})]^2 = (\hat{\mathbf{p}} + e\mathbf{A}) \cdot (\hat{\mathbf{p}} + e\mathbf{A}) + i\sigma \cdot (\hat{\mathbf{p}} + e\mathbf{A}) \times (\hat{\mathbf{p}} + e\mathbf{A})], \tag{1.16}$$

and, by exploiting the following calculations (where ψ is the electron wavefunction) and the expression for the quantum operator of the linear momentum, $\hat{\mathbf{p}} = -i\hbar\nabla$,

$$\begin{aligned}
&[(\mathbf{p} + e\mathbf{A}) \times (\mathbf{p} + e\mathbf{A})]\,\psi = e\,[\mathbf{p} \times (\mathbf{A}\psi) + \mathbf{A} \times (\mathbf{p}\psi)] = \\
&= -ie\hbar\,[\nabla \times (\mathbf{A}\psi) + \mathbf{A} \times (\nabla\psi)] = -ie\hbar\,[\psi\,(\nabla \times \mathbf{A}) - \mathbf{A} \times (\nabla\psi) + \mathbf{A} \times (\nabla\psi)] = \\
&= -ie\hbar\mathbf{B}\psi,
\end{aligned}$$

we can write

$$[\sigma \cdot (\hat{\mathbf{p}} + e\mathbf{A})]^2 = (\hat{\mathbf{p}} + e\mathbf{A})^2 + e\hbar\sigma \cdot \mathbf{B}. \tag{1.17}$$

If we define the spin angular momentum by

$$\hat{\mathbf{S}} = \frac{1}{2}\hat{\sigma}, \tag{1.18}$$

the kinetic operator finally becomes[6]

$$\hat{K} = \frac{(\hat{\mathbf{p}} + e\mathbf{A})^2}{2m} + g\mu_B\mathbf{B} \cdot \mathbf{S}. \tag{1.19}$$

[5] Here we use the case of $\mathbf{a} = \mathbf{b}$. So, eq.(1.11) becomes $(\sigma \cdot \mathbf{a})^2 = \mathbf{a}^2$.

[6] The second term can be derived by considering the relation between the spin angular momentum and the corresponding magnetic moment $\vec{\mu} = -\mu_B g\vec{S}$, and the Zeeman energy of interaction between such magnetic moment and the magnetic field, $E = \vec{\mu} \cdot \vec{B}$.

By considering the electric potential energy, the final Hamiltonian has the following form

$$\hat{H} = \frac{(\hat{\mathbf{p}} + e\mathbf{A})^2}{2m} + g\mu_B \mathbf{B} \cdot \hat{\mathbf{S}} + V, \tag{1.20}$$

where $g = 2$. This is also called Pauli Hamiltonian for a spin-1/2 particle interacting with an external e.m. field. It is the non-relativistic limit of the Dirac equation, when applied to particles with a velocity much lower than the speed of light.
Now, we can write the complete Hamiltonian of all the Z electrons of an atom. By remembering the total orbital angular momentum due to the electrons

$$\hbar \mathbf{L} = \sum_i \mathbf{r}_i \times \mathbf{p}_i, \tag{1.21}$$

and by using the following gauge

$$\mathbf{A}(\mathbf{r}) = \frac{\mathbf{B} \times \mathbf{r}}{2}, \tag{1.22}$$

we obtain

$$\hat{H} = \sum_{i=1}^{Z} \left(\frac{[\hat{\mathbf{p}} + e\mathbf{A}]^2}{2m} + V_i \right) + g\mu_B \mathbf{B} \cdot \hat{\mathbf{S}}. \tag{1.23}$$

Since[7]

$$(\hat{\mathbf{p}} + e\mathbf{A})^2 = \hat{\mathbf{p}}^2 + 2e\hat{\mathbf{p}} \cdot \mathbf{A} + e^2 \mathbf{A}^2, \tag{1.24}$$

by exploiting 1.21, 1.22 and the fact that the scalar triple product is unchanged under circular shift of its three operands, the total Hamiltonian becomes

$$\hat{H} = \sum_i \left(\frac{\hat{\mathbf{p}}}{2m} + V_i \right) + \mu_B (\mathbf{L} + g\mathbf{S}) \cdot \mathbf{B} + \frac{e^2}{8m} \sum_i (\mathbf{B} \times r_i)^2, \tag{1.25}$$

The first term is the unperturbed hamiltonian, the second and third terms are respectively the paramagnetic and diamagnetic term. The paramgentic term (Zeeman term) is usually the dominant perturbation and it is due to the interaction of the atom's own magnetic moment with the magentic field. The diamagnetic term is always present, also for those atoms without any magnetic moment.

The Zeeman contribution, as derived in the present section, will now allow us to derive the Hamiltonian of a ferromagnet.

[7] Actually, here we have considered $\nabla \cdot \mathbf{A} = 0$ so that $[\hat{\mathbf{p}}, \mathbf{A}] = 0$.

1.1.3 Ferromagnetism

First, let us see some hints about the behaviour of ferromagnets. Materials of this type show a spontaneous magnetization even in the absence of an external field, contrary to paramagnets, that have a zero magnetization if no external field is present. However, above a certain temperature (Curie temperature, T_C) the spontaneous magnetization vanishes and the system behaves as a standard paramagnet. There are other features typical of ferromagnetic materials. One of them is the so called magentic hysteresis and it is due to the fact that ferromagnets have "memory" of the past. By looking at fig.1.3, if we apply a magnetic field B to a ferromagnet showing no magnetization, M grows along OA line (first magnetization curve) and approaches the saturation value M_∞ (A). Then, if we reduce B, the magnetization follows a new line that takes to a state of so called "residual magnetization" (M_0) at $B = 0$. Only if we reach the coercive field (B_c), we can fully demagnetize the ferromagnetic sample. By further increasing B along the negative axis, the magnetization changes sign and approaches the saturation value $-M_\infty$ (A'). Now, if we come back toward positive values of the external magnetic field, a new curve will be chosen by the magnetization and it is the line AA' inverted with respect to the origin, O. So, the curve traced by the system

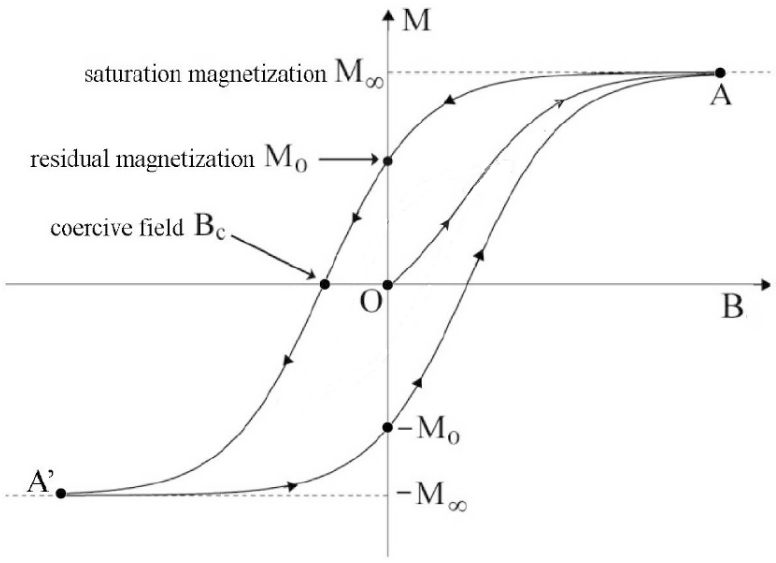

Figure 1.3: Sketch of the hysteresis loop of a ferromagnetic material[14].

on the plane (B,M) is called hysteresis loop and it is observed only if the ferromagnet temperature is below T_c.

The first (classical) model for ferromagnetism was developed by Pierre-Ernest Weiss in 1907. The main hypothesis at the basis of its model is the presence of a mean field, felt by each magnetic moments of the ferromagnet, proportional to the magnetization itself. For all the rest, the model was the same of that for paramagnets of Langevin. The only difference is the magnetic field felt by each atom, which now includes also the mean field: $B = B_{ext} + \lambda M$, where lambda is a proportionality constant. This model is able to explain the spontaneous magnetization and the hysteresis loop of ferromagnets. However, it does not explain the nature of dipoles' interaction generating such mean field. Before talking about the origin of the ferromagnetic interaction, we want to add some other details to our description of a ferromagnet.

By thinking about the spontaneous magnetization, we might wonder how magnetic dipoles decide the particular direction along which to be aligned. When we deal with solid state physics, we have to consider that atoms are no more isolated, spherically symmetric systems, instead they live within a crystalline lattice, whose symmetry is lower than the one of the single atom (e.g. cubic, hexagonal, ...). This means that there are preferential atomic orbitals, chosen by the electrons, such that their Coulombian interaction energy is minimized. The particular geometry of the preferential orbitals defines the direction of the orbital angular momentum. Due to the spin-orbit interaction, the orbital momentum influences the orientation of the spin angular momentum. Since the latter is the main culprit of spontaneous magnetization in ferromagnets, the crystal symmetry eventually determines the preferential direction for the magnetization. These favoured directions are called *crystallographic axes* and can be studied by pointing the field along different directions. This allows to find the easy axis (i.e. the favoured one), along which the saturation is reached faster, and hard axes, characterized by a slower achievement of the ferromagnet's saturation.

Another question that could arise in our minds refers to all those pieces of iron (a ferromagnetic element) that do not show any magnetization. This anomalous behaviour is due to the organization in *magnetic domains* of our ferromagnet. A magnetic domain is a region of the material with a fixed magnetization axis (as we have previously described). Real materials are

made by many domains, even if we consider single-crystals, and they have different easy axes. This means that the total magnetization can be zero, even if each single domain reached saturation. Actually, real materials can be made by more than one crystal. Within one crystal we have many domains, that could have the same easy axes, but with a different orientation for each crystal. Also in this case, the total magnetization could be zero.

1.1.4 Exchange interaction

The first interaction that comes to our minds in magnetic materials is the magnetic dipole interaction

$$E = \frac{\mu_0}{4\pi r^3}\left[\boldsymbol{\mu}_1 \cdot \boldsymbol{\mu}_2 - \frac{3}{r^2}(\boldsymbol{\mu}_1 \cdot \boldsymbol{r})(\boldsymbol{\mu}_2 \cdot \boldsymbol{r})\right], \tag{1.26}$$

but it is too weak, being comparable to thermal energy only when T is of the order of $1K$ (too far from the temperature where ferromagnetism is observed). Moreover, it favours antiparallel coordination of nearest dipoles.

In fact, ferromagnetism has quantum origin. The main ingredient needed to achieve spontaneous magnetization is the **exchange interaction**. This kind of interaction is usually introduced when the problem of an ion with two electrons is studied. By following this idea, let us consider for the moment our two electrons as identical independent particles. If we limit ourselves to a two-level energy spectrum, we can define two wave functions $\psi_a(\mathbf{r})$ and $\psi_b(\mathbf{r})$. Since the two electrons are independent, the joint wave function of the two electrons can be written in the following way

$$\psi(\mathbf{r}_1, \mathbf{r}_2) = \psi_a(\mathbf{r})\psi_b(\mathbf{r}), \tag{1.27}$$

where we have put the origin of the reference system in the nucleus, and $\mathbf{r}_1$ and $\mathbf{r}_2$ are the position vectors of the two electrons. However, we have said that our two electrons are identical particles. From quantum mechanics, this means that exchange symmetry (i.e. particle exchange) has to be obeyed. The wave function 1.27 does not satisfy this property. Thus, we need to build two new wave functions, from a linear combination of $\psi_a(\mathbf{r}_1)\psi_b(\mathbf{r}_2)$ and $\psi_a(\mathbf{r}_2)\psi_b(\mathbf{r}_1)$, that will behave properly under the operation of particle

exchange. They are

$$\psi(\mathbf{r}_1,\mathbf{r}_2)_S = \frac{1}{\sqrt{2}}[\psi_a(\mathbf{r}_1)\psi_b(\mathbf{r}_2) + \psi_a(\mathbf{r}_2)\psi_b(\mathbf{r}_1)]$$
$$\psi(\mathbf{r}_1,\mathbf{r}_2)_A = \frac{1}{\sqrt{2}}[\psi_a(\mathbf{r}_1)\psi_b(\mathbf{r}_2) - \psi_a(\mathbf{r}_2)\psi_b(\mathbf{r}_1)],$$

and we call them respectively, symmetric and antisymmetric wave function. The last ingredient that we need is the spin angular momentum. Let us consider a single domain (i.e. a region of the material with one easy axis). The magnetization prefers to point along its easy axis, that we call z-axis. We have already seen the algebra needed for the spin of the electron. Since the spin components belong to $M_2(\mathbb{C})$, their eigenstates live within $\mathbb{C}^2$. This means that all of them can be written as linear combination of the canonical basis $\mathbf{e}_1, \mathbf{e}_2$

$$\mathbf{e}_1 = \begin{pmatrix}1\\0\end{pmatrix}, \qquad \mathbf{e}_2 = \begin{pmatrix}0\\1\end{pmatrix}. \tag{1.28}$$

Hence the eigenstates are

$$|\uparrow_z\rangle = \begin{pmatrix}1\\0\end{pmatrix} \qquad |\downarrow_z\rangle = \begin{pmatrix}0\\1\end{pmatrix}, \tag{1.29}$$

$$|\uparrow_x\rangle = \frac{1}{\sqrt{2}}\begin{pmatrix}1\\1\end{pmatrix} \qquad |\downarrow_x\rangle = \frac{1}{\sqrt{2}}\begin{pmatrix}1\\-1\end{pmatrix}, \tag{1.30}$$

$$|\uparrow_y\rangle = \frac{1}{\sqrt{2}}\begin{pmatrix}1\\i\end{pmatrix} \qquad |\downarrow_y\rangle = \frac{1}{\sqrt{2}}\begin{pmatrix}1\\-i\end{pmatrix}, \tag{1.31}$$

where, for each spin component, the up and down-eigenstate have respectively eigenvalue $+\frac{1}{2}$ and $-\frac{1}{2}$. As we can see, the z-component eigenvectors are the canonical basis, so the x and y-component eigenstates are written as a linear combination of $|\uparrow_z\rangle$ and $|\downarrow_z\rangle$. In general, the spin wave function is written as a linear combination of the z-component eigenstates

$$\chi = a|\uparrow_z\rangle + b|\downarrow_z\rangle. \tag{1.32}$$

From now on, we will omit the subscript z by taking for granted that we will use the z-component eigenstates as a basis. In our case of two electrons, the general state is

$$\chi = a|\uparrow\uparrow\rangle + b|\uparrow\downarrow\rangle + c|\downarrow\uparrow\rangle + d|\downarrow\downarrow\rangle, \tag{1.33}$$

where $\chi \in \mathbb{C}^4$, and

$$|\uparrow\uparrow\rangle = \begin{pmatrix}1\\0\\0\\0\end{pmatrix}, \qquad |\uparrow\downarrow\rangle = \begin{pmatrix}0\\1\\0\\0\end{pmatrix}, \qquad |\downarrow\uparrow\rangle = \begin{pmatrix}0\\0\\1\\0\end{pmatrix}, \qquad |\downarrow\downarrow\rangle = \begin{pmatrix}0\\0\\0\\1\end{pmatrix}, \tag{1.34}$$

are the canonical basis $\{\mathbf{e}_1, \mathbf{e}_2, \mathbf{e}_3, \mathbf{e}_4\}$. Now, we can write the complete wave function of the two-electron system

$$\psi = \psi(\mathbf{r}_1, \mathbf{r}_2)\chi. \tag{1.35}$$

Whatever the exchange symmetry of the spatial wave function, the spin wave function must have the opposite exchange symmetry. The states $|\uparrow\uparrow\rangle$ and $|\downarrow\downarrow\rangle$ are symmetric under the exchange of the two electrons. The states $|\uparrow\downarrow\rangle$ and $|\downarrow\uparrow\rangle$ are neither symmetric nor antisymmetric. Thus we need linear combinations of the them, one symmetric and the other one antisymmetric

$$\frac{|\uparrow\downarrow\rangle + |\downarrow\uparrow\rangle}{\sqrt{2}}, \tag{1.36}$$

$$\frac{|\uparrow\downarrow\rangle - |\downarrow\uparrow\rangle}{\sqrt{2}}. \tag{1.37}$$

These two states, together with $|\uparrow\uparrow\rangle$ and $|\downarrow\downarrow\rangle$, are a basis since they are the eigenstates of a particular Hamiltonian

$$\hat{H} = A\mathbf{S}^a \cdot \mathbf{S}^b, \tag{1.38}$$

where $\mathbf{S}^a$ and $\mathbf{S}^b$ are the spin operators for two particles (e.g. the two-electron system we are studying). To prove this, we simply have to use the matrix representation of the operator $\mathbf{S}^a \cdot \mathbf{S}^b$. We can do this by using the basis $\{|\uparrow\uparrow\rangle, |\uparrow\downarrow\rangle, |\downarrow\uparrow\rangle, |\downarrow\downarrow\rangle\}$ that we have seen previously, and remembering that S_x^a, S_y^a, S_z^a operators act only on the part of the spin wave function connected with the spin of the first particle (the operators with superscript b obviously refers only to the spin of the second particle). By following this procedure,

we obtain

$$S_z^a = \frac{1}{2}\begin{pmatrix} 1 & 0 & 0 & 0 \\ 0 & 1 & 0 & 0 \\ 0 & 0 & -1 & 0 \\ 0 & 0 & 0 & -1 \end{pmatrix} \qquad S_z^b = \frac{1}{2}\begin{pmatrix} 1 & 0 & 0 & 0 \\ 0 & -1 & 0 & 0 \\ 0 & 0 & 1 & 0 \\ 0 & 0 & 0 & -1 \end{pmatrix},$$

$$S_y^a = \frac{1}{2}\begin{pmatrix} 0 & 0 & -i & 0 \\ 0 & 0 & 0 & -i \\ i & 0 & 0 & 0 \\ 0 & i & 0 & 0 \end{pmatrix} \qquad S_y^b = \frac{1}{2}\begin{pmatrix} 0 & -i & 0 & 0 \\ i & 0 & 0 & 0 \\ 0 & 0 & 0 & -i \\ 0 & 0 & i & 0 \end{pmatrix},$$

$$S_x^a = \frac{1}{2}\begin{pmatrix} 0 & 0 & 1 & 0 \\ 0 & 0 & 0 & 1 \\ 1 & 0 & 0 & 0 \\ 0 & 1 & 0 & 0 \end{pmatrix} \qquad S_x^b = \frac{1}{2}\begin{pmatrix} 0 & 1 & 0 & 0 \\ 1 & 0 & 0 & 0 \\ 0 & 0 & 0 & 1 \\ 0 & 0 & 1 & 0 \end{pmatrix}.$$

Now, it is easy to compute the matrix of the operator $\mathbf{S}^a \cdot \mathbf{S}^b$

$$\mathbf{S}^a \cdot \mathbf{S}^b = \frac{1}{4}\begin{pmatrix} 1 & 0 & 0 & 0 \\ 0 & -1 & 2 & 0 \\ 0 & 2 & -1 & 1 \\ 0 & 0 & 0 & 1 \end{pmatrix}, \tag{1.39}$$

and the associated set of eigenvectors and eigenvalues

$$\{|\uparrow\uparrow\rangle, \frac{|\uparrow\downarrow\rangle + |\downarrow\uparrow\rangle}{\sqrt{2}}, |\downarrow\downarrow\rangle\} \rightarrow \lambda_{I,II,II} = \frac{1}{4}$$

$$\frac{|\uparrow\downarrow\rangle - |\downarrow\uparrow\rangle}{\sqrt{2}} \rightarrow \lambda_{IV} = -\frac{3}{4},$$

as we anticipated before. Now, we know also the eigenvalues of the operator $\mathbf{S}_a \cdot \mathbf{S}_b$. The set of eigenvectors with eigenvalue $\frac{1}{4}$ is called *triplet*. The eigenvector with eigenvalue $-\frac{3}{4}$ is called *singlet*. Now, we can write the complete wave function, by taking into account the exchange symmetry property. We

have two possibilities

$$\psi_S = \frac{1}{\sqrt{2}}[\psi_a(\mathbf{r}_1)\psi_b(\mathbf{r}_2) + \psi_a(\mathbf{r}_2)\psi_b(\mathbf{r}_1)]\chi_S \tag{1.40}$$

$$\psi_T = \frac{1}{\sqrt{2}}[\psi_a(\mathbf{r}_1)\psi_b(\mathbf{r}_2) - \psi_a(\mathbf{r}_2)\psi_b(\mathbf{r}_1)]\chi_T, \tag{1.41}$$

where χ_T is one of the triplet states, and χ_S is the singlet state. The energies of these two possible states are

$$E_S = \int \psi_S^* \hat{E} \psi_S d\mathbf{r}_1 \mathbf{r}_2, \tag{1.42}$$

$$E_T = \int \psi_T^* \hat{E} \psi_T d\mathbf{r}_1 \mathbf{r}_2, \tag{1.43}$$

where $\hat{E}$ is the Hamiltonian of our two-electrons system. Now, let us remember our scope: finding a Hamiltonian whose ground state is the ferromagnetic one, a state with all magnetic momenta pointing in the same direction. Since the magnetic momentum is proportional to the spin angular momentum[8], we want our ground state to be the one with all the spins pointing in the same direction. In our two-electron model, this means we want the triplet states to be the ones more favourable from an energetic point of view. So, by defining the exchange interaction constant, J

$$J = \frac{E_S - E_T}{2} = \int \psi_a^*(\mathbf{r}_1)\psi_b^*(\mathbf{r}_2)\hat{E}\psi_a(\mathbf{r}_2)\psi_b(\mathbf{r}_1)d\mathbf{r}_1 d\mathbf{r}_2, \tag{1.44}$$

we can build the ferromagnetic Hamiltonian, by exploiting the results we obtained about the $\mathbf{S}_a \cdot \mathbf{S}_b$ operator, with eigenvalues E_S and E_T if the complete wave function is respectively ψ_S or ψ_T

$$\hat{E} = \frac{1}{4}(E_S + 3E_T) - (E_S - E_T)\mathbf{S}_a \cdot \mathbf{S}_b. \tag{1.45}$$

By applying $\hat{E}$ on ψ_S or ψ_T, it is easy to see that the corresponding energy is E_S or E_T.

[8]Here we are not considering the orbital angular momentum since, as we have said previously, the spin is the main actor in ferromagnetism. For example, 3d metals are characterized by the quenching of the orbital angular momentum (i.e. $\langle \mathbf{L} \rangle = 0$), so the magnetic momentum is due only to electrons' spin.

In order to have $E_T < E_S$, so the ferromagnetic state favoured, we need $J > 0$. If $J < 0$, the favoured magnetic order is obviously the antiferromagnetic one (because the singlet state with opposite spin is favoured). Now, our patience is going to be paid back. The Heisenberg Hamiltonian for ferromagnetism is obtained from 1.45 and by neglecting the constant part

$$\hat{H}_{ferr} = -\sum_{ij} J_{ij}\mathbf{S}_i\mathbf{S}_j + g\mu_B \sum_j \mathbf{S}_j \cdot \mathbf{B}, \tag{1.46}$$

where we have extended the interaction between the spins of the two-electron model to the interactions of a lattice of atomic spins (only nearest neighbours interaction is considered here), with a different exchange interaction constant J_{ij} for each pair of nearest neighbours, and the paramagnetic term of interaction with the external magnetic field $\mathbf{B}$ is considered. This Hamiltonian can be studied by doing the mean-field approximation of the Weiss model, taking to an Hamiltonian form similar to the one of a paramagnet.

This is the Hamiltonian that we need in order to study ferromagnets (in our case, the BK noise properties of a ferromagnet).

1.2 Crackling phenomena: the BK noise

As we know, BK noise is an effect of the irregular magnetization process of a magnetic sample when a slowly varying external magnetic field is applied. The irregularity (of the domain walls' motion) is due to the defects of the sample.

We can better grasp what is happening by looking at fig.1.4, where the magnetization reversal process is represented. The point A represents a metastable state reached by the system during the phase transition. It is represented also in the right part of the figure, where a graphical representation of the examined portion of the magnetic material is used. Within the area of the ellipse, a fraction has a magnetization already aligned with the external field. This metastable state is due to the presence of a defect. By increasing the amplitude of the magnetic field, the only effect is the bowing of the domain wall (point B), instead the system remains in the state of point A. In order to free the system from such metastable state, we need to increase the field of a quantity ΔH. Indeed, it gives enough energy to the

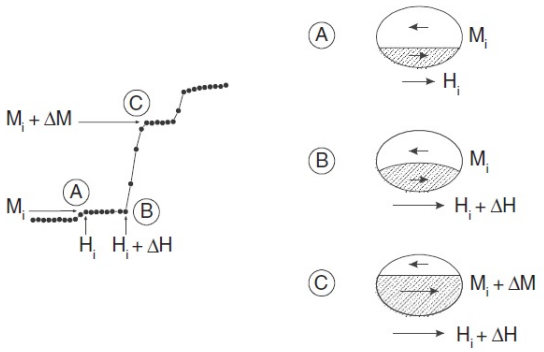

Figure 1.4: Evolution of the system during the inversion of the magnetization.

system in order to overcome the potential barrier due to the pinning defect and jump to the next metastable state (point C). The transition from B to C is an abrupt event, similar to avalanches formed in mountain slopes[9]. The amplitude of an avalanche is here measured by ΔM.

We have already talked about the typical power-law behaviour of avalanches' distribution, $P(\Delta M) \sim (\Delta M)^{-\tau}$, in BK noise, like the one found by Puppin [24]. In this case, the BK noise is said to belong to the class of crackling noise. Systems exhibiting this type of noise respond with discrete events of a variety of sizes, when pushed slowly. In fact, there are systems showing different types of BK effect. We can distinguish between *small BK effect* and *large BK discontinuities*. The former includes all those materials whose field-driven transition is characterized by a large number of small avalanches. Often, soft magnetic materials after annealing show mainly the small BK effect. The latter refers to those magnetic materials exhibiting large jumps in the magnetization. The power-law case is the transition between these two limiting-cases. And that is what interests us.
The model we will use to study the avalanches' statistics is the Random Bonds Ising Model (RBIM), already mentioned in the introduction. The RBIM is characterized by the presence of frozen disorder, controlled by a parameter (R) that turns out to control the avalanches' dimension. At weak disorder, we get one large avalanche with small precursors and aftershocks

[9]Domain wall (DW) motion is the microscopic mechanism behind this abrupt event. Once the pinning potential has been overcome, DW proceeds its motion with a jump (or avalanche).

(large BK discontinuities). At strong disorder, we have a large number of small avalanches (small BK noise). An ideal power-law behaviour of the avalanches' distribution is obtained, within RBIM, at a critical value of the disorder parameter, R_C. It is worth mentioning that, for other values of R (but still close to R_C), similar distributions are found, but with a cut-off for large avalanche's sizes (for an example in RFIM, look at [10]). We call critical

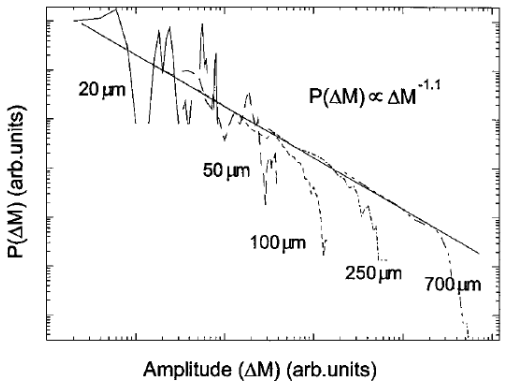

Figure 1.5: Distribution of magnetization steps ΔM in a 90 nm Fe film. From [24]

such value of the disorder parameter, because it is characterized by the appearance of a power-law distribution for the avalanches' size, and power-laws are signature of critical phenomena (in particular continuous phase transitions).

There is a couple of properties deserving to be mentioned about power-laws. The first one is their scale invariance. Given a relation $P(\Delta M) \sim (\Delta M)^{-\tau}$, scaling the argument ΔM by a constant factor c causes only a proportional scaling of the function itself

$$P(c\Delta M) \sim c^{-\tau}(\Delta M)^{-\tau} \propto P(\Delta M). \tag{1.47}$$

This behaviour shows that the relative likelihood between small and large avalanches is the same, no matter how small or large are the avalanches themselves.
A second important property is universality. Magnetic materials are not the only known example of systems characterized by crackling noise phenomena.

For example, the Earth responds with violent and intermittent earthquakes as two tectonic plates rub past one another. A slowly crumpled piece of pa-

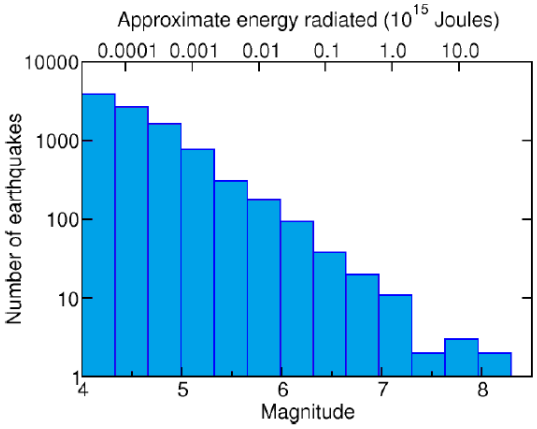

Figure 1.6: Histogram of number of earthquakes in 1995 as function of their magnitude (or, alternatively, their energy release). From the world-wide earthquake catalog of CNSS (Council of the National Seismic System).

per crackles too. Superconductor vortices, microfractures and charge-density waves show this kind of noise too. The intriguing thing is that different phenomena exhibit the same scaling exponent, τ. In this case, they are said to belong to the same universality class. In addition, via renormalization group theory, it has been proven that systems, belonging to the same universality class, share the same dynamics. So, by describing one of them, we would be able to better understand the others too. This is a reason why BK noise in magnets is studied: it is much easier to reproduce crackling phenomena in a ferromagnet, because we can do as many experiments as we want within our lab. Instead, if we want to study earthquakes, we have to wait for an earthquake to happen (we can not produce it), and it is far more difficult to study an earthquake than a ferromagnet sample.

Most of the models for BK noise work only for the zero-temperature case, whereas most experimental data on BK noise have been obtained at room temperature, like Puppin did in [24]. Furthermore, Puppin and Zani [23] tested the statistical properties of BK noise in a thin Fe film for different temperatures and they proved that there is a significant difference at T = 10K and

T = 300K. In both cases, a power-law was found. But different critical exponents were observed. At T = 10K, $P(\Delta M) \sim (\Delta M)^{-1.8}$, while at T = 300K, $P(\Delta M) \sim (\Delta M)^{-1}$. Our scope is to model this behaviour through the RBIM.

Within this project, the simulations were done on a 2D system in order to compare them with experiments of Puppin and Zani[23, 24]. In fact, the literature on BK noise considers mainly 3D materials, because the magnetic phenomena within a thin film are more problematic: stray fields' influence in the direction perpendicular to the sample is non negligible, and it creates complex patterns in the magnetized areas. Many questions remain to be solved and this makes 2D modelling an interesting and promising field of study.

Since we are approximating a thin film with a 2D model, we need to know whether the film's thickness influences the experimental results. Wiegman [27] proved that there is not strong thickness dependence (see fig.1.8).

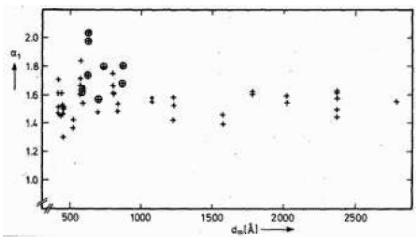

Figure 1.7: Values of the power-law coefficient τ ($\alpha 1$ in Wiegman's notation) for permalloy films as a function of the thickness.

1.3 Phase transitions

In the previous chapters, we have mentioned more than once the phenomenon of the phase transitions. By speaking in general, it is characterized by the transition of a material from one state to a different one. By being more precise, the phase transition is associated to a variation of the symmetry of the equilibrium configuration of the system. The symmetry can be measured through some parameters, called order parameters. For example, at zero field, in magnetic materials we can have a phase transition between the

paramagnetic and the ferromagnetic phase, and the two are distinguished thanks to the magnetization, i.e. an order parameter. Another example of phase transition is the one between two states of matter, gas and liquid. In this case, the order parameter is the densities difference.

In *first order* phase transitions, the system absorbs or yields a given amount of heat (latent heat), during the phase separation. Examples are the crystallization of a liquid, or the fusion and sublimation of a solid. The field-induced transition in a ferromagnet from all spin-up to all spin-down configuration. The liquid/gas transition is a transition of this kind too. All these transitions show an abrupt change in the thermodynamic quantities. For example, once we are in a ferromagnetic phase, we have an abrupt change from down to up magnetization (or vice versa), due to the change of sign of the external magnetic field. The first order transitions are also characterized by the coexistence of the two phases (e.g. magnetic domains in a ferromagnet), and by the presence of hysteresis loops (in ferromagnets, once the magnetic field has changed its sign, the phase transition does not happen, and the system remains in the previous phase which now is metastable)

But, at variance with the first two examples, the line separating the liquid and gas phases on the (P,T) plane ends at a *critical point*, and the down/up magnetization transition shows a similar end point in the (B,T) plane too. Close to such point, the thermodynamic quantities do not show the discontinuous changes typical of first-order phase transitions, but rather a continuous change. Close to this point, thermodynamic quantities are described by power-laws and the fluctuations and spatial correlations of the order parameter becomes increasingly larger. These continuous transitions are called *second order* transitions.

Our main interest will be obviously the magnetic case. The para-ferromagnetic transition is the second-order phase transition that we would face by fixing to zero the external field and moving temperature from below to above the critical point. Such transition is characterized by a continuous change of the order parameter (i.e. the magnetization). The magnetic susceptibility is characterized by a power-law behaviour, with a divergence at T_c.

In the next chapters, we will study the temperature-induced second order phase transition and the field-induced first order phase transition for mag-

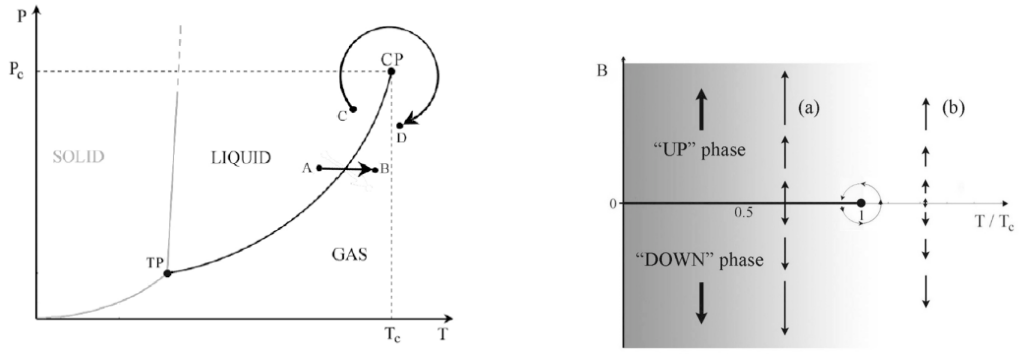

Figure 1.8: Phase diagrams in (P,V) and (B,T) planes respectively for liquid/gas and magnets. Critical points, for liquid/gas and up/down magnetization transitions, are shown.

nets, within the Ising model.

It is interesting to mention that, as we have seen for the magnetic case, also a fluid, if brought close to the critical point along the critical isotherm curve, shows a divergence for the compressibility (i.e. the analogous of the magnetic susceptibility). This is due to a deep physical similarity between fluids and magnets. In fact, in both cases we have spontaneous symmetry breaking, i.e. the systems move from a disordered phase fully invariant to rotation (gas or paramagnet), to a less symmetrical ordered phase (because the invariance to rotation is broken!).

About critical phenomena, we want to mention that one [4, 5] of the theoretical models proposed for the Barkhausen effect involves the theory of Self-Organized Criticality (SOC)[6]. SOC is a property of certain dynamical systems that have a critical point. From a macroscopic point of view , these systems show the scale-invariance typical of critical phenomena, but without the need to set a control parameter to a precise value: it is the system itself that evolves toward the critical point.

Chapter 2

Ising Model

In this chapter, we will describe the Ising model, and the Monte Carlo method, a computational algorithm that we used to study the equilibrium configurations of the Ising model.

2.1 Introduction

The Ising model is a very simple model which proves however able to simulate simulate the magnetic response of a physical ferromagnetic substance. Its main virtue lies in the fact that, even if simple, it has a behaviour very similar to the one of a real ferromagnet. Furthermore, in its two-dimensional implementation, it can be exactly solved within the realm of Statistical Mechanics. In particular, it provides one of the simplest examples of complex systems where phase transitions can be worked out with mathematical rigor. In the Ising model the system considered is an array of N fixed points called lattice sites that form a d-dimensional periodic lattice ($d = 1, 2, 3$). The geometrical structure of the lattice may for example be cubic or hexagonal. Associated with each lattice site is a spin variable s_i (i=1,...N) which is a number that is either +1 or -1. There are no other variables. If $s_i = 1$, the i-th site is said to have spin up, and if $s_i = -1$, it is said to have spin down. A given N-tuple of numbers s_i specifies a configuration of the whole system. The energy of the system in the configuration specified by s_i is defined to be

$$E_I\{s_i\} = -\sum_{<ij>} J_{ij} s_i s_j - H \sum_{i=1}^{N} s_i \tag{2.1}$$

where the subscript I stands for Ising and the symbol $< ij >$ denotes a nearest-neighbour pair of spins. There is no distinction between $< ij >$ and $< ji >$. Thus the sum over $< ij >$ contains $\frac{\gamma N}{2}$ terms, where γ is the number of nearest neighbours of any given site. The parameters J_{ij} are the exchange interactions between all the spin pairs.

We focused on a 2D square-lattice Ising model (d=2), with constant exchange interaction J[1]. It is one of the simplest model in Statistical Mechanics exhibiting a second order phase transition. An analytic solution was found by Lars Onsager (1944). This means that we have analytic results for comparison with our simulations' results. Let us start with the first definition, the magnetization. Its expression is

$$M = \sum_{i=1}^{N} s_i. \tag{2.2}$$

Actually, we used the magnetization per spin,

$$m = \frac{M}{N}, \tag{2.3}$$

and we computed the approximation of its mean value[2],

$$m = \frac{\langle M \rangle}{N}, \tag{2.4}$$

where $\langle \cdot \rangle$ is the mean value of a physical quantity, within the canonical ensemble (look at eq.(2.9) for the definition). The critical temperature and the mean magnetization per spin for the 2D square-lattice Ising model are given by

$$T_c = \frac{2J}{k_B \ln(1+\sqrt{2})} \simeq 2.269185314 \cdot \frac{J}{k_B},$$
$$m(T) = \begin{cases} 0 & ,(T > T_c) \\ \{1 - [\sinh(2\beta J)]^{-4}\}^{\frac{1}{8}} & ,(T < T_c). \end{cases}$$

In fig.2.1, the plot of Onsager's magnetization solution.

[1] In chapter 4 we will use a model with non constant J.

[2] Here we used the letter m both for magnetization per spin and its mean value. All over this work, m will be meant for the mean magnetization per spin.

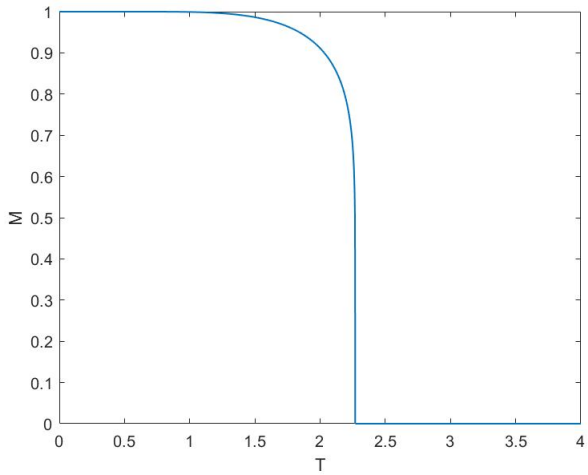

Figure 2.1: Mean magnetization per spin as a function of temperature (Onsager). This is the continuous phase transition, induced by temperature, introduced in the previous chapter.

2.1.1 n-vector model

Before continuing with the Ising model case, we will here briefly review the mathematical models used to describe interacting spins systems. And, at the basis of each one of them, there is the Heisenberg Hamiltonian 1.46 that we have previously derived by taking into account quantum mechanics and spin.

The Ising model is just one of the existing models that we could use for the study of magnetic phase transitions' properties (the temperature and field induced transitions we have introduced in the previous chapter). In particular, the so called Potts model, the XY model, the Heisenberg model have been deeply studied. In fact, these mentioned models are special cases of a general model: the n-vector model or O(n) model, describing a system of interacting spins on a crystalline lattice. In this model, the spins s_i have no longer just one component like in the Ising model (where s_i can be ± 1 only), instead they have n components embedded into a d-dimensional lattice. The Hamiltonian has the usual form, but now the spins are no longer scalar so we have to introduce the inner product:

$$H = -J \sum_{<i,j>} \mathbf{s}_i \cdot \mathbf{s}_j \tag{2.5}$$

and $< i, j >$ still means the interaction between nearest neighbours is just considered. According to the number of components of the spins vectors, n, we can have a different model. The Ising model has $n = 1$. The Potts model is a more general case than the Ising model, with the spin variable taking one of q possible values, distributed uniformly about the circle, at angles $\theta_n = \frac{2\pi n}{q}$ where $n = 0, 1, ..., q-1$ and the Hamiltonian given by

$$H = J \sum_{<i,j>} cos(\theta_{s_i} - \theta_{s_j}). \tag{2.6}$$

In the limit as $q \to \infty$, the Potts model becomes the XY model. This one is a case of the n-vector model with $n = 2$. The Heisenberg model has $n = 3$, i.e. the spins are elements of $\mathbb{R}^3$. Each one of these models can be applied to whatever d-dimensional lattice.

In our case, we have studied the 2D Ising model (n=1, d=2).

2.2 Statistical Mechanics

As we said in the previous chapter, the physical properties of the systems of our interest are determined by the interaction between a very large number of individual elements.
Statistical Mechanics is mainly focused on the calculation of properties of condensed matter systems. Deriving exactly the dynamics of all elements would be a very hard task due to the very large number of components in the system. The number of equations of motion makes it impossible to solve the mathematics exactly. A common example arises from a volume of gas in a container: the number of molecules is of the order of the Avogadro constant ($\approx 10^{23}$), all moving around and colliding with one another and with the walls of the container. Too many Hamilton's equations to solve for these systems. Yet, by looking at the macroscopic behaviour of a gas we find well-behaved and predictable properties like temperature or pressure. So there's some mechanism that averages out the solutions of all the equations to give us a predictable behaviour of the entire system. Statistical Mechanics aims directly to the calculation of these average properties of large systems by studying them from a probabilistic point of view.

Here are some conclusions that we can reach without specifying the exact form of the dynamics.
Suppose our system is in a state μ. Let us define $R(\mu \to \nu)dt$ to be the probability that it is in state ν a time dt later. $R(\mu \to \nu)$ is the **transition rate** for the transition from μ to ν. We assume the transition rate to be time independent. Now, the probabilistic treatment of the problem comes in. We define a set of weights $w_\mu(t)$ which represent the probability that the system will be in state μ at time t. These weights represent our entire knowledge about the state of the system. At this point, we write a **master equation** for the evolution of $w_\mu(t)$:

$$\frac{dw_\mu}{dt} = \sum_\nu [w_\nu(t)R(\nu \to \mu) - w_\mu(t)R(\mu \to \nu)] \tag{2.7}$$

by considering transitions both to and from the state μ.
The probabilities w_μ must also obey the sum rule

$$\sum_\mu w_\mu(t) = 1 \tag{2.8}$$

for all t, since the system must always be in some state.
Since we're interested into the macroscopic properties of the system, let us define the expectation value of a quantity Q at time t for our system as

$$\langle Q \rangle = \sum_\mu Q_\mu w_\mu(t) \tag{2.9}$$

If we want to find the **equilibrium state** we have to put (2.7) equal to zero. The values of the transition rates $R(\mu \to \nu)$ depend on the type of interaction between the system and the thermal reservoir. Here we know a priori the values at equilibrium of the weights w_μ and we denote them by:

$$p_\mu = \lim_{t\to\infty} w_\mu(t). \tag{2.10}$$

Gibbs showed that for a system in thermal equilibrium with a reservoir at temperature T, the equilibrium occupation probabilities are

$$p_\mu = \frac{1}{Z} e^{-\frac{E_\mu}{k_B T}}. \tag{2.11}$$

where E_μ is the energy of state μ and usually it is defined the quantity $\beta = (kT)^{-1}$. The probability distribution in 2.11 is known as the **Boltzmann**

distribution. At this point we can define the expectation value of a quantity Q for a system in equilibrium:

$$\langle Q \rangle = \sum_{\mu} Q_{\mu} p_{\mu} = \frac{\sum_{\mu} Q_{\mu} e^{-\beta E_{\mu}}}{\sum_{\mu} e^{-\beta E_{\mu}}}. \tag{2.12}$$

Obviously when talking about statistical quantities we have to consider also the standard deviation, which gives us information about the fluctuations of the quantity we are looking at. An interesting result is that the variance of the energy is proportional to the specific heat, a macroscopic property. This means that, since the heat capacity is an extensive quantity, the energy fluctuations scale like $\sqrt{V}$ with the volume V of the system. And the energy itself scales like V, so that the relative size of the fluctuations compared to the internal energy decreases as $\frac{1}{\sqrt{V}}$ as the system becomes large. So, if we consider a large system, we can neglect fluctuations. For this reason, the limit of a large system is called the **thermodynamic limit**. The problem is that for Monte Carlo simulations it is not feasible to simulate a system large enough that its behaviour is a good approximation to a large system.
So, also if Statistical Mechanics has produced very elegant formula, the process of calculating the properties of a particular model is very complex. For example if we have to calculate the partition function Z we have to perform a sum over a potentially very large number of states. Indeed we are interested in the thermodynamic limit where the sum is over an almost infinite number of states. Only for a few statistical models it has been found an analytic expression for the partition function, like the 2D Ising model (Onsager 1944). This is why some approximate techniques have been developed. We are interested in computational techniques, in particular in Monte Carlo simulations.

2.3 Monte Carlo method

At this point we can introduce the general ideas behind equilibrium thermal Monte Carlo simulations. We will focus on "importance sampling", "detailed balance" and "acceptance ratios". As we previously said, we want to find a method that gets as close as possible to the observable behaviour of a thermal system. Since we have said that formulas from Statistical Mechanics are tractable only for very small systems (see the example about the partition

function Z, just a few lines above), in large systems the best we can do is to choose a subset of states from the phase space by following a specific probability distribution p_μ.
So, if we want to estimate the expectation value of a quantity Q we won't use the correct formula (2.12). Instead, by supposing our subset of states is $\{\mu_1, ..., \mu_M\}$, our best estimate of the quantity Q will be:

$$Q_M = \frac{\sum_{i=1}^{M} Q_{\mu_i} p_{\mu_i}^{-1} e^{-\beta E_{\mu_i}}}{\sum_{i=1}^{M} p_{\mu_i}^{-1} e^{-\beta E_{\mu_i}}}. \tag{2.13}$$

Q_M is the **estimator** of Q.

The more M states we sample, the more the estimator becomes an accurate estimate of $\langle Q \rangle$. Arrived to this point a question rises: how should we choose the probability distribution p_μ? The goodness of the estimator depends on this too. In order to answer to this question we have to keep in mind that the sums appearing in 2.12 may be dominated by small number of states. Like in the case of a physical system in thermal equilibrium with a reservoir: it does not sample all its states with equal probability, instead it samples them by using the Boltzmann distribution that we have seen previously. So what Monte Carlo methods do is finding these M most important states, and neglecting the others, by picking states so that the probability that a particular state μ gets chosen is 2.11. This procedure is called **importance sampling**. Then our estimator becomes just

$$Q_M = \frac{1}{M} \sum_{i=1}^{M} Q_{\mu_i}. \tag{2.14}$$

In order to pick our sample of states so that each one appears with its correct Boltzmann probability it is convenient to use a **Markov process**. In our case, a Markov process is a mechanism which, given a system in one state μ, generates a new state of that system ν. The probability of generating the state ν given μ is called the **transition probability** $P(\mu \to \nu)$. For a true Markov process all the transition probabilities have to be such that the probability of the Markov process generating the state ν starting from the state μ is always the same, irrespective of anything else has happened before μ. The transition probabilities must also satisfy the following constraint:

$$\sum_{\nu} P(\mu \to \nu) = 1, \tag{2.15}$$

since some state ν has to be generated by the Markov process when the system is in the state μ. Note that $P(\mu \to \mu)$ can be different from zero. During our Monte Carlo simulation, the Markov process is used repeatedly to generate a **Markov chain** of states. We are interested into a Markov process that creates a succession of states which appear with probabilities given by the Boltzmann distribution, if it is run for long enough and starting from any state of the system (we call the process of reaching the Boltzmann distribution "coming to equilibrium", since it is exactly the process that a real system goes through as it reaches equilibrium at a certain temperature). This is possible if other two conditions are satisfied by our Markov process: ergodicity and detailed balance.

2.3.1 Ergodicity

Our Markov process is ergodic if it is in principle able to reach any state of the system if we run it for long enough. This requirement is necessary if we want to generate states according their correct Boltzmann probabilities. Indeed, every state ν has a non-zero Boltzmann probability p_ν, and if that state were inaccessible from another state μ no matter how long we continue our process for, then our goal is impossible if we start in state μ: we will have zero probability of finding ν in our Markov chain of states, and not p_ν probability as we require it to be.

2.3.2 Detailed balance

The detailed balance condition ensures that we reach the Boltzmann distribution after we run the Markov process for long enough, i.e. after we have reached the equilibrium. First, our Markov process reaches the equilibrium when

$$\sum_\nu p_\mu P(\mu \to \nu) = \sum_\nu p_\nu P(\nu \to \mu), \tag{2.16}$$

that actually is just a discrete-time version of the one we would get if we were to set to zero the derivative in the master equation 2.7, as we have already noticed in section 2.2. By exploiting eq.(2.15), we can rewrite this in the following way:

$$p_\mu = \sum_\nu p_\nu P(\nu \to \mu). \tag{2.17}$$

since the first sum is on ν and so p_μ can be taken out of it. Simply finding the set of transition probabilities satisfying this equation is not sufficient to guarantee that the probability distribution will tend to p_μ from any state of the system if we run the process for long enough. This can be seen in the following way. Let us define the Markov matrix $\mathbf{P}$ for the Markov process as the matrix whose elements are the transition probabilities $P(\mu \to \nu)$. By supposing we are dealing with a physical system whose Hamiltonian has a discrete set of n eigenvalues and eigenvectors, and writing explicitly the eigenvalue corresponding to a state, we have the following form for $\mathbf{P}$

$$\begin{bmatrix} P(E_1 \to E_1) & P(E_2 \to E_1) & \cdots & P(E_n \to E_1) \\ P(E_1 \to E_2) & P(E_2 \to E_2) & \cdots & P(E_n \to E_2) \\ \vdots & \vdots & \ddots & \vdots \\ P(E_1 \to E_n) & P(E_2 \to E_n) & \cdots & P(E_n \to E_n) \end{bmatrix}$$

where $\mu, \nu = 1, \ldots, n$. By recovering the notation we used for the master equation, if we measure the time in steps along our Markov chain, then the probability $w_\nu(t+1)$ of being in state ν at time $t+1$ is given by

$$w_\nu(t+1) = \sum_\mu P(\mu \to \nu) w_\mu(t). \tag{2.18}$$

In matrix notation

$$\mathbf{w}(t+1) = \mathbf{P} \cdot \mathbf{w}(t), \tag{2.19}$$

where $\mathbf{w}$(t) is the vector whose elements are the weights $w_\mu(t)$. The Markov process can reach a simple equilibrium state $\mathbf{w}(\infty)$ as $t \to \infty$ for which the following identity is true

$$\mathbf{w}(\infty) = \mathbf{P} \cdot \mathbf{w}(\infty) \tag{2.20}$$

or a dynamic equilibrium in which the probability distribution $\mathbf{w}$ periodically oscillates between a number of different values. Such a rotation is called *periodic chain*. In this case $\mathbf{w}(\infty)$ would satisfy

$$\mathbf{w}(\infty) = \mathbf{P}^n \cdot \mathbf{w}(\infty) \tag{2.21}$$

where n is the period of the chain. We want to avoid this last case. The detailed balance condition allows us to get around this problem. Mathematically, it can be written in the following way

$$p_\mu P(\mu \to \nu) = p_\nu P(\nu \to \mu). \tag{2.22}$$

Clearly, any set of transition probabilities which satisfy this condition also satisfy eq.(2.16). It tells us that on average the overall transition rate from μ to ν is equal to the one from ν to μ. In a limit cycle, some of the states' probabilities occupation vary in a cyclic way. For these states the detailed balance condition is violated on any particular step of the Markov chain. For instance, if the occupation probability of a state increases, there must be more transitions into that state than out of it on average. So, detailed balance condition avoids this kind of dynamics. Now that we have removed limit cycles, we can show that the system will always converge to the probability distribution p_μ as $t \to \infty$. From stochastic matrices theory, we know that as $t \to \infty$, $\mathbf{w}(\mathrm{t})$ will tend exponentially towards the eigenvector corresponding to the largest eigenvalue of $\mathbf{P}$. Being the Markov matrix a stochastic matrix, its higher eigenvalue is one. It is easy to prove that all Markov matrices have at least one eigenvector with corresponding eigenvalue one. From eq.(2.15), we know that all the columns of a Markov matrix give sum equal to one. This means that the vector $(1, 1, 1, 1, 1, \dots)$ is a left eigenvector of $\mathbf{P}$ with eigenvalue one. A left eigenvector is a row vector defined by the following equation:

$$u\mathbf{P} = ku \tag{2.23}$$

where k is a scalar and $\mathbf{P}$ is our Markov matrix. By taking the transpose of this last equation

$$\mathbf{P}^\top u^\top = ku^\top \tag{2.24}$$

we observe that a left eigenvector is equal to the transpose of the right eigenvector of $\mathbf{P}^\top$, with the same eigenvalue. $\mathbf{P}$ and $\mathbf{P}^\top$ have the same eigenvalues, since a matrix and its transpose have the same characteristic polynomial. Thus, the eigenvalues of the left eigenvectors of a matrix are the same of the right eigenvectors of the same matrix. Summing up: our Markov matrix has at least one eigenvector with corresponding eigenvalue equal to one. In order to see that one is the highest possible eigenvalue for a Markov matrix, here it is an elementary proof. Let us suppose that $\mathbf{P}x = \lambda x$, for some $\lambda > 1$ eigenvalue and x corresponding eigenvector of $\mathbf{P}$. Since we have seen that Markov matrix entries are smaller than one (and positive), we can say that each element of the vector $\mathbf{P}x$ can be no greater than the maximum component of x, x_{max}. On the other hand, at least one element of λx is greater than x_{max}. This proves that $\lambda > 1$ is not possible. Now, if we express the eq.(2.17) in matrix notation we obtain

$$\mathbf{p} = \mathbf{P}\mathbf{p}, \tag{2.25}$$

where $\mathbf{p}$ is the vector whose elements are the probabilities p_μ, we can see that $\mathbf{p}$ is that eigenvector of the Markov matrix with eigenvalue equal to one. By putting this together, the equilibrium probability distribution $\mathbf{w}(\infty)$ is exactly $\mathbf{p}$. This means that $\mathbf{w}(\mathrm{t})$ must tend exponentially to $\mathbf{p}$ as $t \to \infty$. At this point, we have proved that the probability distribution of the states generated by our Markov process will converge to whatever distribution p_μ we want, by choosing a set of transition probabilities (i.e. a Markov matrix) which satisfy the detailed balance condition. In particular we want to obtain the Boltzmann distribution weights. This means that the detailed balance condition becomes

$$\frac{P(\mu \to \nu)}{P(\nu \to \mu)} = \frac{p_\nu}{p_\mu} = e^{-\beta(E_\nu - E_\mu)}. \tag{2.26}$$

The constraints on the transition probabilities $P(\mu \to \nu)$ are this last equation and the equation 2.15.

2.3.3 Acceptance ratios

At this point, to simplify the choice of our Markov process we define the transition probabilities in the following way

$$P(\mu \to \nu) = g(\mu \to \nu) A(\mu \to \nu). \tag{2.27}$$

$g(\mu \to \nu)$ is the selection probability, the probability that given an initial state μ, a new state ν will be generate by the algorithm. $A(\mu \to \nu)$ is the acceptance ratio that tells us if we accept or not to move our system into the new generated state ν.

So, what we have to do for building our Monte Carlo algorithm is thinking up an algorithm which generates random new states ν from old ones μ with probability $g(\mu \to \nu)$ and then accepts or rejects those states with acceptance ratios $A(\mu \to \nu)$ that we choose to satisfy

$$\frac{P(\mu \to \nu)}{P(\nu \to \mu)} = \frac{g(\mu \to \nu) A(\mu \to \nu)}{g(\nu \to \mu) A(\nu \to \mu)} = e^{-\beta(E_\nu - E_\mu)}. \tag{2.28}$$

If not accepted, the system remains in state μ and the process is repeated again and again. An example of Monte Carlo algorithm for the Ising model is the single-spin-flip dynamics Metropolis algorithm. But we are interested in the Wolff algorithm [22], the most popular among the so called cluster

algorithms. Before talking about the advantages of this last algorithm respect to the single-flip one, let us look more in details this algorithm.

Chapter 3

Cluster algorithm

In this chapter we describe a particular Monte Carlo method, the Wolff algorithm, which is characterized by the fact that the spins do not evolve one by one towards equilibrium. They are grouped instead in sets of similarly oriented spins (clusters), which are then eventually flipped all together in one go.

We explain how we estimated the mean values of physical quantities, showing the results for the magnetic susceptibility and magnetization.

We will see how these results helped us finding the minimum optimal dimension for the system simulated in our codes.

The Ghost Spin extension, used in order to study the field-induced transition, is introduced too. Finally, the absence of hysteresis loop is explained.

3.1 The Wolff method

With this type of Monte Carlo method we expect to better simulate the avalanche's behaviour in comparison to a single-spin-flip dynamics algorithm, like the single-flip- dynamics Metropolis algorithm used in [15]. In fact, by flipping the spins of the lattice one by one, you can have the following situation. At the n-th MC iteration, the k-th spin is flipped. At the next MC moves, instead of building an avalanche around the k-th spin, the algorithm could end up picking and flipping the $k+1$-th, and the following spins, far from the position of k-th spin. Also, it could be that the k-th spin is picked a

second time, before the avalanche has the possibility to happen. With Wolff we instead give a chance to an avalanche to happen, thanks to the collective evolution of the spins at each MC step.

The following is the strategy proposed by Wolff.

1. Pick at random a spin (seed) from the lattice.
2. Look at its neighbours to see if any of them have the same orientation of the seed.
3. Look at neighbours of those neighbours, and so on, iteratively, until a cluster of spins has been built up.

But, we do not want to flip all the spins with the same orientation of our first seed spin. Indeed, the number of spin we flip should depend on the temperature. For example, we know that in the Ising model at high temperatures the spins tend to be uncorrelated with their neighbours and this means that they flip over in very small clusters (or also individually). By approaching the critical temperature, we know that the sizes of the clusters become much larger, and then, below the critical temperature, an ordered phase appears where spins tend to form big clusters that span the entire lattice. This is why this algorithm has some probability of adding a spin to the cluster which goes up as the temperature falls.
The last step of the strategy.

4. Once the cluster has been built, since there are no more similarly oriented spins to add to the cluster, the algorithm flips the cluster with some acceptance ratio.

3.2 Acceptance ratio for the Wolff method

The formula for the probability of adding a spin to the cluster according to the temperature of the system is

$$P_{add} = 1 - e^{-2\beta J} \tag{3.1}$$

and the acceptance ratios for both forward and backward moves between two states are always equal to the unity (i.e. every proposal is accepted),

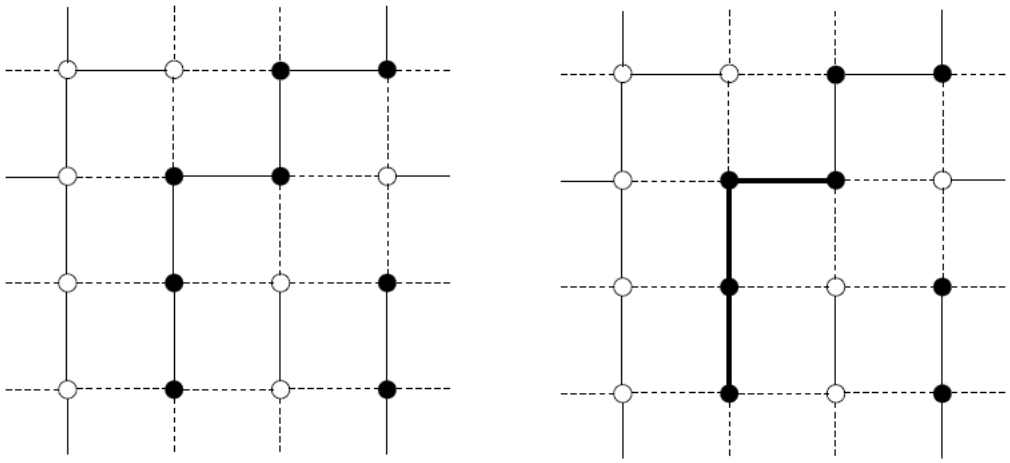

Figure 3.1: On the left, a periodical square lattice, with black and white circles representing up- and down-spins respectively. The solid lines represent the clusters that may be built in it. On the right, the same periodical lattice, showing a possible cluster (thicker solid line) within it.

independently of any properties of the two states, or the temperature, or anything else at all. This is the best possible value for the acceptance ratios in order to speed up the convergence of the algorithm.

Let us see how these choices for P_{add} and acceptance ratios still allow for detailed balance condition to be satisfied. Consider two states of the system, μ and ν, like those illustrated in the figure 3.2 below. The difference between the two configurations is the flipping of a cluster of similarly oriented spins, whose edge is indicated by the line in the figure. Now, we have to focus on the way the spins are oriented around this edge. Both in μ and ν state, outside of the cluster there are some spins oriented like those within the cluster. When the cluster is flipped, the bonds between these spins and the ones in the cluster have to be broken. And those that are not broken moving from μ to ν, of course have to be broken with the reverse move.

At this point, let us consider a move that takes our system from μ to ν. Actually, there are many of these moves. For the moment, however, let us just consider one particular move, starting with a particular seed spin and then adding the other to it in a particular order. Consider also the reverse

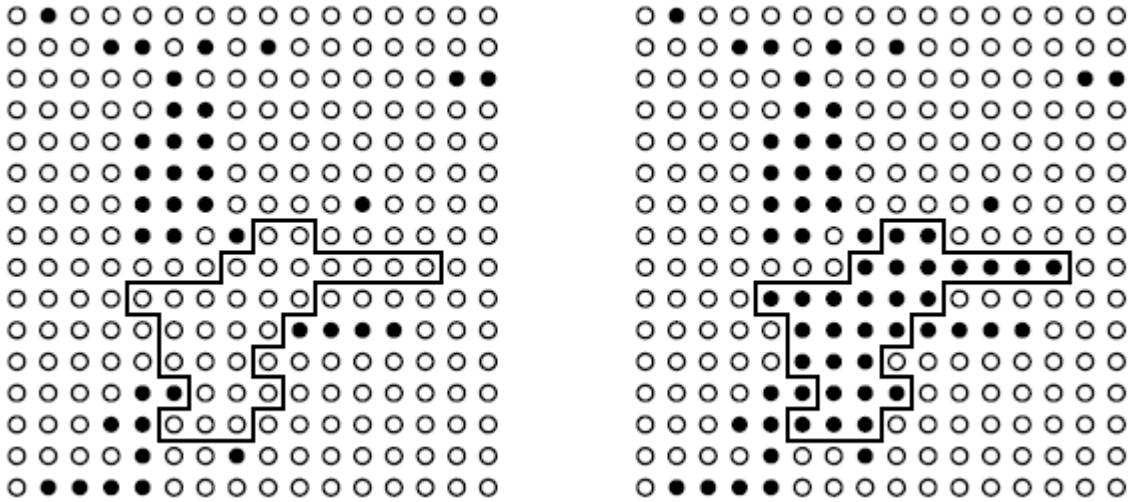

Figure 3.2: Two different configurations, μ on the left and ν on the right, of our 2D lattice of spins. The black and white circles represent the up- and down-spins in the model. (source [12])

move, from ν to μ, starting with the same seed spin and adding all the others in the same way as in the forward move. The only difference between the two moves is the probability of breaking bonds at the edge of the cluster. Because, as we have already noticed, the bonds which have to be broken are different in the two cases.

Suppose we have m broken bonds for the forward move. This means that moving from μ to ν there are m spins close to the edge of the cluster that are not added to the cluster itself. The probability of not adding these spins is $(1 - P_{add})^m$, and it is proportional to the selection probability $g(\mu \to \nu)$. In the reverse move, suppose we have n broken bonds. Then, the probability of doing it will be $(1 - P_{add})^n$. The condition of detailed balance becomes

$$\frac{P(\mu \to \nu)}{P(\nu \to \mu)} = \frac{g(\mu \to \nu)A(\mu \to \nu)}{g(\nu \to \mu)A(\nu \to \mu)} = (1 - P_{add})^{m-n} \frac{A(\mu \to \nu)}{A(\nu \to \mu)} = e^{-\beta(E_\nu - E_\mu)}, \quad (3.2)$$

where the change in energy, $E_\nu - E_\mu$, also depends on the bonds which are broken. In particular, we have for our Ising model

$$E_\nu - E_\mu = 2J(m - n) \quad (3.3)$$

that leads us to rewrite equation 3.2

$$\frac{A(\mu \to \nu)}{A(\nu \to \mu)} = [e^{2\beta J}(1 - P_{add})]^{n-m}. \tag{3.4}$$

Now, we see how the value of P_{add} in 3.1 actually implies acceptance ratios for forward and backward moves equal to one, if we want to satisfy 3.4. So, every move proposed is accepted by the algorithm. This algorithm satisfies also the ergodicity requirement. Indeed, it is enough to note that there is the possibility at any move to build a cluster of only one spin, which is then flipped. Thus, the appropriate succession of such moves will take the system from one state to any other in a finite time.
So, the Wolff algorithm, if run for long time, is able to generate a series of states of the system which will appear with their correct Boltzmann probabilities.

Here it is the precise procedure for the Wolff cluster algorithm for the Ising model:

1. Choose a seed spin at random from the lattice.

2. Look in turn at each neighbours of that spin. If they are pointing in the same direction as the seed spin, add them to the cluster with probability $P_{add} = 1 - e^{-2\beta J}$.

3. For each spin that was added in the last step, examine each of its neighbours to find the ones which are pointing in the same direction and add each of them to the cluster with the same probability P_{add}. During the growth of the cluster, we may pick some neighbours that are already within the cluster, and in this case we do not have to consider adding them again. Also, spins that have already rejected to join the cluster get another chance to get in when we ask them another time. This step is repeated until there are no more spins left in the cluster whose neighbours have not been considered for inclusion in the cluster.

4. Flip the cluster.

3.3 Implementation on a computer code

The Ising model we have described in the previous chapter can be in any dimension (as we have already seen) and with any kind of boundary conditions.

Since we want to develop a model able to mimic the experimental results obtained by Zani and Puppin [23] studying Fe films, we will use a 2D square lattice with size L, composed by $N = L \times L$ spins. So, $\gamma = 4$, i.e. any spin will have four nearest neighbours. About the boundary effects, we set periodic boundary conditions to our square lattice, that is, the spins on one edge of the lattice are neighbours of the corresponding spins on the opposite edge. In this way, all the spins have the same number of neighbours and local geometry.
From a computational point of view, we stored the spin lattice in a vector of dimension N, following the numbering of fig.3.3. In this way, we had to use

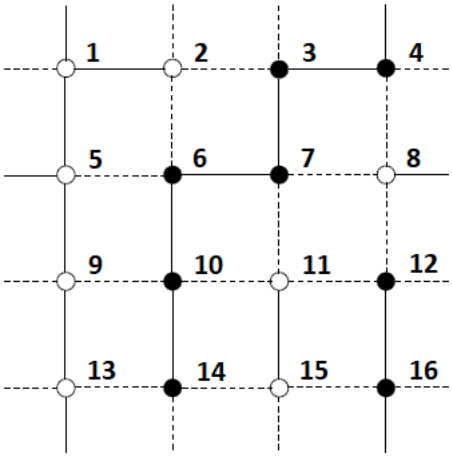

Figure 3.3: Here an example of enumeration of the spins within a 2D square lattice with L=4)

only one index in order to move within the lattice. For the implementation of the Wolff algorithm, the developed code is the following one. In particular, we are going to see the function, that I called **Cluster**, that moves the system from one state μ to a new state ν, by creating and flipping one cluster within the lattice. Obviously, this function is then called repeatedly within the code, in order to implement the Markov process that we have previously described.

Algorithm: generation of a cluster

Define two vectors *guests* and *guests1*, of dimension N;
guests will contain the position, within the lattice, of those spins belonging to the growing cluster and will be used for updating the initial state (if it is the case);
guests1's n-th entry will be zero, if the n-th spin of the lattice is not within the cluster, or one, if the n-th spin of the lattice belongs to the cluster;
Define the initial state μ;
Randomly pick a seed spin, $s \in [0, N-1]$;

guests[0]=s;
guests1[s]=1;

Let us call the **Cluster** function, that updates the vector *guests*, storing in it the position of all the spins belonging to the built cluster, and the vector *guests1*, exploited within the **Cluster** function itself in order to check if a spin is already within the cluster. Also, it returns the area of the built cluster;

```
int Cluster (...) {
 ⋮
 for l=0; l < N; l++
    i=guests[l];                  //the i-th spin is within the cluster
    for j=0; j < 4; j++           // j runs over the four n.n. of the i-th

        if j-th neighbour has different orientation than i-th spin then
          check = 1;
        end
        if j-th neighbour is already within the cluster then
          check = 1;
        end
        if check ≠ 1 then
          h = −2J/T;
          p = random real ∈ [0, 1];
          if p < (1 - exp(h)) then
            k = k + 1;
            guests[k] = j-th neighbour of the i-th spin;
            guests1[j-th neighbour] = 1;
          end
        end
        check = 0;
    end
    if l == k then       //the cluster is built, leave the Cluster function
      return k;
    end
 end
}
```

3.3.1 Equilibration and Measurement

In the previous chapters, we already noticed that whenever detailed balance and ergodicity conditions are fulfilled, the Markov process will end up by choosing the states of the Markov chain according to the desired probability distribution, if "run for long enough". What does "run for long enough" mean? Being a numerical method, a Monte Carlo algorithm needs a certain amount of iterations, so of time, in order to reach convergence, i.e. equilibrium condition where we will be able to pick states according to the Boltzmann probability weights, $p_\mu = \frac{1}{Z} e^{-\beta E_\mu}$. This leads us to the definition of an **equilibration time**, τ_{eq}. When we reach the equilibrium, the system

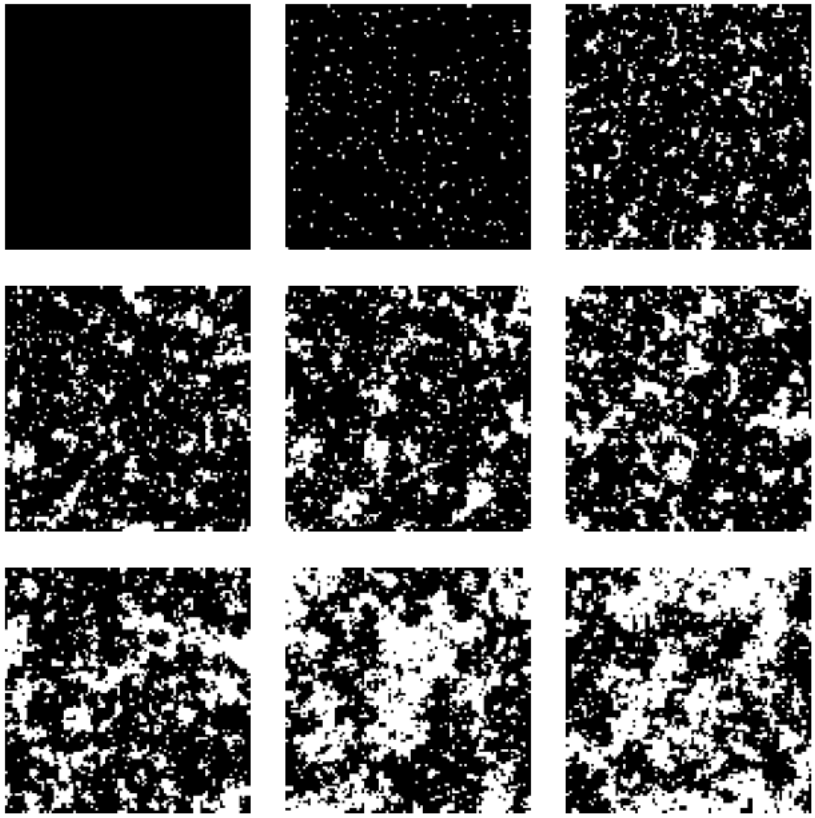

Figure 3.4: Example of convergence process: snapshots of an Ising model on a square lattice coming to equilibrium at some finite non-zero temperature, starting from an ordered configuration. (source [12])

spends the greatest part of the time in a small subset of states, in which the physical observables take a narrow range of values. So, in order to estimate the value of this equilibration time we can look at some physical quantity (e.g. magnetization, energy, ...) and looking at the time when its value will stabilize and oscillate around a steady mean value with a certain standard deviation. Once we have reached the equilibrium, we have to evaluate the estimator (see eq.(2.14)) of whatever physical quantity we are interested in. In order to do this, we need to know how many samples we have to take to get a good estimate of the expectation value of these physical quantities. And, how to pick such samples. Thus, we have to introduce a new time variable, the correlation time (τ_{corr}) of the algorithm we are using, that tells us the time the system takes to move from a state to another one significantly different. At this point, our interest is to determine equilibration and correlation time for different temperatures. This is necessary for the following simulations. For this analysis we used L=60. Its aim is to show the behaviour of the Ising model at different temperatures. Later we will see that it is important to calibrate also the value of the L parameter, in order to get more precise results (i.e. closer to the thermodynamic limit).

As a yardstick to measure the equilibration and correlation times, we chose to look at the plotted graphs of the magnetization per spin m of the lattice

$$m = \frac{1}{N}\sum_i s_i \tag{3.5}$$

as a function of time (see example in fig.3.5). About the correlation time, we obtained it from the time-displaced autocorrelation $\chi(t)$ of the magnetization per spin. Here it is the discrete time version of this function

$$\chi(t) = \frac{1}{t_{MAX}-t}\cdot\sum_{t'=1}^{t_{MAX}-t}(m(t_0+t')-\mu)(m(t_0+t+t')-\mu), \tag{3.6}$$

where $t_0 > \tau_{eq}$, t_{MAX} indicates how much a run of the algorithm lasts starting from t_0, and μ is the mean value of m at equilibrium calculated starting from t_0. Since the autocorrelation is expected to behave exponentially

$$\chi(t) \sim e^{-\frac{t}{\tau_{corr}}}, \tag{3.7}$$

by doing semi-logarithmic plot of $\chi(t)$ we obtain a straight line, whose slope absolute value is τ_{corr}. This is still not enough if we want a τ_{corr} that can be

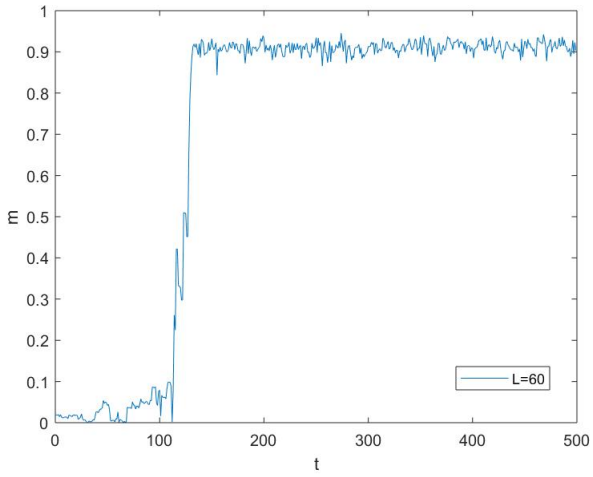

Figure 3.5: Magnetization plot. The Wolff's simulation started at T=∞ (i.e. random configuration) and cooled to equilibrium at T=2.0. Time (t) is measured in Wolff steps.

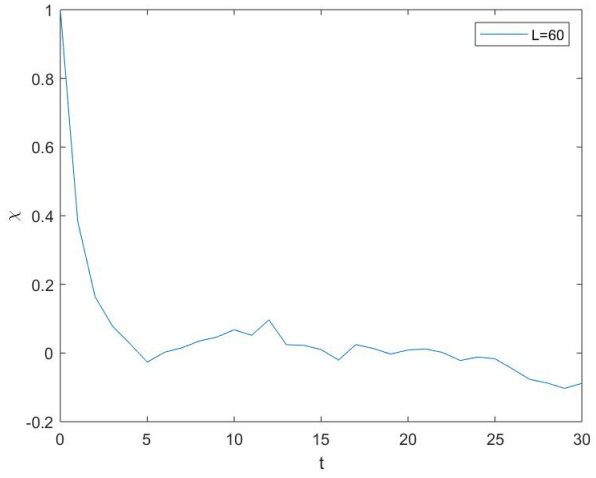

Figure 3.6: Magnetization correlation function, T=2.0.

compared with the one of other algorithms like Metropolis (and, later I will explain in which cases Wolff algorithm wins this comparison). Metropolis time is usually measured in *steps per lattice site*, where one of these steps is also called *lattice sweep*. This because, on average, the algorithm should have flipped each one of the spin of the lattice within one step per lattice site. In this way, the attempt frequency (i.e. the average frequency with which a spin is chosen for flipping) is independent of the total number of spins within the lattice. This is what happens in nature: an atom in a small sample changes as often as the one in a bigger sample. In the Wolff algorithm, the time needed to complete one step is proportional to the number of spins n in the built cluster. Since such a cluster covers a fraction $\frac{n}{N}$ of the whole lattice, the correct way to define the correlation time is the following one

$$\tau_{corr} \propto \tau_{steps} \frac{\langle n \rangle}{N}, \tag{3.8}$$

where τ_{steps} is the correlation time measured in Wolff steps, and $\langle n \rangle$ is the average cluster size in equilibrium.

The following are the results for $L = 60$. Both these two plots have sources

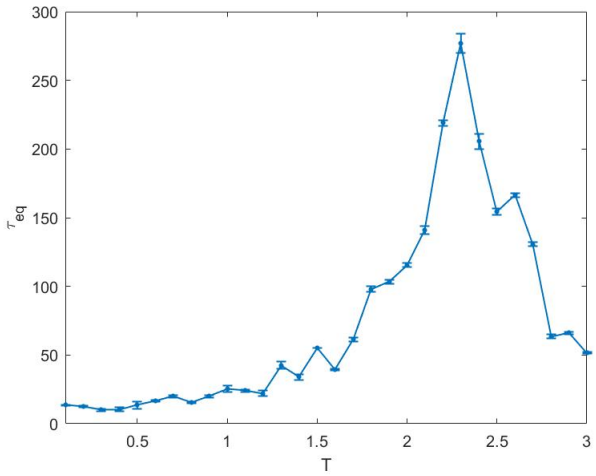

Figure 3.7: Equilibration time τ_{eq}. The errorbars were built by doing three different experiments for each temperature.

of error. For the τ_{eq}, we used a graphical method to compute the equilibration time. This means that there can be some imprecisions due to human

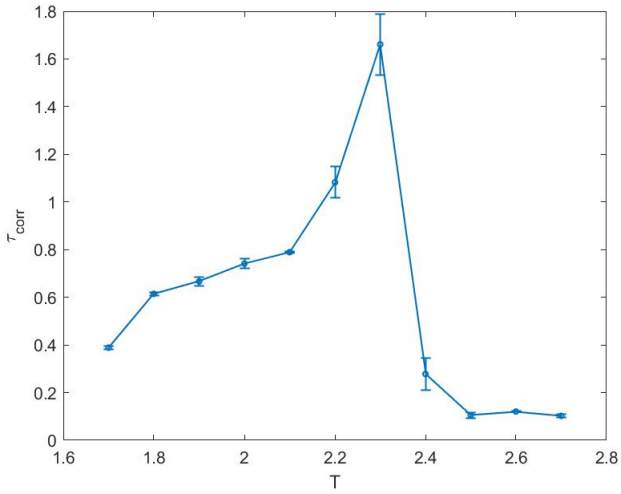

Figure 3.8: Correlation time τ_{corr}. The errorbars were built by doing three different experiments for each temperature.

errors at looking where the magnetization exactly starts to stabilize itself. For τ_{corr} there are causes of error too. The first one is that we should sum over infinite time in order to compute $\chi(t)$, but this is impossible in numerical analysis. Then, when t gets closer to t_{MAX}, the time interval on which we are integrating, using 3.6, becomes smaller (actually this source of error here is reduced by taking a time window far from t_{MAX}). This means that the statistical error on $\chi(t)$, due to the random fluctuations of $m(t)$, may become large. In the end, we have also to consider an error in the computation of the $log(\chi(t))$ slope (i.e. τ_{steps}).

But, the main information that we have to keep from this analysis is the peak around T_c (here, due to the small dimension of the lattice the critical temperature is 2.30). For the next simulations, we know that for the greatest part of the used temperature range, the same equilibration and correlation time can be used. The only exception is the small set of temperatures close to the critical one. For such temperatures, bigger times are required. Another important detail is the dimension of the errorbars, getting bigger when we come close to T_c, both from lower and higher temperatures.

The reason for these large errorbars is the **continuous phase transition** of

the Ising model, that we have talked about previously. By approaching T_c, the cluster[1] size ξ, also called *correlation length*, starts increasing. At T_c, the range of clusters' size is significantly wider than at any other temperature. This means we can find vary large clusters, that produce big fluctuations in the value of m (i.e. big value of the variance of magnetization) because of their orientation's flipping. We call them *critical fluctuations*. So, approaching T_c, the size of these fluctuations diverges. As a consequence, the statistical error of magnetization diverges too, since it is proportional to such fluctuations. Just notice that in finite size systems, we do not have an actual divergence but the values of fluctuations and statistical error become very large. Here it is explained the source of larger errorbars close to T_c for quantities linked to magnetization measurement. To make the situation worse, we have that also the correlation time diverges close to T_c (see fig.3.11). This means that we can extract a smaller number of independent measurements from a simulation of a certain length. This effect causes an increase of errors on measurements, even without the large critical fluctuations. So, if we want to reduce this second source of error we need longer simulations. This is called **critical slowing down** of the algorithm, and it is a property of the algorithm itself and not of the model we are studying. This is why the Wolff algorithm has been developed: it is faster than Metropolis close to T_c, i.e. it has a smaller correlation time.

There is another important thing to notice: the magnetization per spin is never negative (fig3.5). In fact, what we have plotted in fig.3.5 is its absolute value, $|m|$. This is due to the fact that the expectation value of the magnetization, below T_c, is zero. We can understand this looking at the expressions for the expectation value of a physical quantity, eq.(2.12), the one defining the energy of the system, eq.(2.1), and finally that of magnetization

$$M = \sum_{i=1}^{N} s_i. \tag{3.9}$$

Since the Hamiltonian of the Ising model is invariant when the sign of all the spins of a certain configuration is changed (for zero external field), the contribution of every spin configuration s_i is cancelled by that of $-s_i$. Thus,

[1]Here, cluster is a set of spin within a configuration with same orientation. So, there can be more than one cluster in a configuration. We are not referring to the cluster built during a Wolff's step

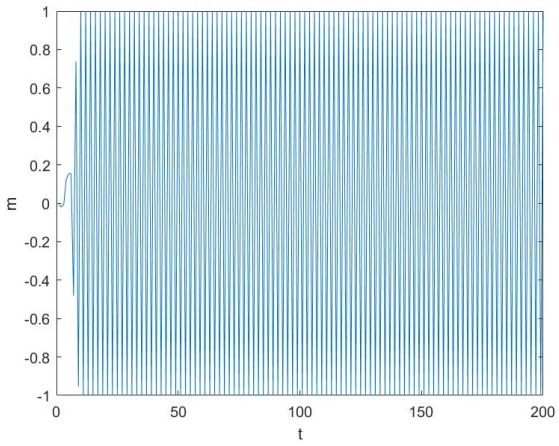

Figure 3.9: Plot of magnetization for a L=60 2D square Ising model, T=0.1. The system is equally happy to have most of its spins pointing either down or up. In the Wolff algorithm the lower the temperature, the bigger the built clusters are. In this low temperature case, the clusters have always the dimension of the lattice. So, after a termalization phase, we have an oscillation of the system magnetization between -1 and +1.

$\langle M \rangle = 0$. As we go to the thermodynamic limit we expect $|m|$ to agree with the exact solution of the 2D Ising model.

3.3.2 Temperature-driven phase transition

Now, we know the main features of our algorithm. This means we can start to measure physical quantities, like the mean magnetization.

First, let us study the variance of the magnetization. It will be useful for the choice of the optimal lattice size (L) for our simulations, and for computing the critical temperature (especially when we will introduce the disorder, instead for R=0 we already know the value of T_c and it will be only a prove that our algorithm is working well).

The formula for the sample variance we used is the following one[2]

$$\sigma^2 = \frac{1}{n}\sum_{i=1}^{n}(m - \bar{m})^2. \tag{3.10}$$

The first step will be to look for the best possible lattice size for the simulations of the next chapters. Since we have seen that in correspondence of T_c the fluctuations of the magnetization have the maximum value, we can exploit the variance (that is proportional to such fluctuations) in order to find the minimum lattice size getting as close as possible to the critical temperature value of the 2D square Ising model. From fig.3.10, we can observe how

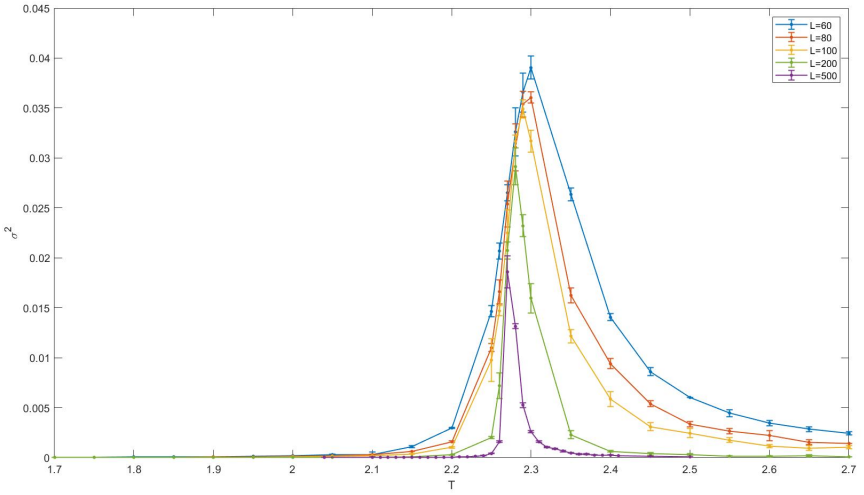

Figure 3.10: Temperature dependence of the magnetization's variance, for different values of L.

going toward the thermodynamic limit the peak of the variance gets lower. As we have already noticed, in this limit whatever measurement related to $|m|$ will converge to the actual one. Also, we notice that the variance does not actually diverge due to the finite size of the lattice used in our simulation. The $L = 500$ lattice is the first one getting closer to T_c, with a critical temperature of $T_c^{500} = 2.27$, as we can appreciate looking at fig3.11. In table 3.1, also the value of T_c for different lattice size is shown. This first analysis

[2]Actually, this formula gives an estimate of the population variance that is biased by a factor of $\frac{n-1}{n}$. Since the samples we used were made by thousands of elements, this factor

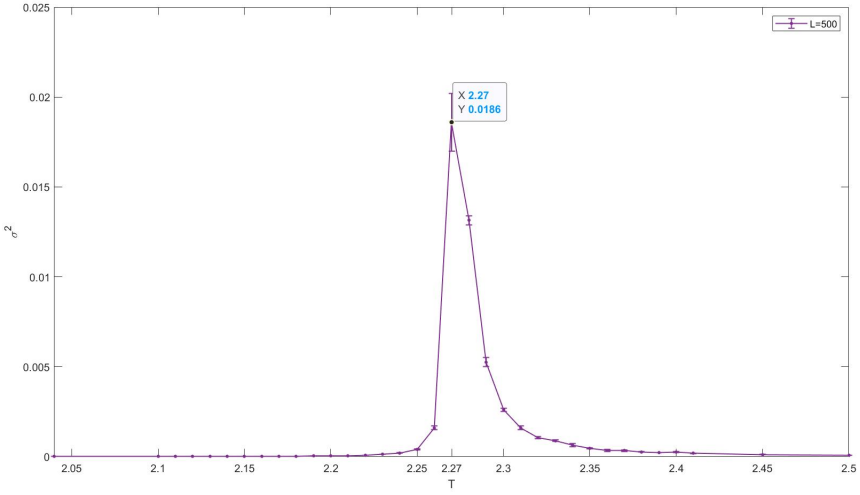

Figure 3.11: Magnetization's variance, L=500.

L	T_c
60	2.30
80	2.30
100	2.29
200	2.28

Table 3.1: The value of T_c for different lattice size.

makes us inclined to choose $L = 500$ as our best candidate for the avalanches' statistics study. In order to be completely sure about our choice, we analysed also the susceptibility, χ. From Statistical Mechanics, we know that this quantity is proportional to the variance

$$\chi = \frac{\partial \langle M \rangle}{\partial H} = \beta \left(\langle M^2 \rangle - \langle M \rangle^2 \right), \tag{3.11}$$

where $\beta = (k_B T)^{-1}$. Actually, here we calculated the susceptibility per spin

$$\chi = \frac{\beta}{N} \left(\langle M^2 \rangle - \langle M \rangle^2 \right) = \beta N \left(\langle m^2 \rangle - \langle m \rangle^2 \right), \tag{3.12}$$

goes to one and we can use 3.10 as a good approximation

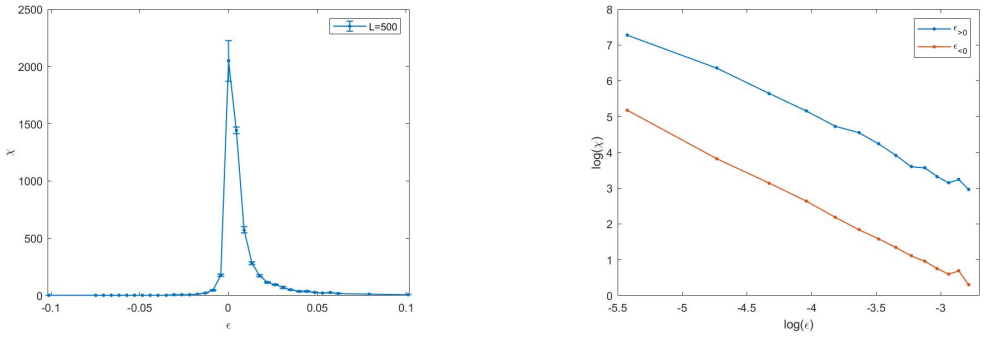

Figure 3.12: On the left, the χ VS ϵ plot. On the right, the linear fitting of the two branches from the picture on the left.

where $m = \frac{M}{N}$. This means that also χ has a power law dependence close to the T_c. From theory, for 2D square Ising model, the exponent τ is equal to $\frac{7}{4}$, if χ is plotted as a function of $\epsilon = \frac{T-T_c}{T_c}$. We checked if this value can be found with a simulation on our $L = 500$ lattice size candidate. From fig.3.12 (the one on the right), we can observe that the two slopes are almost the same. In 3.2, we can observe how much the two values are close to the theoretical value of τ, 1.75. This is another proof in favour of $L = 500$ as the

$\tau_{\epsilon>0}$	$\tau_{\epsilon<0}$
1.71	1.82

Table 3.2: The two values of the critical exponent of the susceptibility.

minimum optimal lattice size. And also a proof of the goodness of the Wolff simulations to determine such parameter. Later on, it will be interesting to see how this parameter τ varies according to the disorder added to the system.

Finally, we can start looking at the behaviour of magnetization as a function of the temperature. For the measurement of $|m|$ VS T we developed a code capable of telling us also the T_c. Below a fixed value of $|m|$ (we chose 0.80), we started to look for the temperature with the highest σ^2 [3]. In this code,

[3]When we will deal with RBIM, we will introduce a disorder parameter R to the "simple" Ising model ($R = 0$) that we are studying here. Obviously, for $R = 0$ we have already seen the value of T_C and it is in agreement with Onsager's value. But, for the model with disorder included we do not have a theoretical value for comparison. So, we

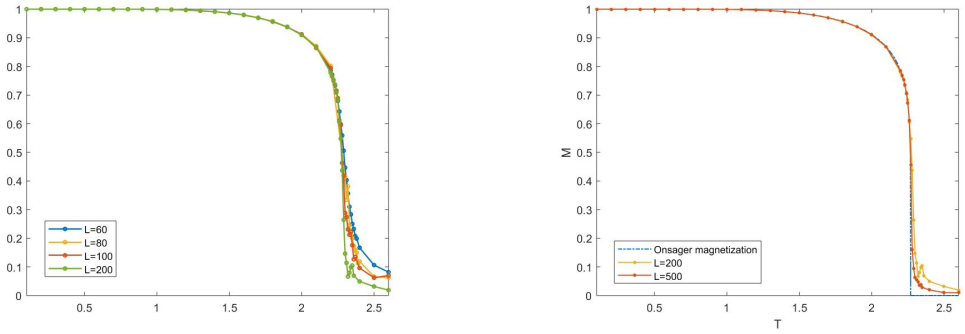

Figure 3.13: On the left, Magnetization's behaviour as a function of T, for different values of L. On the right, a focus on L=200 and L=500, compared with the Onsager exact solution for the magnetization.

we start from $T = 0.1$ and with an initial configuration corresponding to $T = \infty$. Once reached the equilibrium, we start to sample the magnetization. Then, we move on with the next temperature, but in this case the initial configuration is the equilibrium configuration of $T = 0.1$. This means that the system is already close to the equilibrium. For all the next temperatures we followed the same procedure, starting from the equilibrium configuration of the previous temperature. This saved a lot of simulation time.

Fig. 3.13 shows that L=500 is the one closer to Onsager's solution, as we have already noticed from the variance analysis.

Before introducing the random Ising model that we have studied, let us look at the case of the complete Ising Hamiltonian, the one with the external magnetic field included (till to this point we did not considered it).

3.3.3 Magnetic field-driven phase transition: Ghost Spin

In this subsection, we want to introduce some features about the Wolff algorithm, when the contribution of an external magnetic field is added to our

will exploit the fact that σ^2 has a peak in correspondence of T_c in order to find it.

spin lattice. Here it is the complete Hamiltonian of the Ising model

$$E_I\{s_i\} = -\sum_{<ij>} J s_i s_j - H\sum_{i=1}^{N} s_i, \tag{3.13}$$

where the H is the external magnetic field.

The effect of such field has been introduced by considering a variation of the Wolff algorithm, called Ghost spin extension. A first verion of such extension to the Wolff cluster method was proposed by Dotsenko, Selke, and Talapov [16]. The idea behind the algorithm we implemented is to consider the external field like a spin entity outside of the system, which is not involved in the MC dynamics. Hence the name: ghost spin. Let us give more details about this. We can start rewriting the Hamiltonian 3.13

$$E_I\{s_i\} = -\sum_{<ij>} J s_i s_j - |H|\sum_{i=1}^{N} s_i s_0 \tag{3.14}$$

where

$$s_0 = \begin{cases} +1, & if H \geq 0 \\ -1, & if H < 0 \end{cases} \tag{3.15}$$

This can be seen like the Hamiltonian of the following lattice made by the

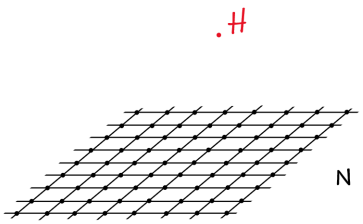

Figure 3.14: The "new" lattice within the Ghost Spin frame.

previous lattice (N spins) plus the Ghost Spin, i.e. the field. eq.(3.14) can be written in a more compact way

$$H = -\sum_{<ij>} \tilde{J}_{ij} s_i s_j, \tag{3.16}$$

where

$$\tilde{J}_{ij} = \begin{cases} J, & if \quad i,j > 0 \\ |H|, & if \quad i = 0 \vee j = 0 \end{cases} \tag{3.17}$$

Pay attention that the ghost spin can not flip (it is the field!). Thus, build up the cluster as in the Wolff method but keep in mind there is also the ghost spin:

1. Choose the initial spin, s_i, randomly. Put it first on the growing cluster's list.

2. Generate the cluster starting from s_i, like we did for the Wolff method. But, now we have to consider a new neighbour for each spin of the lattice: s_0. This means that we have to take into account a possible activation of the "link" of a lattice spin with s_0, when s_i has the same sign of s_0 (i.e. the sign of the magnetic field, H). The probability of adding a spin to the cluster can thus be written in a more general form:

$$P_{add} = 1 - e^{-2\beta\tilde{J}_{ij}} = \begin{cases} 1 - e^{-2\beta J_{ij}}, & if \quad j \neq 0 \\ 1 - e^{-2\beta|H|}, & if \quad j = 0 \end{cases} \tag{3.18}$$

3. Since the ghost spin can not flip, if s_0 is added to the cluster, we have to stop building it and restart from point (1). Hint: of all the nearest neighbours (in our 2D square lattice they are 5, the 4 lattice spins and the ghost spin), check the ghost spin out first.

4. If the ghost spin has not entered the cluster, come back to step (2), and move to s_{i+1} within the growing cluster's list. If there are no more spin to visit within the list, flip all the cluster.

In order to prove that this algorithm still satisfies ergodicity and detailed balance, let us recall the proof of the Wolff method we have seen in section 3.2. By considering also this time the μ and ν configurations, the condition of detailed balance becomes:

$$\frac{P(\mu \to \nu)}{P(\nu \to \mu)} = \frac{g(\mu \to \nu)A(\mu \to \nu)}{g(\nu \to \mu)A(\nu \to \mu)} = (1-P_{add})^{m-n}(1-P'_{add})^{k}\frac{A(\mu \to \nu)}{A(\nu \to \mu)} = e^{-\beta(E_\nu - E_\mu)}, \tag{3.19}$$

where k is the number of spins within the built cluster (and the number of times the ghost spin has been rejected to enter the cluster), and P'_{add} is the

probability for the ghost spin to enter the cluster. As we can notice, here we are supposing the external field H is pointing as the spin within the cluster of configuration μ. This means that the selection probability $g(\nu \to \mu)$ is simply proportional to $(1 - P_{add})^n$, where n is the number of broken bonds in the $\nu \to \mu$ transition, because we are 100% sure that the ghost field can not enter the cluster. The change in energy, $E_\nu - E_\mu$, is

$$E_\nu - E_\mu = 2J(m - n) + 2k|H|, \tag{3.20}$$

where m is the number of broken bonds in the $\mu \to \nu$ transition, and H is the external field. This leads us to rewrite equation 3.19

$$\frac{A(\mu \to \nu)}{A(\nu \to \mu)} = [e^{2\beta J}(1 - P_{add})]^{n-m} \cdot [e^{2\beta H}(1 - P'_{add})]^{-k}. \tag{3.21}$$

Since, as in the Wolff method, the acceptance ratios we use are both equal to 1, we need

$$P_{add} = 1 - e^{-2\beta J}$$
$$P'_{add} = 1 - e^{-2\beta|H|},$$

in order to satisfy eq.(3.21). About ergodicity, it is satisfied as in the Wolff algorithm because there is a finite probability of building clusters with only one spin.

In this chapter, all the field-induced transition simulations use a variation of the magnetic field $\Delta H = 0.001$.

The first important thing to notice about this algorithm is the absence of hysteresis loop. In order to understand this, let us consider the clusters' average area ($\langle A \rangle$) at equilibrium[4] for the point of the simulation where $H = 0.001$, and for the three temperatures shown in fig.3.15. Let us suppose that the final configuration, at $H = 0$, in which the system is left after MC iterations, is the one with the spins all ordered downward. This is what we actually expect from a ferromagnetic domain starting at $m = -1, H = -\infty$ and taken to $H = 0$ by varying continuously the field. At this point, if we look at the

[4]Like we did for the MvsT analysis, here too we look for the equilibrium configuration, for a certain temperature and field values, by starting from the equilibrium configuration of the previous value of the field. So, the system is already really close to the equilibrium, when the MC simulation for a certain field starts.

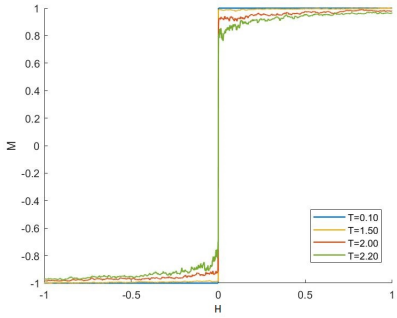

Figure 3.15: $\tau_{eq} = 20$, which is the termalization time for $T = 0.1, R = 0, L = 60$.

T	$\langle A \rangle$	P
0.1	3600	97.3%
1.50	3500	97%
2.00	3000	95%

Table 3.3: Values' table

table 3.3 we can see that, whatever it is the temperature we consider, the first MC iteration at $H = 0.001$ will produce a very big cluster (are we forgetting the ghost spin? No. Here the magnetic field has the same sign of each spin within the lattice. Thus, it can be ignored because we are sure it will not be included within the cluster), so the system will change its magnetization sign. Now, the ghost spin joins the game. Indeed, for the next iteration the field has the same sign of the nearly totality of the lattice spin. The fact that $1 - e^{-2\beta|H|} \sim 0.1\%$ could mislead us to think that with very low probability the ghost spin will interfere with the formation of another big cluster. But, it is exactly the huge dimension of the cluster that makes possible for the field to stop the building of the cluster, as we can see by looking at the third column[5] of table 3.3, where the probability for the ghost spin to get included within the cluster, for the corresponding average area, is reported. All the three values of P are close to 100%. This means that, almost certainly, the ghost spin is accepted within the cluster that, consequently, is not flipped. So, the system is left in the previous configuration. Obviously, it can happen

[5]The value P, in the third column of table 3.3, is easy to compute. It is $P = 1 - (1 - P'_{add})^{\langle A \rangle}$.

a MC step in which the ghost spin dose not interfere with the cluster building, but still, on average, over all the MC steps during sampling phase, these kind of steps are much less common. Then, increasing the field magnitude, the probability of accepting the ghost spin becomes even bigger. This means that our system will get stuck with $m = 1$. So, no hysteresis loop will be seen.

So, unlike the Metropolis algorithm, where we observe our system stuck in a metastable state (i.e. not absolute minimum) until $H = 4J$ (which is the value to overcome the tendency induced by the four neighbours), with the Ghost Spin extension to the Wolff method we are able to always lead our system toward the absolute minimum of its free energy. This is also a difference with real ferromagnets, that usually prefer to stay in a metastable state until a big enough field is applied, giving rise to the typical hysteresis loop of ferromagnets.

This behaviour of the Wolff algorithm can be understood from a more physical point of view. Let us suppose we have a spin pointing upward, surrounded by equal-sign nearest neighbours. If you want to flip that spin within single-flip Metropolis, more energy is needed since it will flip on its own against the equal-sign nearest neighbours, compared to the Wolff algorithm where also the nearest neighbours have the chance to enter the cluster that will be flipped. So, in Metropolis you need the energy provided by a field $H = 4J$, instead in Wolff it is enough $H > 0$ in order to get the first-order phase transition.

Chapter 4

Random-Bond Ising Model

In this chapter we introduce the Random-Bond Ising model (RBIM) we will study in the following chapters. The RBIM aims at reproducing the real behaviour of ferromagnets introducing randomness in the bonds within the spins of the lattice, thanks to the disorder parameter R.

Within this model, we studied how the temperature dependent behaviour of the magnetization's variance changes according to the disorder parameter. This helped us to build the para-ferromagnet phase diagram within the (T, R) plane.

4.1 Definition

In RBIM the exchange interaction constant will not have a fixed value anymore. Instead, according to the $\langle i, j \rangle$ couple of nearest neighbours that we are considering, we have a J_{ij} value representing the spin interaction. And, J_{ij} is picked by a Gaussian distribution

$$f(J_{ij}) = \frac{1}{\sqrt{2\pi R}} e^{-\frac{(J_{ij}-\bar{J})^2}{2R}}, \tag{4.1}$$

with mean value $\bar{J} = J$ and variance $\sigma^2 = R$. Without any loss of generality we may set $J = 1$. In this way the temperatures will be measured in units of J/k_B, with k_B the Boltzmann constant. We can notice that there is a non-zero probability of having $J_{ij} < 0$, i.e. an antiferromagnetic bond between

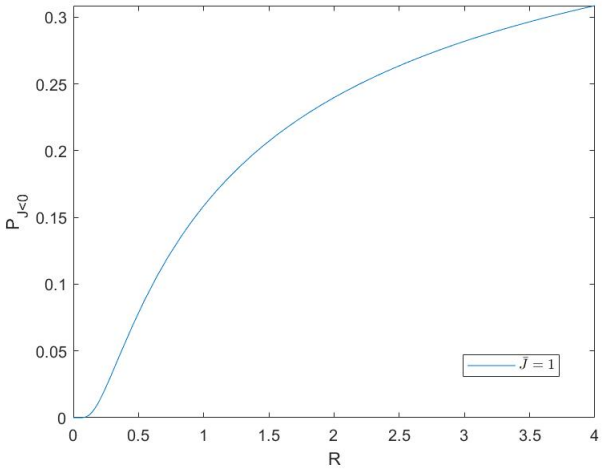

Figure 4.1: $P_{J<0}(R)$, $\bar{J} = 1$.

the spin of the $\langle i, j \rangle$ couple. Such probability, $P_{J<0}$, is equal to

$$P_{J<0} = \int_{-\infty}^{0} f(J_{ij}) dJ_{ij} = \frac{1}{2} erfc\left(\frac{1}{\sqrt{2R}}\right), \tag{4.2}$$

where $erfc(x) = \frac{2}{\sqrt{\pi}} \int_x^{\infty} e^{-t^2} dt$ is the complementary error function. This probability represents the fraction of antiferromagnetic bonds over all the $4N$ bonds within our 2D square lattice. Actually, it is a function of R. In fig.4.1, the R-dependence of $P_{J<0}$ is plotted.

4.2 Temperature-driven phase transition analysis

4.2.1 Correction of the algorithm

As it happened with the magnetic field, also in this case we have to modify the Wolff algorithm we have introduced in the previous chapter. In particular, we are going to prove that the "old" version of the algorithm does not satisfy the detailed balance condition in the RBIM, precisely due to the fact that some J_{ij} can be less than zero (as we have previously seen). Fig.4.2 helps us with this. The red lines represent links with negative J_{ij}. Here we are

Figure 4.2: Like we did in order to prove that Wolff satisfies detailed balance when $J = constant$, also here we consider two configurations, A and B. The red lines represent links with negative J_{ij}. • and × are spin of opposite direction.

considering the configuration A, where the • represents the randomly picked spin (i.e. s_i) and the built cluster is made only by •, since we do not even consider its nearest neighbours because of their opposite sign. This is the move $A \to B$, and $P(A \to B) = 1$. Then, looking at the configuration B, the central, randomly picked, spin has opposite direction now. In this case we consider the nearest neighbours, since they have the same sign of the seed spin. But, the adding probability

$$P_{add} = 1 - e^{-2\beta J_{ij}}, \tag{4.3}$$

is negative because the exchange interactions between the spins are all negative. This means that also here the cluster is made by the only seed spin, and we get back to the configuration A. So, this is the inverse move $B \to A$, and also here $P(B \to A) = 1$. Now, we can write the detailed balance equation

$$\frac{P(A \to B)}{P(B \to A)} = \frac{1}{1} = 1 \neq e^{-\beta \Delta H}, \tag{4.4}$$

where ΔH is the energy difference between A and B configurations, that is obviously different from zero due to the higher energy of the A configuration.

This means that our algorithm's rules need to be checked and changed in order to satisfy the detailed balance condition. The change to apply refers to how we treat two nearest neighbours with opposite sign. If their link is positive, we do not activate their link as we did in the implementation of the

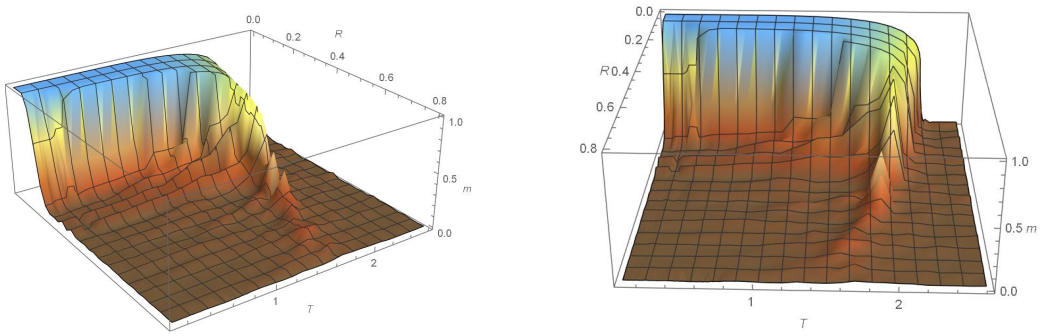

Figure 4.3: m VS T, L=500.

classical Wolff algorithm. But, in case of negative J_{ij}, an antiferromagnetic ordering is favoured. This means that the link between the two opposite sign spin has the possibility to be activated! A new definition for the adding probability is needed

$$P_{add} = 1 - e^{-2\beta J_{ij} s_i s_j}, \tag{4.5}$$

where $J_{ij} < 0$ does not mean any more 100% probability of rejecting the link for a couple $\langle i, j \rangle$ of opposite-sign spins.

4.2.2 Cluster growth

In the last section we have identified a correct algorithm which obeys the detailed balance principle, and thus guarantees converge towards equilibrium. With this, we can start studying the RB Ising model. Our first interest has been to study the dependence of T_c from the disorder parameter R. But, we had to face a first problem. By exploiting the code, we have previously described, for the computation of m VS T plot, we found the behaviour shown in fig.4.3. This was something not expected, since for values of R around 0.1, and for low temperature, the system's magnetization falls down instead of being close to the maximum value. For $R = 0.1$, the magnetization climbs up to 1 close to $T = 0.5$. Instead, for higher values of R we have to wait temperatures closer to the critical region[1] in order to see values of the m closer to 1.

Actually, if we think about this apparently strange behaviour of our code, it is not so difficult to grasp the correct interpretation of what is happening.

[1]We will talk about T_c as soon as we have solved this problem.

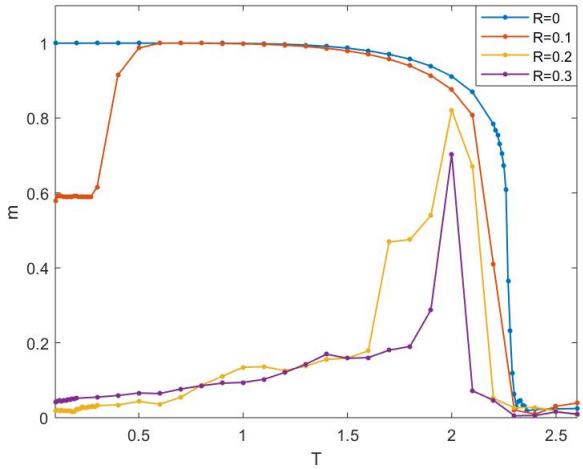

Figure 4.4: Magnetization of a $L = 500$ lattice, for different values of the disorder parameter R. These are some slices of the plot in fig.4.3.

The main culprits are the negative links and the too big clusters built by the Wolff algorithm. Even if the values of R, for which the m value starts to be far from 1 for low temperatures, are still low (i.e. the percentage of negative links is very low), they are enough for our algorithm to get stuck within the initial configuration (i.e. $T = \infty$). This is due to the fact that at low temperatures the P_{add} of the Wolff method is nearly 1, thus the algorithm includes within the cluster almost everyone of the same sign spins it visits, creating very big clusters. So, also if the number of negative links is very low respect to the total number of links within the lattice, there is a good chance, while we are building a big cluster, to meet one of these links, between two opposite sign spins. This means from that point on, our cluster will change sign. So, we end up with a big cluster made of both positive and negative spins that more or less compensate each other in the computation of magnetization, that, as a consequence, gets stuck to the nearly zero value of the initial configuration. Obviously, growing R, the number of negative links will increase and this behaviour will become dominant, leading to clusters as large as the lattice itself.

By looking at fig.4.5 we can observe also a clusters' area analysis, for a lattice size $L = 60$, that confirms what we have said about the tendency of the Wolff

algorithm to build too big clusters at low temperatures. For $L = 60$ too, we have such behaviour, but the decrease of $|m|$, for low temperatures, starts at slightly higher values of R, fig4.6 (this is obvious, for example for $R = 0.1$ we still do not see any decrease of the magnetization because the probability of having even just one negative link is nearly zero). We can see how the red line's (high T) distance from the lower temperatures lines becomes bigger and bigger if we increase the R parameter. In particular, the lower temperatures have a deficit for those values of the cluster's area that are not too big neither too small, so the ones necessary for the system to move toward the equilibrium. This is the reason for the low temperature slowness to converge of the Wolff algorithm, for growing values of R. In literature, this behaviour was already noticed in [17].

4.2.3 Physical quantities analysis

In order to solve this problem, we started our simulations from a completely ordered configuration (e.g. all spins up). In this way, we obtained fig.4.7. In

	$\tau_{\epsilon>0}$	$\tau_{\epsilon<0}$
$R = 0.2$	1.49	2.18
$R = 0.3$	1.17	2.21
$R = 0.4$	0.99	2.05

Table 4.1: Value of susceptibility critical exponent τ, for $R = 0.2$, $R = 0.3$ and $R = 0.4$.

order to complete the interesting analysis about the critical exponent of the susceptibility that we have done for the case $R = 0$, here we show how that exponent varies with R. The difference between $\tau_{\epsilon>0}$ and $\tau_{\epsilon<0}$ increases with R.

The behaviour of the magnetization variance as a function of T and R is shown in fig.4.8.

Another interesting result to mention is the R-dependence that we found for the critical temperature (fig.4.9), i.e. the para-ferromagnet phase diagram in the (T, R) plane. For $R = 0$, we have the critical temperature of the Ising model without disorder that we have estimated in the previous chapter, $T_C = 2.27$. Note that the line separating the paramagnetic and ferromagnetic

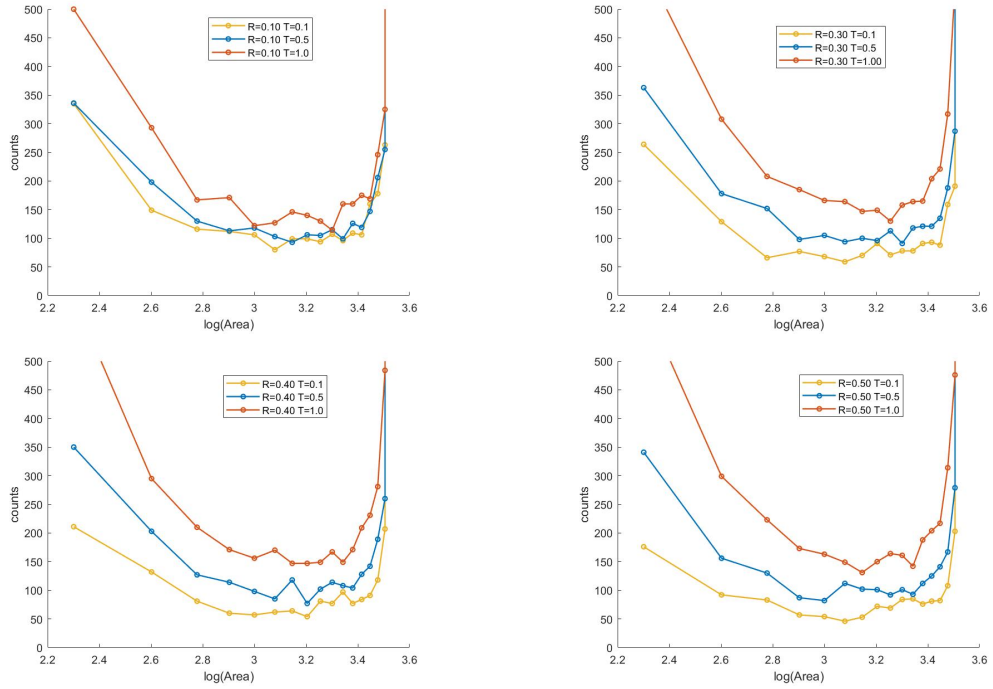

Figure 4.5: Fixed the value of R, the analysis is done on 600 simulations for each temperature. $L = 60$. Each simulation starts from $T = \infty$ configuration, reaches the equilibrium and continues for other iterations. For each temperature the same number of cluster's areas is measured. The counts' axis is not completely shown, in order to highlight the range of less probable areas for lower temperatures (i.e. those areas that would allow the simulations to reach the equilibrium).

Figure 4.6: m VS T, L=60.

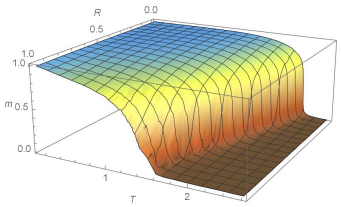

Figure 4.7: Magnetization of a $L = 500$ lattice, starting from an ordered configuration at $T = 0.1$ for each value of R.

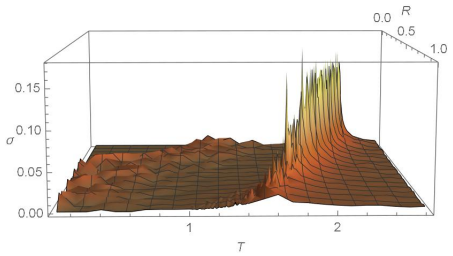

Figure 4.8: Variance, $L = 500$. The peak's position at T_c moves with R.

phases resembles a linear dependence, as the dashed line in fig.4.9 suggests. In the next chapter, we will improve the (T, R) phase diagram, when the spin glasses will be introduced. As we have already anticipated in the previous chapter, we derived the T_c looking at the maximum value of the magnetization variance, for each value of R.

At this point, we have almost all we need to study the avalanches' statistics induced by an external field. We only miss a further analysis, on the value of R, ensuring us to work within the ferromagnetic domain. It can be that for a too big value of the disorder parameter, the system free energy begins to show new minima besides the ferromagnetic one.

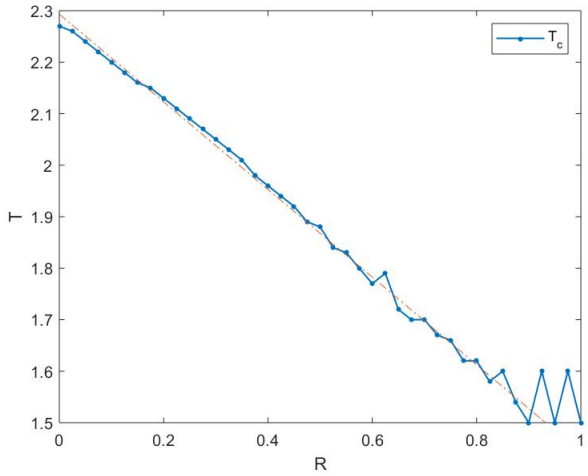

Figure 4.9: Para-ferromagnet phase diagram in the (T, R) plane. $L = 500$.

Chapter 5

Spin Glasses

Before we continue with the study of the Random-Bond Ising model, it is necessary to check if there is a value for the R parameter such that our system stops behaving like a ferromagnet. Indeed, the destruction of the ferromagnetic order is expected, at $T = 0$, when the percentage of antiferromagnetic bonds is equal to the 15% of all the bonds within the lattice [13]. We want to check if the same works for $T \neq 0$, or if there is a different threshold for the concentration of antiferromagnetic bonds, and consequently determine the value of the R parameter needed to reach such limiting value. This will be useful for the study of the avalanches distribution, as we will see in the next chapter. Before doing this, let us move through an overview about the new magnetic phase that the critical antiferromagnetic bonds' concentration would generate: the spin glass phase.

5.1 The spin glass phase

In simple words, a spin glass is a collection of spins (i.e. magnetic moments) whose low-temperature state is a **frozen disordered** one. This means a completely different situation from the one of conventional magnets where we observe uniform or periodic patterns. It appears that in order to produce such a state, two ingredients are necessary: there must be competition among different interactions between the magnetic moments (i.e. no single configuration of the spins is uniquely favoured by all the interactions, this what usually we call 'frustration') and these interactions must be at least partially random, otherwise the magnetic transition will be of the standard

ferromagnetic or antiferromagnetic type of long-range order.

5.1.1 Frustration

Let's consider as an example the case of Ising model on the lattices in fig.5.1, where only the nearest-neighbour antiferromagnetic interactions operate (i.e. the exchange interaction constant is negative).

By looking at the square lattice, it is easy to see that the requirement of an-

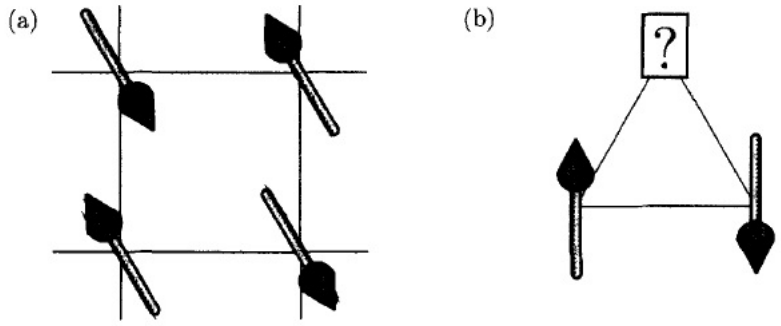

Figure 5.1: Antiferromagnetic nearest-neighbour interactions on the (a) square lattice and (b) triangular lattice

tiparallel nearest-neighbours spins can be satisfied. Instead, in the triangular lattice case, introduced for the first time by Wannier [18], it is not possible to satisfy all the interactions. As shown in fig.5.2, if two adjacent spins are placed antiparallel, one is faced with a dilemma for the third spin. Whatever configuration we will choose, one of the two-neighbour pairs will not have its energy minimized. The system therefore cannot achieve a state that entirely satisfies its microscopic constraints, but does possess a multiplicity of equally unsatisfied states. And, since this effect occurs for each spin, the ground state is sixfold degenerate.

This is a simple example of frustration due to conflicting inter-atomic forces (in our case, the exchange force between magnetic moments of the atoms of the lattice) in turn due to the geometry of the system. Such frustrated systems are experimentally realized in a variety of crystal structures. For

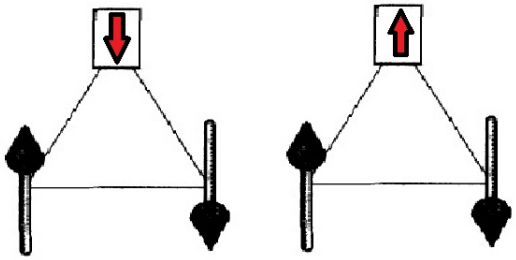

Figure 5.2: Two degenerate ground states for the upper vertex

instance, in 2D, in addition to the triangle (hexagonal) lattice, we have the Kagomé lattices characterized by corner-sharing triangles.

5.1.2 Randomness

The second ingredient for spin glasses are random competing interactions. The randomness can be introduced in many different ways. First is site-randomness, which can be achieved in an alloy. The first kind of system that was studied widely consisted of dilute solutions of magnetic transition metal impurities in noble metal hosts. The impurity moments magnetically polarize the host metal conduction electrons around them, whit a positive sign at some distances and negative at others. Other impurity moments then feel the local magnetic field produced by the polarized conduction electrons and try to couple with it. This is actually the RKKY (Ruderman–Kittel–Kasuya–Yosida) interaction between distant magnetic atoms (i.e. this is an example of indirect exchange interaction, happening when orbitals of magnetic atoms are too far from each other in order to make possible the short range direct exchange interaction). Here the coupling depends on the distance between magnetic ions and has the following form:

$$J_{RKKY}(r) \propto \frac{cos(2k_F r)}{r^3} \tag{5.1}$$

at large r (assuming a spherical Fermi surface of radius k_F). Because of the random placement of the impurities, some of interactions are positive (i.e.

favouring parallel alignment of the moments) and some are negative. Thus we have not only random but also competing interactions (i.e. frustration), the two requirements for being a spin glass. A commonly studied spin glass with site-randomness is $Cu_{1-x}Mn_x$ with $x \ll 1$ in which the substitution of small amounts of Mn into the Cu matrix occurs completely randomly with no short-range ordering.

Another kind of disorder is due to bond-randomness in which the nearest neighbour interaction bonds vary and are randomly distributed throughout the sample. This can be done by modulating the indirect exchange interactions between magnetic ions in a regular crystalline lattice. This is performed in $Rb_2Cu_{1-x}Co_xF_4$ for which both Cu and Co are magnetic ions. In this case the Ising character is given to the magnetic moments by the uniaxial single ion anisotropy. A kind of anisotropy due to the electrostatic interaction of the magnetic ions' orbitals with the crystal field (i.e. electric field derived from neighbouring atoms in the crystal) that tends to stabilize particular atomic orbitals, fixing, in turn, the angular momentum of the magnetic atom and consequently the easy axis for the magnetization along which the spin-orbit interaction is minimized. However the size and sign of the superexchange interaction (that usually favours antiferromagnetic order) between magnetic ions depends on whether the coupling are between Co and Co, or Co and Cu, or Cu and Cu and which orbital on the Cu is occupied. Automatically, the frustration condition is present in this random-bonds spin glass.

5.2 How to identify a spin glass phase

The expression 'frozen disorder', previously used, suggests that the spin glass state has a nonzero local spontaneous magnetization $m_i = \langle S_i \rangle$ ($S_i = \pm 1$, in a system of Ising spins and $\langle S_i \rangle$ is the thermal average) at a given site i of the lattice, though the average magnetization vanishes. This last feature might lead us to mistakenly think to an antiferromagnet. Instead, neutron scattering experiments come to our help, showing no magnetic Bragg peaks which would have indicated long range order. Then, in order to better characterize our sample's spin glass state, we can carry out a measurement on the susceptibility. Indeed, the local spontaneous magnetizations of the low-temperature spin glass state make their presence felt because they reduce the susceptibility from the value it otherwise would have. This is what ex-

periments show: a spin glass exhibits a marked cusp at a temperature which is rather sharply defined. The connection between the susceptibility and the existence of frozen moments can be made more explicit by using a system of Ising spins ($S_i = \pm 1$) and considering the single-site susceptibility χ_{ii} defined as the amount of magnetization m_i induced at site i by an external field h_i acting only on this site:

$$\chi_{ii} = \frac{\partial \langle S_i \rangle}{\partial h_i} = \frac{\partial m_i}{\partial h_i} \tag{5.2}$$

A fundamental theorem of classical Statistical Mechanics, the linear response theorem, states that the fluctuations in a variable X are proportional to the susceptibility of that variable to its conjugate field, Y:

$$\frac{1}{\beta} \frac{\partial \langle X \rangle}{\partial Y} = \langle X^2 \rangle - \langle X \rangle^2 \tag{5.3}$$

So (in units where the Boltzmann constant $k_B = 1$), we can write:

$$T\chi_{ii} = \langle (S_i - \langle S_i \rangle)^2 \rangle = \langle S_i^2 \rangle - \langle S_i \rangle^2 = 1 - m_i^2 \tag{5.4}$$

where we have used the fact that $S_i^2 = 1$ and the magnetic field is conjugate to the spins. Averaging over all the sites in the system gives

$$\chi_{loc} \equiv \frac{1}{N} \sum_i \chi_{ii} = \frac{1 - N^{-1} \sum_i m_i^2}{T}. \tag{5.5}$$

From this we can see that the reduction of the average local susceptibility χ_{loc} from the Curie law ($\propto \frac{1}{T}$) characteristic of free moments is a direct measure of the mean square local spontaneous magnetization in the frozen state. Actually the experiments do not measure the local susceptibility χ_{loc}, but rather its average, the uniform susceptibility χ. Nonetheless, it can be proved that if χ_{loc} has a cusp then χ to will exhibit it. So, the experiments on susceptibility really indicate the existence of a nonzero frozen spontaneous magnetization, a spin glass state.

Actually, the susceptibility we are talking about is the real part of the a.c. susceptibility $\chi(\omega, T)$ (see fig 5.3). In this technique the magnetic susceptibility is measured using a very small alternating magnetic field of frequency ω, sometimes with a constant (d.c.) magnetic field also applied. The freezing temperature T_f turns out to depend on the frequency of the applied magnetic

field, a feature that is not present in other magnetic systems and therefore confirms the spin glass phase (see fig 5.3). The 'true' T_f should therefore be defined by the limit of vanishing frequency. Furthermore, the cusp is not completely sharp as shown in fig 5.3 for CuMn.

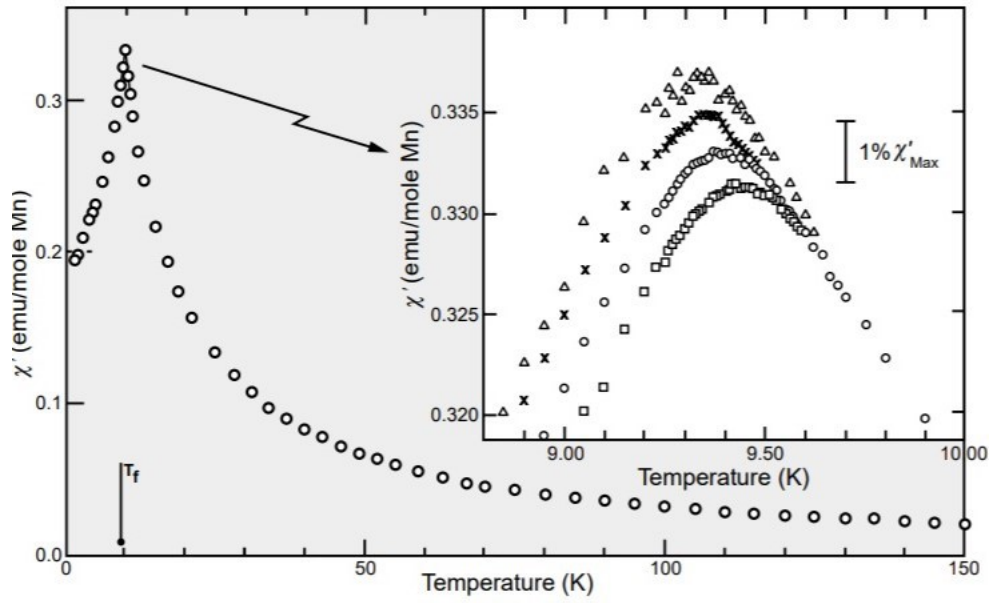

Figure 5.3: The real part (χ') of the a.c. susceptibility as a function of temperature for Cu-0.9%Mn for frequencies 1.33 kHz (□), 234 Hz (∘), 10.4 Hz (x), 2.6 Hz (△) (from Mulder et al, 1981, 1982)

5.3 Spin glass theory: a brief overview

In this section, we will very briefly overview how a spin glass phase is characterized and, therefore, can be recognized in a numerical simulation.

Spin glasses belong to the class of quenched disordered systems. For these systems the disorder is explicitly present in the Hamiltonian, typically under the form of random couplings J among the degrees of freedom

$$H = H(\sigma; J). \tag{5.6}$$

The disorder is specified by its probability distribution $p(J)dJ$ which is the same for each different coupling constant in the system. This is actually the type of Hamiltonian that we are using for the Monte Carlo simulations:

$$H = -\sum_{\langle ij \rangle} J_{ij}\sigma_i\sigma_j, \tag{5.7}$$

where the spins $\sigma_i = \pm 1$ are the degrees of freedom and the couplings J_{ij} are Gaussian random variables. This is a famous model in spin glass theory called Edwards-Anderson model [19]. This is a finite dimensional model, since the sum is performed over nearest-neighbour spins. It is characterized by a quenched disorder, meaning that the J are constant on the time scale over which the σ fluctuate. Within this model, the first problem they had to face was the following one: how to deal with the disorder? Indeed, each observable depends on J. For example the free energy of the system:

$$F_N(\beta, J) = -\frac{1}{\beta N} log \int e^{-\beta H(\sigma;J)} d\sigma \tag{5.8}$$

where N is the size of the system and $Z = \int e^{-\beta H(\sigma;J)} d\sigma$ is the partition function. This is not very pleasant, since it looks like that the physical properties of spin glasses are different for each different realization of the disorder J, i.e. for each different sample. If this was true, it would be impossible to build a theory for spin glasses since we could only build it for a specific piece of material. In fact, both experience and common sense tells us that for sufficiently large systems, physical properties do not depend on J anymore (a property which is called "self-averaging"). For quantities like these, it turns out that in the thermodynamic limit ($N \to \infty$) the extensive thermodynamic potentials, including the free energy, are self-averaging quantities. Thus, the average over the disorder is equal to its J-independent value,

$$F = -\lim_{N\to\infty} \frac{1}{\beta N} \overline{logZ(J)} = F_\infty(\beta) = \lim_{N\to\infty} F_N(\beta, J) \tag{5.9}$$

where,

$$\overline{A} = \int p(J)A(J)dJ \tag{5.10}$$

At this point, a new problem arises when we consider the explicit formula for the free energy:

$$F = -\frac{1}{\beta N} \int dJ p(J)\ log \int e^{-\beta H(\sigma;J)} d\sigma, \tag{5.11}$$

which looks pretty complicated, since we have to integrate the log (of an integral) over J. Here it comes the replica trick, in which the logarithm of the partition function Z is evaluated by calculating the partition function of n replicas of the system, Z^n, and then doing a limit operation:

$$logZ = \lim_{n\to 0} \frac{Z^n - 1}{n} \tag{5.12}$$

that can be easily understood by means of Taylor expansion:

$$\lim_{n\to 0} \frac{Z^n - 1}{n} = \lim_{n\to 0} \frac{e^{n\, logZ} - 1}{n} \tag{5.13}$$

$$= \lim_{n\to 0} \frac{n\, logZ + \frac{1}{2!}(n\, logZ)^2 + ...}{n} \tag{5.14}$$

$$= logZ \tag{5.15}$$

The important thing here is that all the Hamiltonians in Z^n formula have the same realization of the quenched disorder, and in this sense are replicas one of the other. This replica trick allows to treat integrals like the one in 5.11. Indeed, if n is an integer, we have

$$\overline{Z^n} = \int d\sigma_1 ... d\sigma_n \overline{e^{-H(\sigma_1,J)...-H(\sigma_n,J)}}, \tag{5.16}$$

which is much simpler to compute.
Another spin glass model is the one introduced by Sherrington and Kirkpatrick [20] called S-K model for spin glasses. It's a long range interaction model, i.e. each of the N spins of the system is supposed to interact with all the other spins. This is the first difference with our model (i.e. the EA model). Another difference is the mean value of the Gaussian distribution, in our case it is $J = 1$, instead in S-K model it is $J = 0$. By applying the replica trick, this model appeared to be exactly solvable and many of the features of the Edwards-Anderson model were reproduced. However, the "replica symmetry assumption" hypothesizes that all the copies of the spin glass thermalizes within the same minimum of the free energy. This approximation is not correct for a spin glass (instead it is for a ferromagnet), generating not correct results like a negative entropy at low temperatures. It was thought the error was due to an improper interchange of the two limits $n \to 0$ (about replica trick) and $N \to \infty$ (i.e. thermodynamic limit) and that the consequences were confined to low temperature. In order to

avoid this puzzling step in the calculations, Thouless et al. turned to a different approach that confirmed the correctness of SK model solution above and near T_C, but found very different behaviour at low temperatures. The turning point for spin glass theory happened when Almeida and Thouless noticed that the symmetry between replicas should be broken in the spin glass state. This correction correctly takes into account the fact that a spin glass has many possible equilibrium configurations, thus replicas can thermalize in different configurations. On the wave of all these theoretical results, in 1979 Parisi was able to find an equilibrium solution of SK model [21].

5.4 Para - Ferro - Glass phase diagram

However, our purpose here is to find for which value of the bonds variance, R, we obtain a system that is no more a ferromagnet (i.e. a state with only two minima in the free energy) and has become a spin glass (i.e. a state with new energetic minima, different from the ferromagnetic one). Hence the name "critical", not to be mistaken with the R_C defining the power-law regime for the magnetization jumps.

5.4.1 Overlap

We do not study in details the SK model but we simply use here some of the results obtained for that model. In particular we are interested in a quantity that allows us to measure the similarity between two configurations. It is called *overlap* and it is defined as

$$q_{\alpha,\beta} = \frac{\sum_{i=1}^{N} \sigma_i \tau_i}{N}, \tag{5.17}$$

where σ_i and τ_i are the spin variables of two different realizations α, β of our lattice, and N is the total number of spins within the lattice. For example, in a ferromagnet, where the system equally prefers to stay within one of the two minima of the free energy (i.e. the two configurations with magnetization pointing up or down), the overlap is equal to ± 1 because we will always find our system in one of these two configurations. Actually, this is true for a ferromagnet at $T = 0$, where the system has a unique equilibrium configuration (i.e. all spins up or down). Instead, when $T \neq 0$, the configuration is no more unique (e.g. in a ferromagnet with 95% spin up and 5% spin down, it

is unlikely that, within the 5% of down spin, the spins are the same in each computed configuration). Thus, for $T \neq 0$ the overlap maximum value is on average smaller than 1.

In fact, the quantity that we have studied is another one. It is the probability distribution of each possible value of the overlap among realizations, $P(q)$. In a spin glass the overlap will have the ± 1 values (actually, as we have previously said, it is difficult that the configurations are exactly the same so the maximum value of the overlap is on average less then 1), but also some other values in between.

We developed a code generating a number C of configurations of the spin lattice. For each one of the C simulations, we started from the same initial configuration of the spin lattice, i.e. all the initial configurations share the same mean magnetization per spin[1], and let the system evolving toward thermalization. Then, for each couple of configurations, we computed the overlap. In this way, we were able to determine the overlap distribution, $P(q)$, and discriminate whether our system was a ferromagnet or a spin glass.

For a ferromagnet, $P(q)$ is equal to two Dirac's deltas in ± 1. Above T_C, the $P(q)$ becomes a Delta in zero. This can be seen by looking at fig.5.4. If we increase the disorder parameter R, when we are still in the ferromagnetic phase, the two Deltas start to become similar to two Gaussian functions. From spin glass theory, we know that the transition between ferromagnet and spin glass happens when $P(0) \neq 0$. We can look at this transition from fig5.5.

[1]The usual choice for the initial configuration is the random configuration, letting the system choose between one of the energy minima. But, due to the slowness of our algorithm, we started from an initial configuration with a magnetization closer to the one of the two ferromagnetic minima.

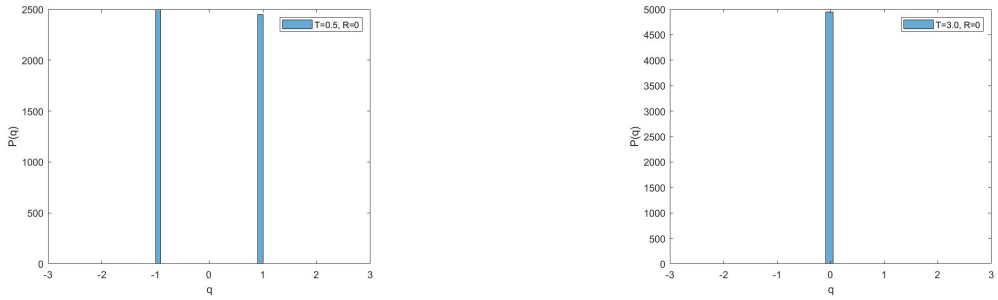

Figure 5.4: On the left, histogram of P(q) for a ferromagnet, L=90, C=100. Since the number of configurations is finite ($\frac{C(C-1)}{2}$ = 4950 is the number of q values that we evaluated), the values of the P(q) in q = +1 and q = −1 are finite, and slightly different. On the right, P(q) for the paramagnetic phase, L=90.

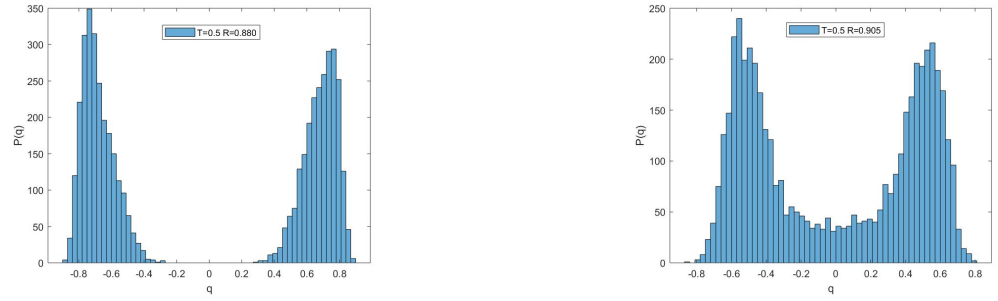

Figure 5.5: On the left, we can see the two Deltas being substituted by two functions with a bell-like shape. On the right picture, the transition to spin glass has happened since we have $P(0) \neq 0$.

5.4.2 Order Parameter q(x)

Now that we have better understood how the $P(q)$ distribution behaves through the ferro-glass transition, we introduce the order parameter for spin glasses. In fact, we will exploit this quantity in order to detect the ferro-glass transition. It is a function that is constant if the system is a ferromagnet. If it is not constant, it means that new energetic minima exist, so it is an indicator of the rising of the spin glass phase. If we define the function $x(q)$ such that

$$\frac{dx}{dq} = P(q), \tag{5.18}$$

where we are considering only the values of $P(q)$ for $q > 0$, the order parameter is the inverse function, $q(x)$, with $x(0) = 0$ as initial condition. In particular, when the derivative in the origin of such order parameter is infinite, it means we are still in the ferromagnetic phase. When it becomes finite, it means the system is in the glassy phase.

The scope of this chapter is to define the region in the (T, R) plane where we are sure to be working with a ferromagnetic system, i.e. we have enriched the plot of the critical temperature as a function of R. This can be helpful for the avalanches' simulations. For the $q(x)$ plot, the values on both axes are normalized to the biggest one. Here, we can see the transition for three different temperatures, $T = 0.5, T = 0.9$ and $T = 1.4$. The range of temperatures we studied goes from $T = 0.5$ to $T = 1.7$ (the triple point).

In fig.5.9, a kind of phase diagram is depicted, showing the three following magnetic phases: ferromagnet, spin glass and paramagnet. On the right of the red line, and below the blue one, the system is a spin glass. Instead, on the left of the red line it is a ferromagnet. Above the blue line, we have the paramagnetic phase. The value of R at $T = 0.5$ needed for the transition from ferromagnetic to spin glass phase, is $R = 0.905$. The value is close to the result for $T = 0$ obtained by [28], where a concentration of 0.15 of antiferromagnetic bonds is the computed value for the transition to spin glass. Such value, in our $J = 1$ model, corresponds to $R = 0.93$. So, by going below $T = 0.5$, we would have found a value close to $R = 0.93$. We stopped at $T = 0.5$ due to the slowness of the RBIM at lower temperatures, inducing a lower accuracy in our simulations. Just one observation, the blue line has been derived for $L = 500$. Instead, the ferromagnet/spin glass transition

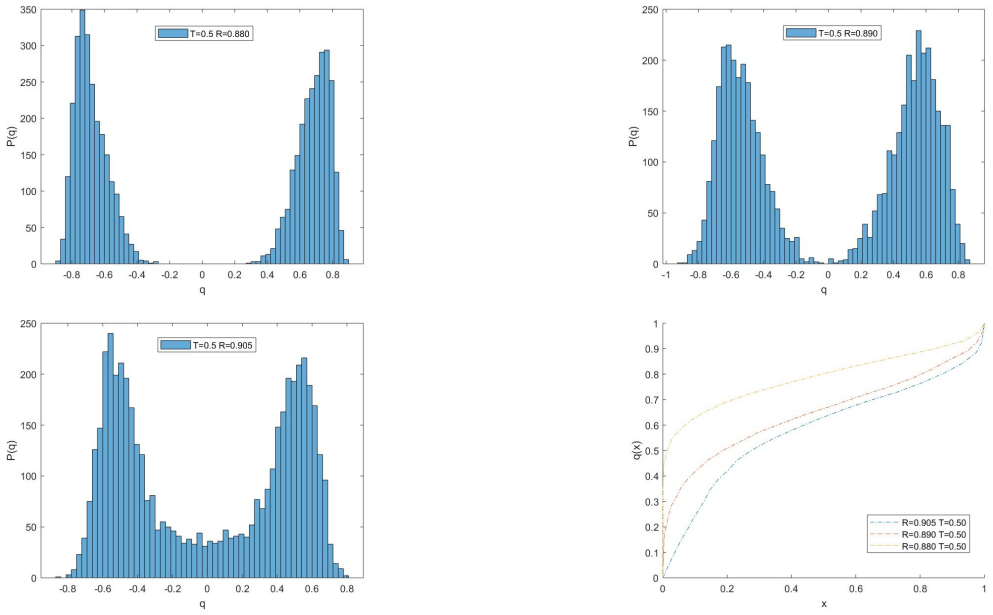

Figure 5.6: The transition is shown both for $P(q)$ and $q(x)$. With $q(x)$ we better appreciate it, because it is clear the value of R such that the derivative in the origin is no more infinite. T=0.5, L=90.

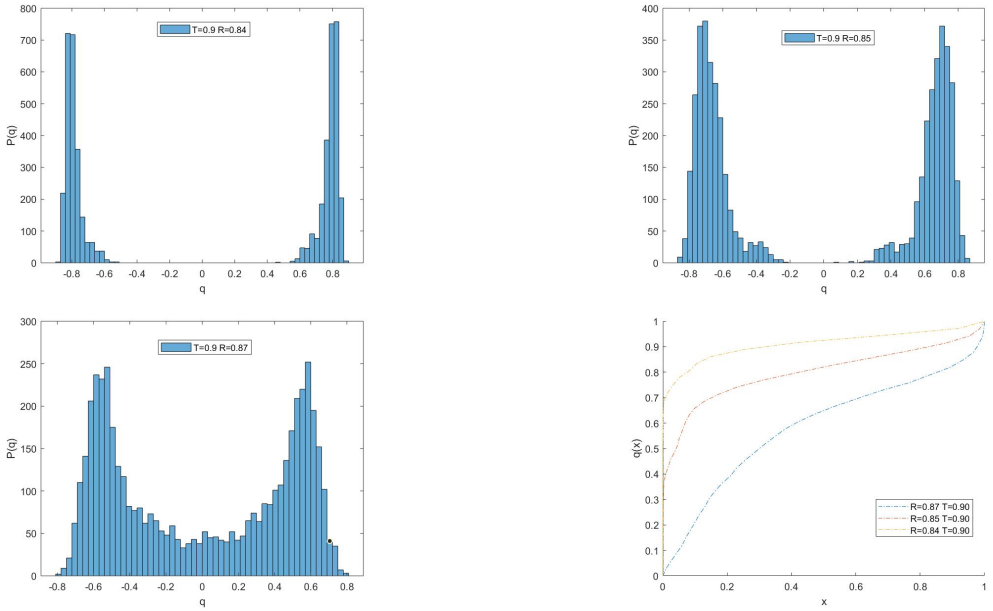

Figure 5.7: The transition is shown both for $P(q)$ and $q(x)$. T=0.9, L=90.

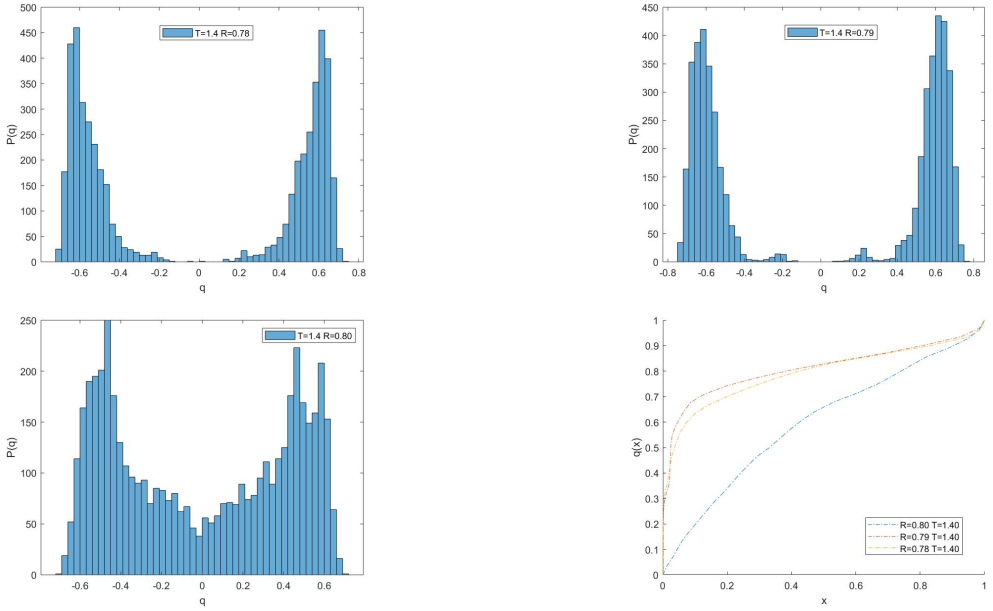

Figure 5.8: The transition is shown both for $P(q)$ and $q(x)$. T=1.4, L=90.

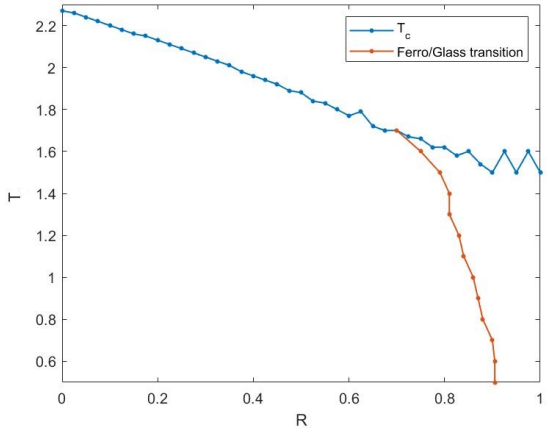

Figure 5.9: Magnetic phase diagram. The intersection point between the blue and red line is called *triple point*, it is located at $T = 1.70$ and $R = 0.70$.

line has been computed on a lattice size $L = 90$, due to the slowness of the algorithm needed to compute the $P(q)$ for $C = 100$. In any case, we have seen in the previous chapter how a lattice size of $L = 60$ is precise to the first decimal digit when it comes to determine the ferromagnet/paramagnet transition temperature at $R = 0$. So, we can suppose the same precision for the ferro/glass transition too, or even better since we used $L = 90$. And, for our scope, that is enough.

Chapter 6

Barkhausen noise analysis

Finally, we are ready to start with the analysis of avalanches' statistics. The lattice size for all the simulations is $L = 500$ (i.e. the optimal one that we have found in Chapter 3). The scope of this chapter is to study the Barkhausen noise generated during a magnetic transition between the up- and down-states, driven by a steadily increasing external magnetic field. In particular, we will study the power-law distributions which emerge in this transition, and focus our attention on the temperature dependence of the of the power-law coefficient of the avalanches' statistics, so that we can compare the theoretical result with the experimental data obtained by Puppin and Zani [23] and Puppin [24]. An analysis on the sign of the avalanches is done too, and the results are compared with the experimental data obtained in [25], by Puppin and Zani.

The amplitude of an avalanche is measured by ΔM, where M is the magnetization of the system. So, what we are going to study is the magnetization jumps' statistics for different temperatures. We expect such statistics to exhibit a power-law behaviour for a critical value of the disorder parameter R. All the plots have log-log axes, so the power-law behaviour becomes a linear behaviour.

The analysis is divided in two parts. In the first part, the simulations will be performed on a system which is allowed to reach thermalization for every single value of the external magnetic field. Because of this, we did not use a too small ΔH, otherwise the simulations would have taken a not reasonable time to be completed.

The second part, instead, is characterized by a single avalanche analysis, based on a particular hypothesis we did about the MC time. Here we were able to use a smaller magnetic field step, so smaller avalanches became visible.

The first analysis is needed to understand how to tune our model's parameter, R, in order to simulate the BK noise, i.e. in order to have an acceptable linear behaviour in log-log plot. The second analysis is, instead, the one we used for the study of the power-law coefficient τ, thanks to the knowledge acquired with the first analysis.

6.1 Thermalization analysis

For these simulations, we used a $\Delta H = 10^{-3}J$, where we recall that we chose to fix the average bond interaction energy $J = 1$ so that all energies (and magnetic fields) are measured in terms of J, and all temperatures are measured in terms of J/K_B, K_B being the Boltzmann constant. For each value of H we waited long enough for our system to reach thermalization[1]. In our case, each MC step had 2000 iterations, with $\tau_{eq} = 1000$ and $\tau_{corr} = 50$ (i.e. 20 samples). Each avalanche plot is reported in log-log axes. On the x-axis there is the amplitude of the magnetization jumps, ΔM. On the y-axis, the counts of how many magnetization jumps are found for a value of ΔM.

A first way to check if we have found the critical parameter R_C is by looking at the plot of magnetization as a function of the external magnetic field. Indeed, in fig.6.1, we can observe what we have anticipated in the first chapter: by tuning the value of R, the system moves from a regime characterized by many small avalanches (high R, here $R = 0.45$), toward a regime where one big avalanche happens during the phase transition (low R, here $R = 0.25$), passing through the power-law regime with a variety of avalanches' sizes (critical R, here $R_C = 0.35$).

[1] In section 3.3.1, we have seen that the highest thermalization time is the one at T_C. In any case, similarly to what we did for the temperature-induced phase transition, for each value of the external field H we started the Monte Carlo simulation from the equilibrium configuration of the previous value of the field. This means that, even for T_C simulation, it was not required to wait the full thermalization time, being our system already close to the equilibrium configuration. This helped us to save a lot of computational time.

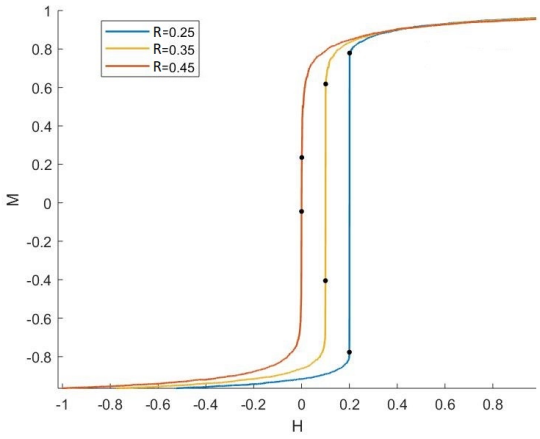

Figure 6.1: MvsB plots for different values of R, at $T = 2.00$. The blue and yellow lines are shifted in order to put in evidence the behaviour close to the transition point, i.e. each magnetization reversal actually happens at $H = 0$. For each branch, the two closest values of the magnetization, around transition point, are highlighted with black points.

In any case, it is not practical looking for power-law behaviour of magnetization's jumps by looking at the magnetization plot. Indeed, we exploited the log-log plot of the magnetizations' jumps in order to identify the value of R for which the linear part of the distribution has the maximum length.

In fig.6.2, we show the results of this kind of analysis. For each value of R, we launched 7 runs of the code. First, we can notice how the linear behaviour covers an increasingly small number of decades as the system's temperature decreases. One cause could be the inability of the Wolff algorithm to build clusters belonging to a wide range of sizes at lower temperatures (see subsection 4.2.2). The highest evidence of this behaviour are the temperatures $T = 1.80$ and $T = 1.85$.

We start seeing linear behaviours covering nearly two decades for temperatures equal or bigger than $T = 1.90$.

The most important thing to notice about this analysis is that, for each

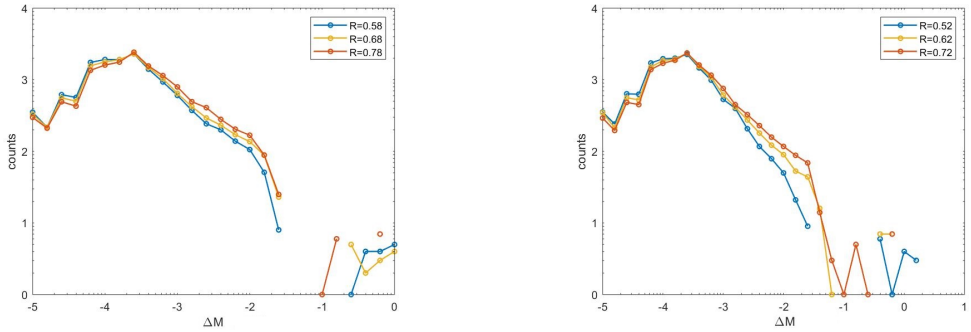

(a)

(b)

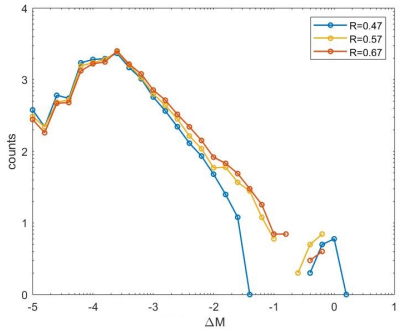

(c)

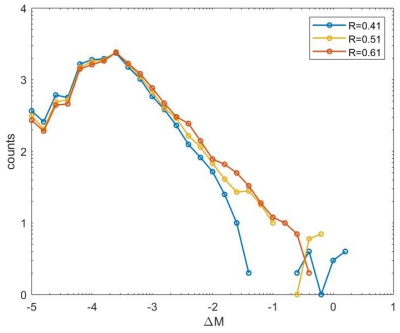

(d)

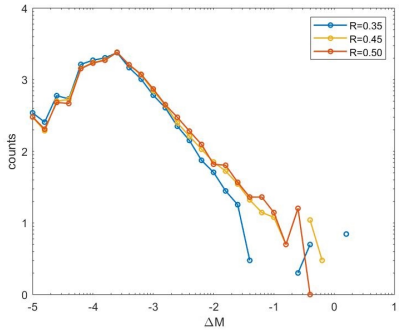

(e)

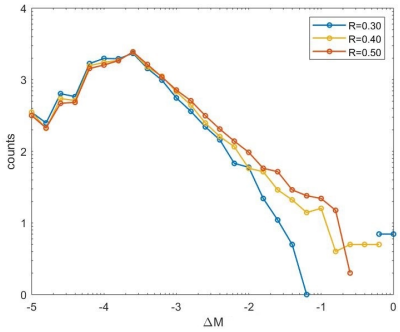

(f)

Figure 6.2: Avalanches' statistics.(a)T = 1.80,(b)T = 1.85,(c)T = 1.90,(d)T = 1.95,(e) T = 2.00,(f)T = 2.05.

temperature T, the value of R with the widest linear behaviour is such that the corresponding temperature is already slightly or well beyond the T_C of the para-ferromagnetic transition. So, the yellow and red lines in the plots of fig.6.2 represent a paramagnetic phase. The blue lines are all within the ferromagnetic region (and close to T_C). For each temperature, the cut-off of the statistics for low values of ΔM is due to the value of ΔH used for the simulations.

This initial analysis indicates that the Wolff algorithm is particularly fit for the study of the avalanches if we put the system close to the T_C. Actually, if we go below $T = 1.90$, even if we choose R such that T is close to T_C, the efficiency for this kind of analysis starts decreasing.

Fig.6.3 is in support of what we have just said. We can see that the linear behaviour gets worse if we choose a value of R such that T is not close to T_C. Also, note that decreasing R, the number of big avalanches increases.

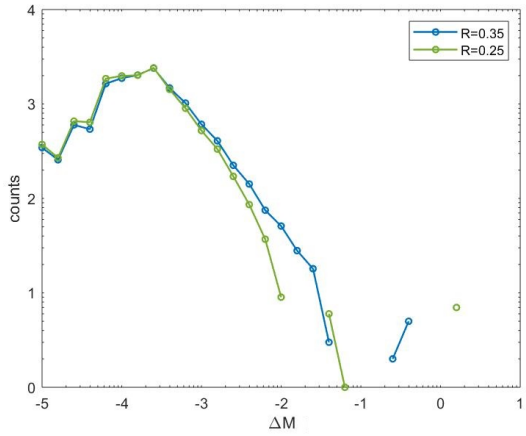

Figure 6.3: Avalanches' statistics not close to the T_C region ($R = 0.25$), and close to T_C ($R = 0.35$) where, instead, the Wolff works better. We can see a decrease of the range of avalanches' sizes covered by the linear part of the distribution for $R = 0.25$. $T = 2.00$

In order to improve the statistics of the blue lines from the previous plots, we first tried reducing the simulation time to 550 iterations per MC step

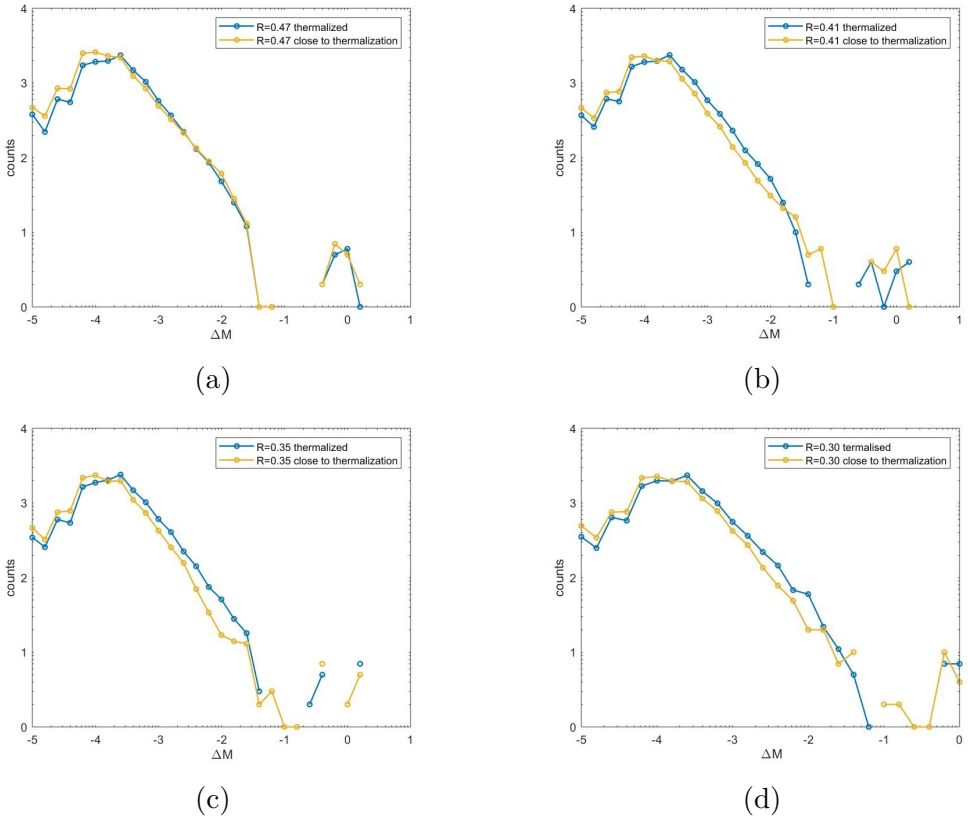

Figure 6.4: Comparison between thermalized and close to thermalization simulations.(a)T = 1.90,(b)T = 1.95,(c) T = 2.00,(d)T = 2.05.

with a τ_{eq} = 250 and τ_{corr} = 15 (i.e. still 20 samples), so, by starting the sampling phase of the MC simulation when still the thermalization was not fully reached, unlike the previous case. The result in fig.6.4. Here the main result is the increase of the counts for small values of the avalanches. This is something expected, since we do not give enough time to the system to reach the equilibrium, so the magnetization difference between two subsequent values of H can be smaller. We can also notice a light filling of the region around $\Delta M = 10^{-1}$.

The following are the main results to keep in mind about this first analysis:

1. The Wolff algorithm is efficient, for BK noise modelling, only if we put the system close to the critical temperature, T_C. This means that the Wolff method is complementary to the single-flip Metropolis method, where the best linear behaviour was found for very low values of the temperature, thus, far from T_C, given a certain R (for the results see [15]).

2. The linear behaviour that we have seen in previous plots (we are considering the blue lines) does not cover more than two decades.

3. By reducing the time of the simulation (i.e. not waiting for full thermalization), the number of small avalanches increases. In each plot of fig.6.4, the linear regions of the two statistics have a similar slope.

4. The linear behaviour would be surely wider, on the side of the lower avalanches, with a smaller ΔH. Indeed, with a smaller variation of the field, some of the big avalanches that we have seen in the previous plots, would reveal to be the sum of many smaller avalanches. As stated above, in this first part we chose a compromise between the value of ΔH and a reasonable computational time.

5. A bigger number of runs (here we always used 7 code's runs for each histogram) surely would improve the statistics. But, still, the time required would increase.

So, here the problem is linked to the required simulation time. Even in the close-to-thermalization simulations, by reducing ΔH and keeping $L = 500$, would require a very long time (on a desktop server in the Physics Department computer, one week for 7 runs, with fixed T and R, against the three days required for the value of ΔH that we used here). The idea for the next analysis will be able to overcome the problem related to the computational time, allowing us to use a smaller step for the magnetic field. So, we postpone the analysis on the power-law coefficient to the next section, where more reliable results will be found.

This first analysis has been useful in understanding, given a certain T, where we have to look to get a power-law behaviour within the Wolff algorithm: close to the value of R characterized by $T_C \sim T$. Indeed, for the next analysis we used fig.4.9 in order to find the suitable range of values for R_C.

6.2 Quasi-equilibrium analysis

In this second part of our analysis on the avalanches' statistics, we start from an hypothesis about the MC time. We mimic the real time with the MC simulation time. So, for a value of H, we do not wait the thermalization for sampling. Instead, we take as a sample the first few iterations of the MC algorithm (we chose 5 iterations). As if our simulated lattice's behaviour, out-of-thermalization, was actually like the real one, where a magnetic domain changes shape and rotation under a continuous tuning of the external magnetic field. In order to keep this out-of-thermalization analysis sufficiently close to equilibrium, we have reduced the amplitude of the external field steps. More precisely, we used $\Delta H = 10^{-5}J$ (a field step two orders of magnitude smaller than before) in order to simulate the experimental conditions of slow but almost-continuous variation of the field. The computational time saved allowed us to increase the number of runs to 21.

For each temperature, the analysis is focused around the lowest value of R from the previous analysis.

In fig.6.5 and 6.6, we can look at the results for a low and high temperature respectively. The plots for the other temperatures were equivalent. As we previously supposed, the linear region of the distribution is larger on the side of smaller avalanches. For the lower temperatures, we still have the tendency of the linear region to cover less decades. Instead, for the highest temperatures, the best linear behaviours are found.

6.2.1 Power-law coefficient and critical R analysis

Finally we can analyse the power-law coefficient (τ, as defined in section 1.2) behaviour, and compare the theoretical results with the experimental ones. For the computation of τ, we obviously focused our linear fitting operations on that part of the distributions that most resembles to a linear trend, as we can notice by looking at the pictures 6.5 and 6.6. For each one of the distribution, the corresponding linear fitting has been plotted too. For the highest temperatures, we focused on the distribution with the best linear trend (always the one with higher R, as we can see from the pictures 6.5 and 6.6), then, for the other two values of R, we chose to consider only those plot's points where the three different distributions were more similar to each other.

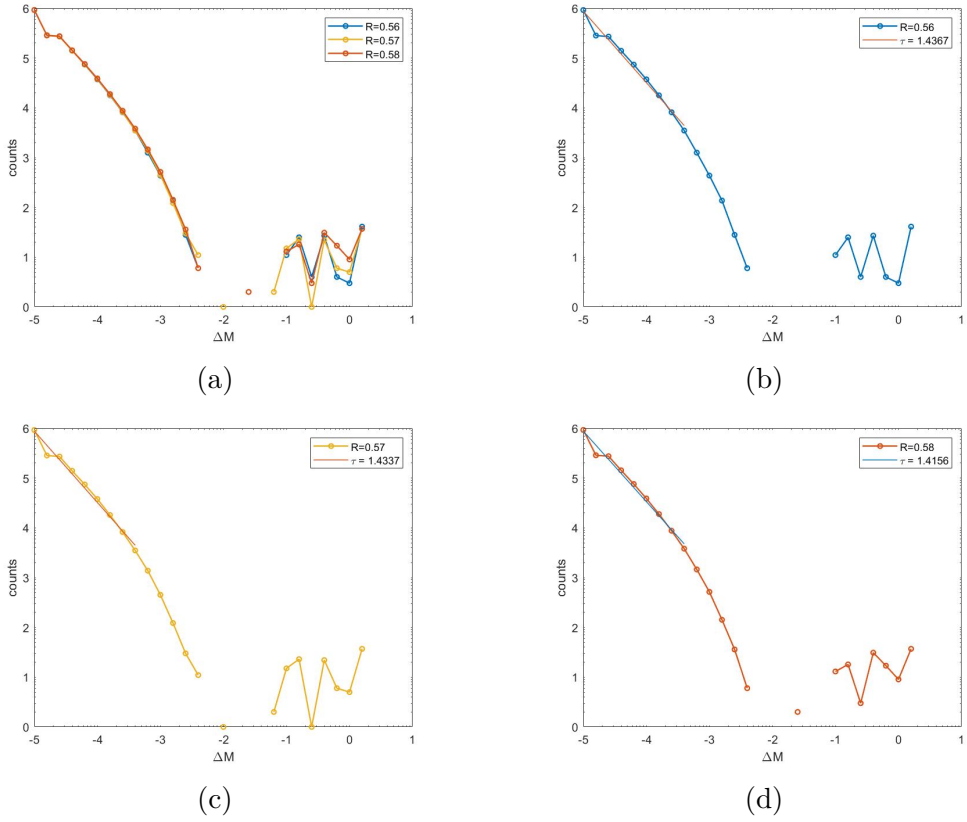

Figure 6.5: Avalanches' statistics.(a)$T = 1.80$,(b)$R = 0.56$,(c) $R = 0.57$,(d)$R = 0.58$.

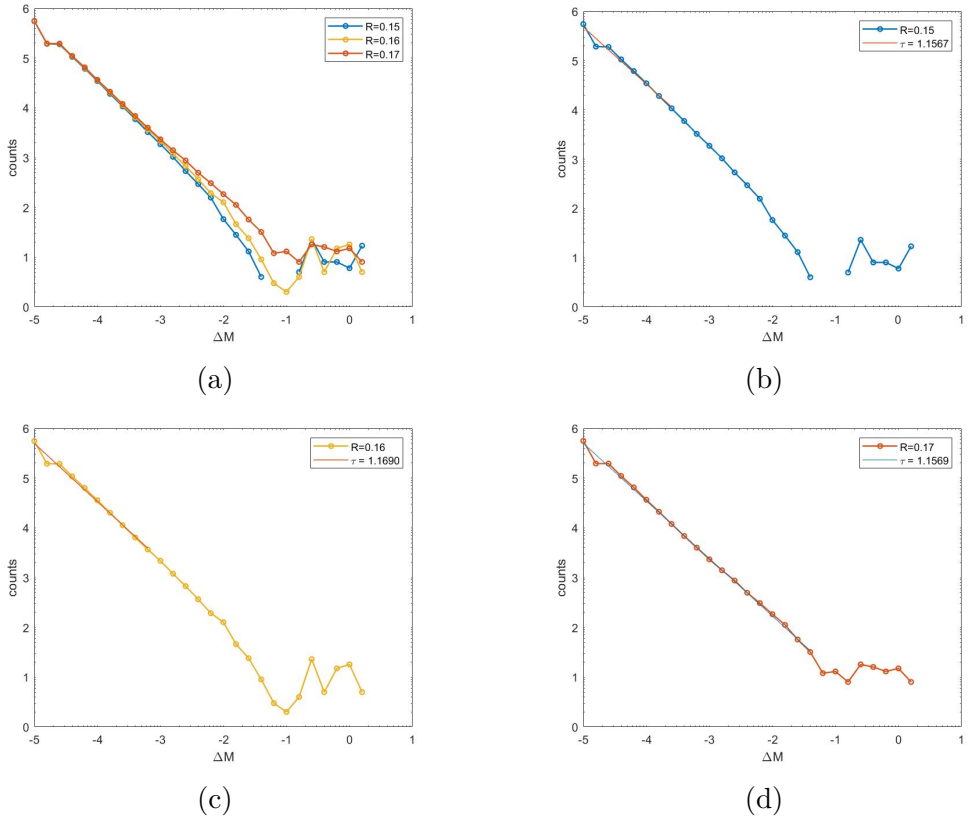

Figure 6.6: Avalanches' statistics.(a)$T = 2.15$,(b)$R = 0.15$,(c) $R = 0.16$,(d)$R = 0.17$.

The temperature dependence of the power-law exponent τ is shown in fig.6.7.

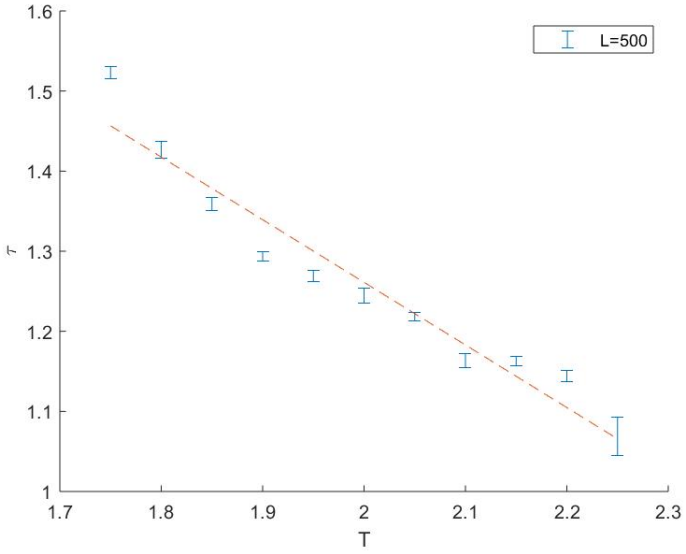

Figure 6.7: Temperature dependence of the power-law coefficient τ. The dotted line indicates the best linear fit to the data obtained.

Since, for each temperature, we tested three different values of the disorder parameter R, we have three values of the coefficient τ for each T. With these three values, we computed the errorbars in fig.6.7.

With this analysis, we did not go below $T = 1.75$ for two reasons:

1. The linear behaviour is already very weak for $T = 1.75$ (i.e. the linear part of the distributions covers only a decade), making it difficult to do a good analysis of the slope of the linear part of the distribution.

2. Since we are moving on the line of the para-ferromagnetic transition (see blue line in fig.5.9) where Wolff is more efficient, going below $T = 1.75$ temperature means getting close to the triple-point of the para-ferro-glass transition (see the intersection point between blue and red line in fig.5.9).

So, a more efficient algorithm far from the critical temperature zone is needed in order to continue the analysis for T below 1.75.

In fig.6.8, we can see the temperature dependence of the critical value of the disorder parameter, R_C, plotted with the disorder dependence of the critical temperature T_C too. This allows to better appreciate that they are one the inverse function of the other.

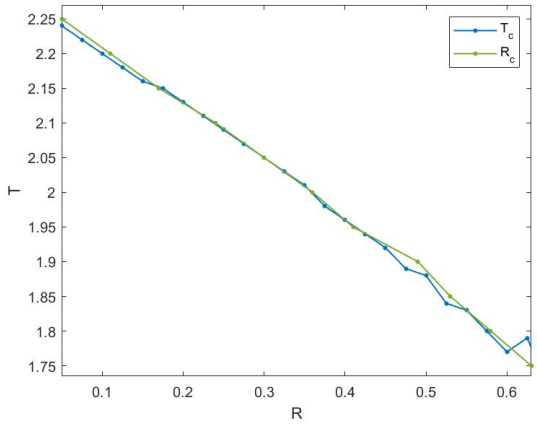

Figure 6.8: Temperature dependence of the critical value of the disorder parameter, R_c. For each T, we choose as a critical R the one with the wider linear behaviour.

If we go above R_C, we enter the small-avalanches regime. In particular, within RFIM, Sethna et al. found a cut off for big size avalanches (see fig.6.9). In fig.6.10, we can see a similar behaviour in our RBIM. Actually, due to limit of the lattice dimension[2] we can not go below $\Delta M = 8 \cdot 10^{-6}$, so we can not appreciate the four lines, in each plot, going toward small size avalanches with the same slope for a couple of decades, like in 6.9. In any case, we can notice a starting trend of the distributions to reach the same slope for small size avalanches. Trend that would be more visible with a bigger lattice size L. Instead, we can see that, by increasing R, the quantity of big avalanches decreases and a cut off appears like the one found by Sethna. As with RFIM, also in RBIM the cut off appears to diverge when we get close to R_C.

[2]For $L = 500$, the minimum magnetization variation is $\Delta M = \frac{2}{250000} = 8 \cdot 10^{-6}$, which in log axis is $\Delta M = -5.09$.

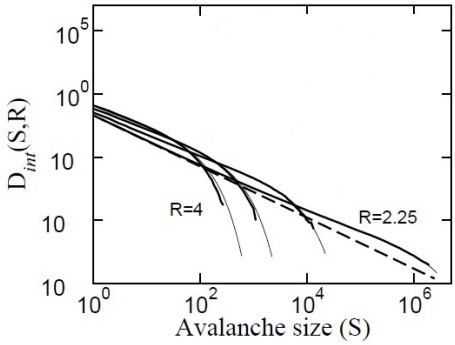

Figure 6.9: Avalanches size distributions, for RFIM. $R_C = 2.16J$ (dotted line), $J = 1$, $3D$, $T = 0$. Up to 50% above R_C, there is still a linear behaviour for small avalanches, similar to the one at lower values of R, with a cut off for big size avalanches. (source [10])

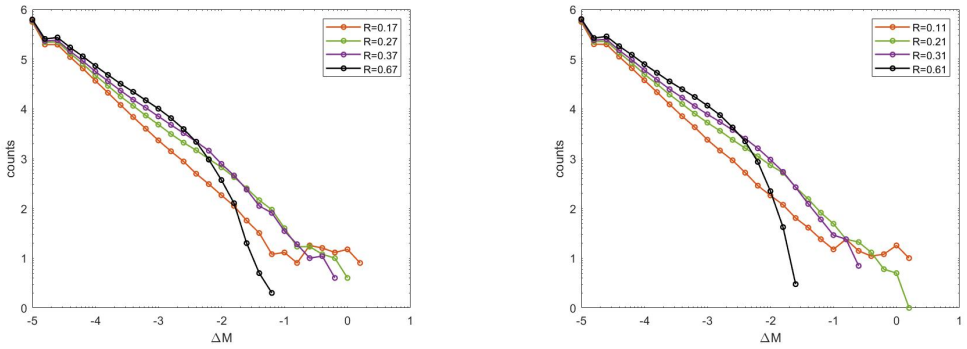

(a) (b)

Figure 6.10: Cut off for big size avalanches within RBIM, for $T = 2.15$ ($R_C = 0.17$) and $T = 2.20$ ($R_C = 0.11$).

6.3 Negative Barkhausen noise

Up to now, we did not distinguish between positive and negative values of ΔM, i.e. all the histograms that we have seen consider both positive and negative avalanches. A negative avalanche is a discontinuity of the area (volume, in $3D$) of the magnetic domain inducing a negative variation of the magnetization of the magnetic sample.

Within this section, we study both the statistics of $\Delta M > 0$ and $\Delta M < 0$. In [25], Puppin and Zani found the same coefficient $\tau = 1.6$ (within experimental error) for positive and negative avalanches' statistics. We look if the same behaviour emerges from RBIM.

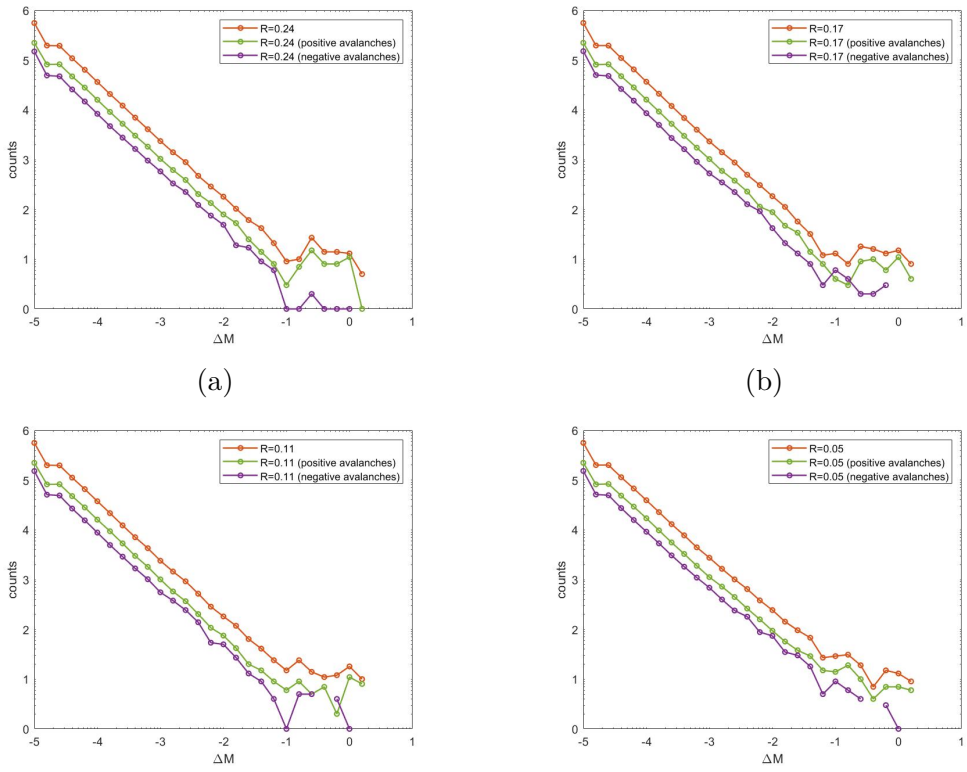

Figure 6.11: Avalanches' statistics.(a)$T = 2.10$, $R_C = 0.24$,(b)$T = 2.15$, $R_C = 0.17$(c) $T = 2.20$, $R_C = 0.11$(d)$T = 2.25$, $R_C = 0.05$.

In fig.6.11, we can compare the whole avalanches' statistics, studied so far, with the positive and negative ones. Only the four highest temperature are shown, since they exhibit a wider linear behaviour respect to lower temperatures. For each on of these four cases, we can notice that there are always more positive avalanches than negative ones (except for some value at big avalanches). This is quite obvious since the external magnetic field moves in the direction of positive avalanches. Also, the slope of positive and negative seems quite similar. This first qualitative impression is confirmed by the plot in fig.6.12. The main differences are found at low temperatures (T = 1.75,

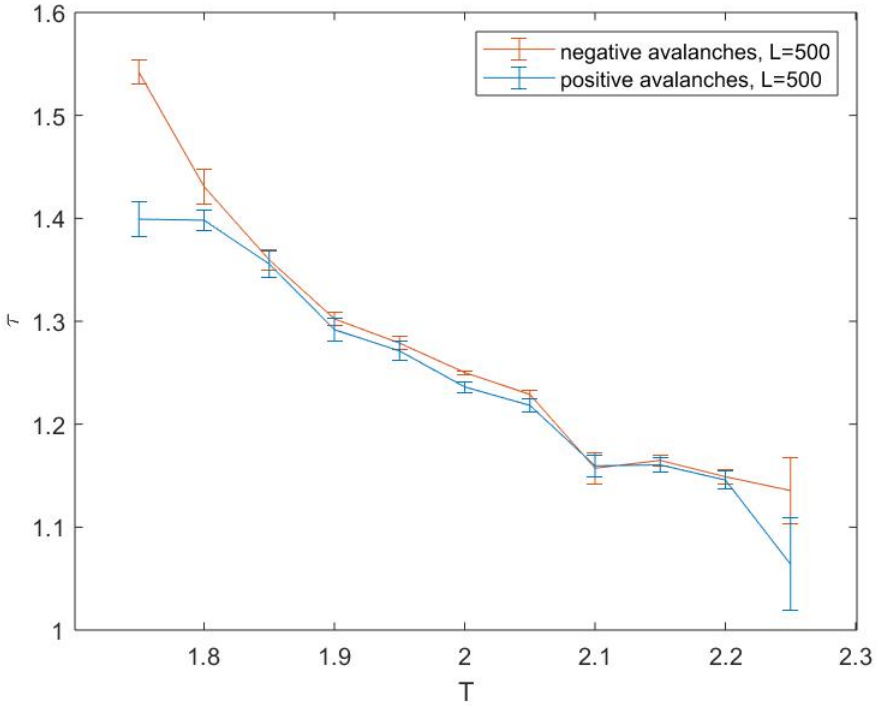

Figure 6.12: Comparison between the temperature dependence of τ for positive and negative avalanches. Here we use the line connecting the points of the plot. In this way it is easier for the reader to observe the similarity between the two cases, positive avalanches and negative avalanches.

T = 1.80), and at T = 2.25, close to the critical temperature (T_C = 2.27, L = 500). For all the other temperatures, we found similar values of τ for

positive and negative avalanches.

Here are some considerations about the possible causes for the temperatures showing big differences in the value of τ:

1. Since at low temperatures the linear region of the avalanches' distribution covers just one decade or less, the analysis of the distribution's slope is affected by a bigger error respect to the higher temperatures.

2. Close to T_C, the critical oscillations of the physical quantities, like the magnetization, affects also the avalanches' statistics, and consequently the estimation of τ.

Chapter 7

Conclusions and Discussion

The main original results of this thesis are three: the para-ferro-glass phase diagram, the temperature dependence of the BK noise power-law exponent τ, and the negative BK noise power-law.

7.1 The para-ferro-glass phase diagram

The para-ferro-glass phase diagram (fig.5.9, here reported as fig.7.1 for the ease of the reader) lives in the (R, T) plane. The line separating the fer-

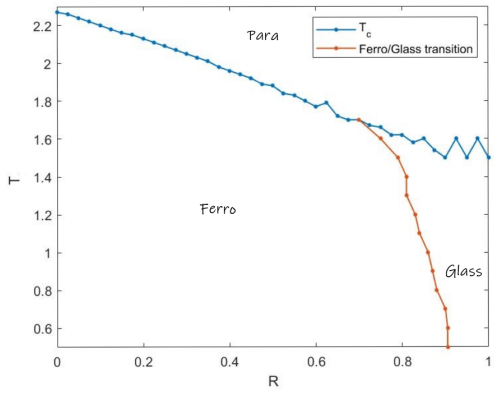

Figure 7.1: Magnetic phase diagram.

romagnetic and spin-glass phases has a low-temperature behaviour in good

agreement with the results of [28]. In this article, the value of negative bonds' concentration inducing the transition from ferromagnet to spin-glass at $T = 0$ is 0.15. By exploiting 7.2, we observe that the 15% of negative bonds cor-

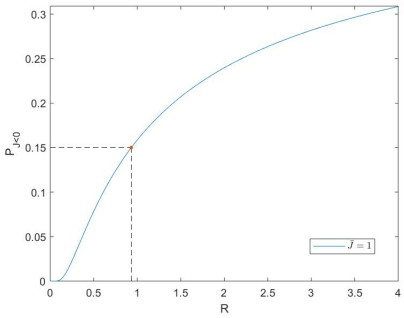

Figure 7.2: Concentration of negative bonds within RBIM with $\bar{J} = 1$ and variance R.

responds to $R \simeq 0.93$. The minimum temperature for which we were able to estimate the value of R, necessary for the transition, is $T = 0.5$. With $R = 0.905$. We can suppose the red line in fig.5.9 tends to $R = 0.93$ as the temperatures goes to zero.
On the other hand, the blue line of the phase diagram is the limit between the paramagnetic and ferromagnetic phases. It has been derived looking at the temperature with the highest value of the magnetization variance, for a fixed R. The intersection between these two lines is called *triple point*, that is located at $T = 1.70$ and $R = 0.70$
Such phase diagram was useful for our avalanches' analysis, by avoiding us ending up in the glassy phase.
We did not study the line separating the glassy phase from the paramagnetic one, so the part of the blue line below $T = 1.70$ should be analysed and possibly confirmed in a separate study.

7.2 Barkhausen noise

We derived a number of results concerning the critical exponent characterizing the BK noise. By looking at results found by Puppin and Zani investigating the magnetization process of a 900Å thick Fe sample grown on MgO (001) substrate, a similarity can be seen with our theoretical values. In [23],

they found τ = 1.8, for T = 10K , and τ = 1, for T = 300K (i.e. room temperature). By looking at fig.6.7, here reported as fig.7.3, we notice how the value

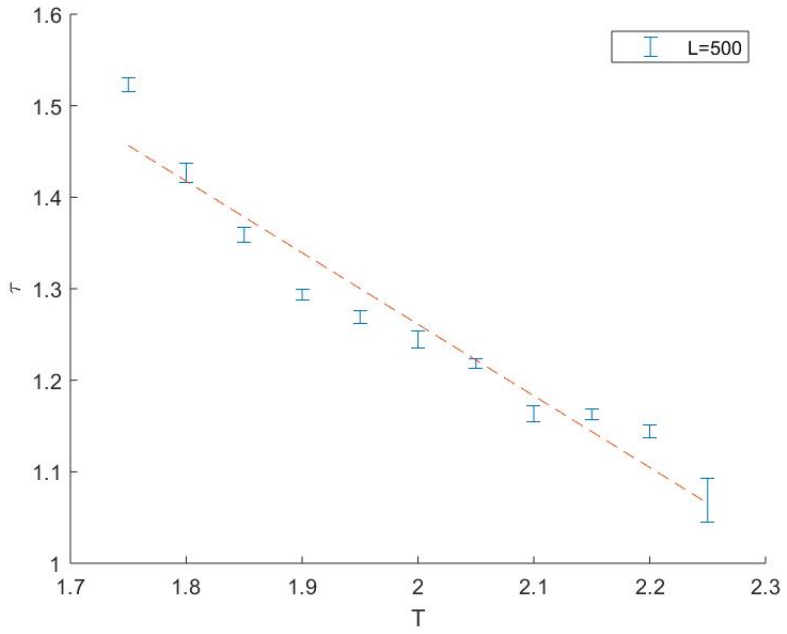

Figure 7.3: Temperature dependence of the critical exponent τ.

of τ gets close to 1 for temperatures close to the critical one (T_C = 2.27, for 2D square Ising model with L = 500). The T_C for iron bulk is 1043K, but, in [23] a thin film of Fe has been studied. It can be that, due to the reduced coordination of spins' links compared to bulk Fe, the critical temperature has decreased respect to the bulk value. Indeed, for the critical temperature T_C, a decreasing trend with the sample thickness was found in [29, 30]. In [24], Puppin found for the same material τ = 1.1, at room temperature. Still similar to our results in the high temperature regime. Another measurement at room temperature, with which the range of values that we have found is in agreement, is the one in [26], where for Co and MnAs thin films a power-law exponent $\tau \sim 1.33$ was found.

If we move towards lower temperatures, the coefficient τ increases. At the lowest temperatures at which the Wolff algorithm delivered reliable results ($T \sim 1.75$), it already reaches values between 1.50 and 1.55. This is in agree-

ment with the trend found in [23], where the lowest temperature has the highest value of τ, i.e. on average the size of the avalanches increases with temperature. Within our simulations, it was not possible going towards too low temperatures, because there the Wolff algorithm is no more optimal for BK noise analysis, since it is characterized by the unbridled growth of too big clusters (see section 4.2.2).

Finally, the good results we found in the single-avalanche analysis (section 6.2) suggest that the Barkhausen effect is a quasi-equilibrium phenomenon. This is an interesting result, especially because we are not aware of other studies in the literature which use the Wolff algorithm in quasi-equilibrium conditions.

7.3 Negative Barkhausen noise

We have also the good agreement between data from negative Barkhausen noise simulations and experimental data found by Puppin and Zani in [25]. In this article, the same value of τ was found both for positive and negative avalanches, at room temperature, in amorphous ribbons of $Fe_{63}B_{14}Si_8Ni_{15}$. Looking at fig.6.12, we can see that, within the range of temperatures from T = 1.80 to T = 2.20, also our results show such similarity between positive and negative avalanches power-law coefficient.

7.4 Future developments

In conclusion, we achieved a good agreement between our theoretical model (Random-Bond Ising Model) and the real systems mentioned above. We have seen that the Wolff algorithm is good, for BK noise analysis, only if we choose the R_C value such that $T \sim T_c$. This makes sense since the Wolff algorithm (and more in general clusters algorithm) have been developed in order to overcome the critical slowness of the single-flip Metropolis algorithm close to T_C (see [22]). Actually, for low temperatures this trick (i.e. moving close to the T_C line in 7.1) is no more efficient, due to the unbridled growth of too big clusters.

For further studies, we suggest the Niedermayer algorithm, where a new

parameter is introduced in order to control the size of the built cluster.

More precisely, this algorithm covers with continuity the intermediate cases between the Metropolis and the Wolff algorithm. Within this method, the acceptance ratio (A) and the P_{add} formulas become

$$A = e^{-\beta(1-\alpha/2)\Delta E},$$
$$P_{add} = 1 - e^{-\alpha\beta J_{ij} s_i s_j},$$

where α is the tunable parameter mentioned above, ΔE is the energy difference between the starting configuration and the new proposed one, J_{ij} is the interaction strength between the two nearest neighbours spins, s_i and s_j. We notice that with $\alpha = 2$ we recover the formulas of the Wolff algorithm (and $\alpha = 0$ gives the Metropolis case).

An interesting analysis would be finding the proper value for the parameter α so that the optimal algorithm, capable to visit lower temperatures compared to those we have reached with the Wolff method, is found.

Bibliography

[1] *Barkhausen effect*, (2020)Wikipedia. Available at:https: //en.wikipedia.org/wiki/ Barkhausen effect (Accessed: 3 October 2020).

[2] H. Barkhausen, *Zwei mit Hilfe der neuen Verstärker entdeckte Erscheinungen*, Physik Z., 20:401-403, 1919.

[3] H. J. Williams and W. Shockley, *A simple domain structure in an iron crystal showing a direct correlation with the magnetization*, Phys. Rev., 75:178-183, 1949.

[4] Cote, P. J., and Meisel, L. V., *Self-organized criticality and the Barkhausen effect.*, Phys. Rev. Lett. 67, 1334–1337, 1991.

[5] Meisel, L. V., and Cote, P. J., *Power laws, flicker noise, and the Barkhausen effect.*, Phys. Rev. B 46, 10822–10828, 1992.

[6] Bak, P., Tang, C., and Wiesenfeld, K., *Self-organized criticality: An explanation of the 1/f noise.*, Phys. Rev. Lett. 59, 381–384, 1987.

[7] E. Vives and A. Planes, *Avalanches in a fluctuationless first order phase transition in a random-bond Ising model.*, Phys. Rev. B, 50:3839-3848, 1994.

[8] K. Dahmen, S. Kartha, J. A. Krumhansl, B. W. Roberts, and J. P. Sethna, and J. D. Shore, *Disorder-driven first-order phase transformations: A model for hysteresis*, J. Appl. Phys. 75, 5946, 1994.

[9] E.M. Purcell, *Elettricità e magnetismo*, La Fisica di Berkeley, Zanichelli, 1986.

[10] O. Perkovic, K. Dahmen, and J. P. Sethna, *Avalanches, Barkhausen Noise, and Plain Old Criticality.*, Phys. Rev. Lett. 75, 4528, 1995.

[11] J. Kent-Dobias, J. P. Sethna, *Cluster representations and the Wolff algorithm in arbitrary external fields.*, Phys. Rev. E. 98(6), 2018.

[12] M.E. Newman, G.T. Barkema *Monte Carlo Methods in Statistical Physics*, Oxford University Press, 1999.

[13] N.K. Jaggi, *Ground state of a two-dimensional frustrated Ising model*, J. Phys. C: Solid St. Phys., 13 (1980) L177-80.

[14] R. Piazza, *Statistical Physics. A Prelude and Fugue for Engineers*, Springer, 2017.

[15] M. Metra, *Barkhausen noise in random Ising models*, Tesi di laurea magistrale in Mathematical Engineering, Politecnico di Milano, A.A. 2017-2018. https://www.politesi.polimi.it/handle/10589/144387

[16] V.S. Dotsenko, W. Selke, L. Talapov, *Cluster Monte Carlo Algorithms for Random Ising Models*, Physica A 170, 278 (1991).

[17] D.A. Kessler, M. Bretz, *Unbridled growth of spin-glass cluster*, Physical Rev. B 41, 7 (1990).

[18] G.H. Wannier, *Antiferromagnetism. The Triangular Ising Net*, Phys. Rev. 79 (2): 357–364.

[19] S.F. Edwards, P.W. Anderson, *Theory of spin glasses*, J. Phys. F: Metal Phys. 5, May 1975.

[20] D. Sherrington, S. Kirkpatrick, *Theory of spin glasses*, Phys. Rev. Lett. 35, 1792 – 1975.

[21] G.Parisi, *Toward a mean field theory for spin glasses*, Physics Letters A, Volume 73, 3, 1979, 203-205.

[22] U.Wolff, *Collective Monte Carlo Updating for Spin Systems*, Phys. Rev. Lett. 62, 361, 1989.

[23] E. Puppin, M. Zani *Magnetic hysteresis and barkhausen noise in thin Fe films at 10 K.*, J. Phys.: Condensed Matter, 16:1183, 2004.

[24] E. Puppin *Statistical properties of Barkhausen noise in thin Fe films.*, Phys. Rev. Lett.84, 5415-5418, 2000.

[25] E. Puppin, M.Zani *Negative Barkhausen jumps in amorphous ribbons of* $Fe_{63}B_{14}Si_8Ni_{15}$., J. Appl. Phys., 94, 9, 2003.

[26] S. C. Shin, K. S. Ryu, D.H. Kim, S.B.Choe, H. Akinaga *Power-law scaling behaviour in Barkhausen avalanches of ferromagnetic thin films.*, J. Magn. Magn. Materials 310, 2599– 2603, 2007

[27] N. J. Wiegman *Barkhausen noise in magnetic thin films: Experimental noise spectra.*, Appl.Phys., 12, 157-161, 1977.

[28] N. K. Jaggi *Ground state of a two-dimensional frustrated Ising model.*, J. Phys. C: Solid St. Phys., 13 (1980) L177-80.

[29] W. Dürr, M. Taborelli, O. Paul, R. Germar, W. Gudat, D. Pescia, M. Landolt *Magnetic Phase Transition in Two-Dimensional Ultrathin Fe Films on Au(100).*, Phys. Rev. Lett. 62, 1989.

[30] A. P. Jaroenjittichai, Y. Laosiritaworn *The competitive effect of non-magnetic defect and films thickness on the ferromagnetic critical temperature in Ising thin-films.*, MATEC Web of Conferences 249, ICMMM 2018.